



**Synthesis and Characterisation of Sesquioxidic
Precipitates Formed by the Reaction of Acid Mine
Drainage with Fly Ash Leachate**



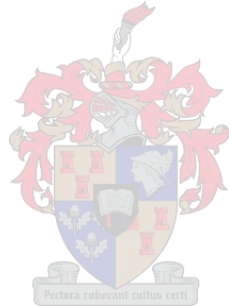
C.L. Burgers

Submitted in partial fulfilment of the
requirements for the degree of
Master of Science (Agriculture)
in the Department of Soil Science
University of Stellenbosch
August, 2002

Declaration

I the undersigned hereby declare that the work contained in this thesis consists in entirety of my own original research. It has not, in whole or in part, been submitted to any other University for the purposes of obtaining a further degree.

Colleen Burgers



Abstract

Coal mining in South Africa is estimated to produce 200 Ml of acid mine drainage (AMD) per day in the Pretoria-Witwatersrand-Vereeniging (PWV) area alone, while electricity production resulted in approximately 27 Mt of ash in 2001. A large number of collieries in South Africa are tied to power stations where these two waste streams, acid mine drainage and fly ash, have the capacity to neutralize each other and provide an opportunity for co-disposal.

The aim of this study was to investigate the reactions that occur during the co-disposal of fly ash leachate (FAL) and AMD and to examine the precipitates that result from the neutralisation reactions. Potentiometric titration was employed to investigate the neutralisation of Al-Fe salt solutions, simulating acid mine drainage (AMD), with alkaline solutions of Ca or Na hydroxide as well as fresh alkaline leachate from fly ash (FAL). The effectiveness of fly ash in removing metals and other salts from acid mine water was examined by analysing the neutralised water and modelling the results thermodynamically. Precipitates, prepared from large scale synthetic AMD and FAL co-disposal at various pH levels and Fe:Al ratios, were characterised according to composition, mineralogy and surface properties.

The experimental neutralisation of synthetic acid mine drainage was achieved through titrating the components of SAMD (Fe and Al salt solutions) and solutions of various Fe:Al mole ratios with different bases in air and N₂, and comparing the SAMD-FAL system with these simple acids and bases. The FAL used in all experiments was produced from fresh fly ash collected at Arnot power station. The SAMD was prepared as a solution with a pH of 2.5 and containing 12.7 mmol/L Al, 10.9 mmol/L Fe and 40.8 mmol/L SO₄. The characterisation of reaction solids was achieved by collecting the precipitates formed from the co-disposal of FAL and SAMD with Fe:Al ratios of 7.3, 0.8 and 2.5.

From the titration experiments it was found that upscale potentiometric titrations of SAMD show buffer zones at pH values of 3.5, 4, 6 and 10 corresponding to Fe(III)

precipitation, Al precipitation, Fe(II) hydrolysis and oxidation, and Al redissolution, respectively, while downscale potentiometric titrations with SAMD show buffer zones at pH values 12 – 11, 9 and 4.5, which correspond to Fe oxidation and precipitation, Al precipitation and Al re-dissolution, respectively. A high concentration of Al in the simulated AMD inhibited the crystallinity of the precipitates and resulted in a large quantity of SO₄ being removed from solution, which suggests that an aluminium sulphate phase is precipitating, but it is not crystalline and cannot be identified by XRD. Titrations performed up-scale by adding FAL to AMD showed near-complete metal and substantial SO₄ removal from solution.

The characterisation of reaction solids by x-ray diffraction, infrared spectroscopy, thermal gravimetric and differential thermal analysis revealed that the precipitates consist of poorly crystalline, highly Al-substituted goethite and ferrihydrite with large amounts of SO₄ included in the structure. Poorly crystalline bayerite appears at a high pH and high Al concentration, and calcite is present in precipitates made by adding SAMD to FAL. High surface charges of between 330 cmol/kg positive and 550 cmol/kg negative charge and potentially large specific surface areas between 7 and 236 m²/g suggest a strong potential for the precipitates to function as low-grade adsorbents in wastewater treatment. The similarity of these ochre precipitates to soil minerals implies that land disposal of the neutralised solids is also viable.

Uittreksel

Steenkool mynbou in SA produseer na benaming 200 ML suur mynwater per dag in die PWV area alleenlik, terwyl opwekking van elektrisiteit naastenby 27 Mt vliegas geproduseer het in 2001. 'n Groot aantal steenkoolmyne in SA word verbind met krgsentrales, waar hierdie twee strome afval, suur mynwater en vliegas, die kapasiteit het om mekaar te neutraliseer en die weg te baan vir gesamentlike wegdoening.

Die doel van hierdie studie was om die reaksies wat plaasvind gedurende gesamentlike wegdoening van vliegas loog (VAL) en suur mynwater (SMW) te ondersoek, asook die neerslae wat mag vorm as gevolg van neutralisasie reaksies. Potensiometriese titrasies was gebruik om die neutralisering tussen Al:Fe-sout oplossings te ondersoek as nabootsing van SMW met gebruikmaking van alkaliese oplossings van Ca of Na hidroksied asook vars loog van VA. Die effektiwiteit van VA om metale en soute uit SMW te verwijder was getoets deur outleding van die geneutraliseerde water en modellering van die termodinamika. Neerslae berei uit groot-skaal sintetiese SMW en VAL en met gelyktydige storting by verskeie pH vlakke en Fe:Al verhoudings, was gekarakteriseer volgens samestelling, mineralogie en oppervlak eienskappe.

Die eksperimentele neutralisering van sintetiese suur mynwater (SSMW) was gedoen deur titrering van die SSMW komponente en oplossings van verskeie Fe:Al molêre verhoudings met verskillende basisse in lug en N₂, en vergelyking van SSMW-VAL sisteem met hierdie eenvoudige sure en basisse. Die VAL gebruik in alle eksperimente was geproduseer van vliegas verkry van die Arnot krgsentrale. Die SSMW was berei as 'n oplossing met 'n pH van 2.5 en bevat 12.7 mmol/L Al, 10.9 mmol/L Fe en 40.8 mmol/L SO₄. Die karakterisering van vastestowwe uit die reaksie was gedoen deur die bemonstering van neerslae gevorm as gevolg van die gelyktydige wegdoening van VAL en SSMW met Al:Fe verhoudings van 7.3, 0.8 en 2.5.

Die was waargeneem in die titrasie eksperimente dat hoër-skaal potensiometriese titrasie van SSMW buffersones, by pH waardes 3.5, 4, 6 en 10, ooreenstem met Fe(III) presipitasie, Al presipitasie, Fe(II) hidrolise en oksidasie, en Al her oplossing, terwyl laer skaal potensiometriese titrasie met SSMW buffer sones by pH waardes 12 - 11, 9 en 4.5 ooreenstem met Fe(III) presipitasie en oksidasie, Al presipitasie en heroplossing respektiewelik. 'n Hoë konsentrasie Al in die sintetiese SMW het kristalliniteit van die neerslae geïnhieber en veroorsaak dat 'n hoeveelheid SO₄ uit oplossing verwijder is, wat suggereer dat die AlSO₄ fase neerslaan maar nie kristallyn is en gevoglik nie opgetel word met x-straal diffraksie nie. Titrasië gedoen by hoërskaal deur byvoeging van VAL tot SSMW, het feitlik volledige metaal en SO₄ verwydering uit oplossing getoon.

Die karakterisering deur x-straal diffraksie, infrarooispektroskopie, termies gravimetries en differentiële termiese analise, het getoon dat die presipitate bestaan uit swak kristallyne, hoë Al-gesubstitueerde goethiet en ferrihidriet met groot hoeveelhede SO₄ vasgevang in die struktuur. Swak kristallyne bayeriet verskyn by hoë pH en hoë Al-konsentrasies en kalsiet is teenwoordig in neerslae gevorm deur byvoeging van SSMW tot VAL. Hoë oppervlakladings van tussen 330 cmol_c/kg positief en 550 cmol_c/kg negatiewe lading en ook potensieel groot spesifieke oppervlak van tussen 7 en 236 m²/g, duif op 'n sterk potensiaal vir neerslae om as laegraadse adsorbeermiddels in afvalwaterbehandeling gebruik te word. Die ooreenstemming in hierdie geelbruin neerslae met grond minerale, impliseer dat die land storting van geneutraliseerde vastestowwe ook lewensvatbaar is.

Acknowledgements

The author would like to thank the following people and organisations without whose support this thesis could not have been completed:

- Prof. Martin Fey for his supervision of this project and his boundless enthusiasm for the subject;
- Richard O'Brien for all his help and advice in the lab, with analytical equipment and with the occasional chat;
- The Water Research Commission for financial support;
- The Eskom Tertiary Education Support Programme (TESP) for financial support
- The National Research Foundation for financial support;
- The WRC project group at UWC, Leslie Petrik, Dr. Richard White, Michael Klink and Vernon Somerset for knowledge sharing;
- Matt Gordon for the analyses of many water samples by AAS and IC;
- Gerry Masters at UWC for his help with BET analyses;
- Suzana Vasic at UCT for the TGDTA analyses;
- Dr. Paul Verhoven for his introduction to the FTIR;
- All those in the Soil Science department for help, support and good humour;
- Jason Burke for his support and caring and for giving up his computer time;
- My family and friends who were ever willing to lend a caring ear.

Table of contents

Abstract (English)	i
Abstract (Afrikaans)	iii
Acknowledgements	v
Table of contents	vi
List of figures	x
List of tables	xii
Abbreviations and acronyms	xiv
Chapter 1. Introduction	1
Chapter 2. The genesis, remediation and environmental impacts of fly ash and acid mine drainage and the mineralogy of precipitates formed by sulphide oxidation: a literature review	
2.1 Introduction	6
2.2 Fly ash	6
2.2.1 Introduction	6
2.2.2 Products of coal combustion	6
2.2.2.1 Fly and bottom ashes	6
2.2.2.2 Flue gas desulphurisation wastes	7
2.2.3 Mineralogy, physical characteristics and elemental composition of fly ash	7
2.2.4 The disposal of fly ash	9
2.2.5 Environmental impacts of fly ash	11
2.2.5.1 Plant response	11
2.2.5.2 Soil Response	11
2.2.6 Chemistry of leachates and extracts	12
2.3 Acid mine drainage	13
2.3.1 Introduction	13
2.3.2 Sources of acid mine drainage	14
2.3.3 Generation of acid mine drainage and metal mobility	14
2.3.3.1 Rate of AMD production	16

2.3.3.2	Role of bacteria	17
2.3.3.3	Factors affecting the production and transport of AMD	18
2.3.4	Environmental impacts of acid mine drainage	19
2.3.5	Treatment of AMD	21
2.3.5.1	Active treatment	21
2.3.5.2	Passive treatment	23
2.4	Mineralogy of precipitates formed through sulphide oxidation	24
2.4.1	Introduction	24
2.4.2	Hydrated metal salts containing divalent cations	25
2.4.2.1	Melanterite group	25
2.4.2.2	Epsomite group	25
2.4.2.3	Hexahydrite group	26
2.4.2.4	Rozenite group	26
2.4.2.5	Kieserite group	26
2.4.3	Hydrated metal salts containing trivalent cations	26
2.4.4	Mixed divalent-trivalent salts	27
2.4.4.1	Copiapite group	27
2.4.5	Fe and Al hydroxysulphates	27
2.4.5.1	Al hydroxysulphates	28
2.4.5.2	Fe hydroxysulphates	29
2.4.6	Fe and Al oxides and hydroxides	30
2.4.6.1	Fe oxides and hydroxides	30
2.4.6.2	Al hydroxides	32
2.5	Conclusions	32

Chapter 3. Experimental neutralisation of synthetic acid mine drainage

3.1	Introduction	33
3.2	Materials and methods	34
3.2.1	Sample preparation	34
3.2.1.1	Fly ash leachate	34
3.2.1.2	Synthetic acid mine drainage	34
3.2.2	Potentiometric titrations	36
3.2.2.1	Experiment 1: Components of SAMD titrated with different bases in oxic and anoxic environments	36

3.2.2.2 Experiment 2: Acidic solutions with differing Fe:Al mole ratios	38
3.2.2.3 Experiment 3: The SAMD-FAL system compared with simple acids and bases	38
3.2.2.4 Reproducibility of potentiometric titrations	39
3.3 Analysis	40
3.4 PHREEQC solution modelling	41
3.5 Results of potentiometric titrations	41
3.5.1 Experiment 1: Components of AMD titrated with different bases in oxic and anoxic environments	41
3.5.2 Experiment 2: Different Fe:Al ratios titrated with base	44
3.5.3 Experiment 3: The SAMD-FAL system compared with simple acids and bases	45
3.6 XRD data	48
3.7 Anion and cation data	53
3.8 Mineral saturation indices	58
3.9 Discussion	62
3.10 Conclusions	64

Chapter 4. Characterisation of reaction solids

4.1 Introduction	66
4.2 Materials and methods	66
4.2.1 Fly ash leachate	66
4.2.2 Synthetic acid mine drainage	67
4.2.3 Preparation of products for analysis	67
4.3 Analysis	68
4.4 Results	69
4.4.1 Anion and cation data	69
4.4.2 X-ray diffractometry	72
4.4.3 Thermo-gravimetric and differential thermal analysis	73
4.4.4 Infrared spectroscopy	76
4.4.5 Surface area	81
4.4.6 Surface charge	82
4.4.7 PHREEQC modelling of anion and cation data	88

4.5 Discussion	89
4.6 Conclusions	91
Chapter 5: Discussion and conclusions	92
Chapter 6: References	95
Appendix 1: XRD pattern of haematite formed by heating $\text{Fe}_2(\text{SO}_4)_3 \bullet \text{XH}_2\text{O}$	105
Appendix 2: Reproducibility of potentiometric titrations	107
Appendix 3: A replot of figure 3.3 in order to compare the difference between NaOH and the $\text{CaCl}_2/\text{NaOH}$ solution	111

List of figures

Figure 1.1: Coalfields and selected power stations of South Africa.	2
Figure 2.1: The environmental impacts of AMD on an ecosystem.	20
Figure 2.2: Schematic diagram for the active treatment of acid mine drainage.	21
Figure 3.1: Equipment arrangement for titration experiments.	36
Figure 3.2: Titration graphs comparing oxic and anoxic environments.	43
Figure 3.3: Titration graphs of different Fe:Al ratios in oxic and anoxic environments: (a) 1:6 Fe ^{II} :Al, (b) 6:1 Fe ^{II} :Al, (c) 1:2 Fe ^{II} :Al, (d) 2:3 Fe ^{II} :Al.	44
Figure 3.4: Downscale titration graphs of different bases titrated with different bases.	46
Figure 3.5: Titration graphs of FAL and a synthetic FAL with SAMD.	47
Figure 3.6: XRD patterns of the precipitates of FeSO ₄ titrated with different bases in oxic and anoxic environments during experiment 1. Y-axis shows the titration number and each pattern is labelled with a summary of the conditions.	49
Figure 3.7: XRD patterns of the precipitates synthesised from an Fe ₂ (SO ₄) ₃ solution titrated with different bases in oxic and anoxic environments during experiment 1. Y-axis shows the titration number and each pattern is labelled with a summary of the conditions.	50
Figure 3.8: XRD patterns of the precipitates of Al ₂ (SO ₄) ₃ titrated with different bases in oxic and anoxic environments during experiment 1. Y-axis shows the titration number and each pattern is labelled with a summary of the conditions.	50
Figure 3.9: XRD patterns of the precipitates of Fe:Al ratios titrated with a base in oxic and anoxic environments during experiment 2. Y-axis shows the titration number and each pattern is labelled with a summary of the conditions.	51
Figure 3.10: XRD patterns of the precipitates of SAMD titrated with a base in oxic and anoxic environments during experiment 3. Y-axis shows the titration number and each pattern is labelled with a summary of the conditions.	52
Figure 3.11: XRD patterns of the precipitates of Al:Fe = 2:1 titrated with different	

bases in oxic and anoxic environments during experiment 2. Y-axis shows the titration number and each pattern is labelled with a summary of the conditions.	53
Figure 4.1: XRD patterns for products 1 – 6 (y-axis), showing Fe:Al ratios and final solution pH.	71
Figure 4.2: XRD patterns for products 7 – 12 (y-axis), showing Fe:Al ratios and final solution pH. Bayerite and calcite lines are labelled.	72
Figure 4.3: XRD pattern of waste sludge produced by the neutralisation of AMD with lime from Landau colliery.	73
Figure 4.4: DTA and TGA graphs for all products, horizontal divisions are equivalent to 20 °C and 20 mg.	74
Figure 4.5: Infrared spectra for products 1 and 2.	77
Figure 4.6: Infrared spectra for products 3, 4, 12 and 13	78
Figure 4.7: Infrared patterns for products 5 and 6.	78
Figure 4.8: Infrared patterns for products 7 – 11.	79
Figure 4.9: A bridged bidentate metal sulphate complex.	80
Figure 4.10: Surface charge graphs for products 1 – 3, where the point of zero charge (pzc) and the zero point of titration (zpt) are shown.	83
Figure 4.11: Surface charge graphs for products 4 – 6, where the point of zero charge (pzc) and the zero point of titration (zpt) are shown.	84
Figure 4.12: Surface charge graphs for products 7 – 9, where the point of zero charge (pzc) and the zero point of titration (zpt) are shown.	85
Figure 4.13: Surface charge graphs for products 10 – 12, where the point of zero charge (pzc) and the zero point of titration (zpt) are shown.	86
Figure 4.14: Surface charge graph for product 13, where the point of zero charge (pzc) and the zero point of titration (zpt) are shown.	87

List of tables

Table 2.1: Physical properties of fly and bottom ashes.	8
Table 2.2: Thermal transformation of mineral phases.	9
Table 2.3: Bacteria genera <i>Thiobacillus</i> , <i>Leptospirillum</i> and <i>Sulfobacillus</i> and the inorganic substances that they consume.	19
Table 3.1: Selected analyses of some acid drainage, ion concentrations in mmol/L.	35
Table 3.2: The composition of SAMD in this study.	35
Table 3.3: List of titrations done for experiment 1.	37
Table 3.4: Composition of bases and fly ash leachate as determined by acid titration and AAS and IC.	38
Table 3.5: List of up- and downscale titrations performed with different ratios of Al:Fe ^{II}	38
Table 3.6: List of up- and downscale titrations completed for experiment 3.	39
Table 3.7: The total amount of each ion added before and during titration for experiment 1. Values are in mmol _c per volume of solution added.	54
Table 3.8: The total amount of each ion added before and during titration for experiment 2. Values are in mmol _c per volume of solution added and the base is the NaOH-CaCl ₂ solution.	54
Table 3.9: The total amount of each ion added before and during titration for experiment 3. The shaded area indicates downscale titrations and values are in mmol _c per volume of solution added.	55
Table 3.10: Ion concentrations in mmol _c /L in the supernatant solutions upon completion of titrations performed for experiment 1. Final pH measured immediately prior to analysis.	56
Table 3.11: Ion concentrations in mmol _c /L in the supernatant solutions upon completion of titrations performed for experiment 2. Final pH measured immediately prior to analysis.	57
Table 3.12: Ion concentrations in mmol _c /L in the supernatant solutions upon completion of titrations performed for experiment 3. Final pH measured immediately prior to analysis.	58
Table 3.13: The saturation indices for selected phases in the supernatant solutions	

For each titration in experiment 1. The (a) designates amorphous material.	60
Table 3.14: The saturation indices for selected phases in the supernatant solutions for each titration in experiment 2. The (a) designates amorphous material and the base is the NaOH-CaCl solution in all cases.	61
Table 3.15: The saturation indices for selected phases in the supernatant solutions for each titration in experiment 3. The (a) designates amorphous material and the shaded area indicates downscale titrations.	61
Table 4.1: Reaction conditions for precipitation products showing the different SAMD compositions used in percentage. Samples 6-10 are downscale reactions and the initial volume is that of FAL.	68
Table 4.2: Quantities (mmol _c) of ionic reactants used in preparing products of different Fe:Al molar ratios.	70
Table 4.3: Ion concentrations in mmol _c /L in the supernatant solutions upon completion of titration. Final pH measured immediately prior to analysis.	71
Table 4.4: The infrared active bands for some common molecules.	77
Table 4.5: The major infrared peaks for each product and their assignments (Nakamoto, 1963). Titrations 6-10 are downscale.	79
Table 4.6: Surface areas and pore volume and diameters for precipitates.	82
Table 4.7: pH of formation and point of zero charge shown with SAMD composition.	88
Table 4.8: List of phases and their saturation indices in the product supernatant solutions.	89

Abbreviations and acronyms

AAS	Atomic adsorption spectrometry
ALD	Anoxic limestone drain
AMD	Acid mine drainage
BET	Brunauer-Emmett-Teller
DTA	Differential thermal analysis
EC	Electrical conductivity
FAL	Fly ash leachate
IR	Infrared spectroscopy
IC	Ion chromatography
ICP-AES	Inductively coupled plasma-atomic emission spectroscopy
PFA	Pulverised fuel ash
PZC	Point of zero charge
SAMD	Synthesised acid mine drainage
SI	Saturation index
TGA	Thermal gravimetric analysis
XRD	X-ray diffractometry

Chapter 1

Introduction

Low grade coal is mined in South Africa to produce cheap electricity for many countries in Africa. These mining operations result in millions of tons of polluted water, and the power plants that burn coal to produce electricity create vast amounts of waste ash. These two pollutants cause major environmental problems and incur massive clean-up costs. The extent of South Africa's coalfields, the area that they cover and the potential for environmental pollution in the future is shown in Figure 1.1.

Pulverised fuel ash is the material remaining when coal is combusted to power the steam turbines that make electricity. Fly ash (FA) is that fraction of waste that enters the flue gas stream and is collected by bag house precipitators or other emission control devices. This waste is usually disposed of as a slurry to a waste dam site, where it is left to solidify and weather. Fly ash is considered to be a ferro-alumino silicate made up of glass spheres of very small particle size (20 – 80 μm) (Mattigod *et al.*, 1990). The mineralogy of FA is such that it includes a fraction of lime that gives the ash some degree of alkalinity. Fly ash frequently has high pH values (10 – 12) and contains high concentrations of potentially toxic elements that pose a considerable environmental hazard.

Acid drainage is produced when meteoric and ground water come into contact with sulphide minerals that are undergoing oxidation. This occurs primarily in coal and gold mines and their tailings but may also occur in soils that are close to the sea or contained in drained marshlands. Coal mining in South Africa is estimated to produce 175 Ml of acid mine drainage (AMD) per day in the Pretoria-Witwatersrand-Vereeniging (PWV) area alone (van Niekerk *pers.comm.*, 2001) and a further 120 000 Ml are stored. Due to the extremely low pH of AMD many metals such as Fe and Al are present in toxic concentrations. Sulphate is also present at toxic concentrations. Current legislation requires the mines to carry out neutralisation and clarification of all AMD before allowing it to rejoin natural waters. Active neutralisation with lime (CaO or Ca(OH)_2), soda ash (Na_2CO_3) or limestone (CaCO_3) is the most commonly

used method of remediation. The precipitated minerals, called ochres, are classified as hazardous waste and are disposed of in dump sites.

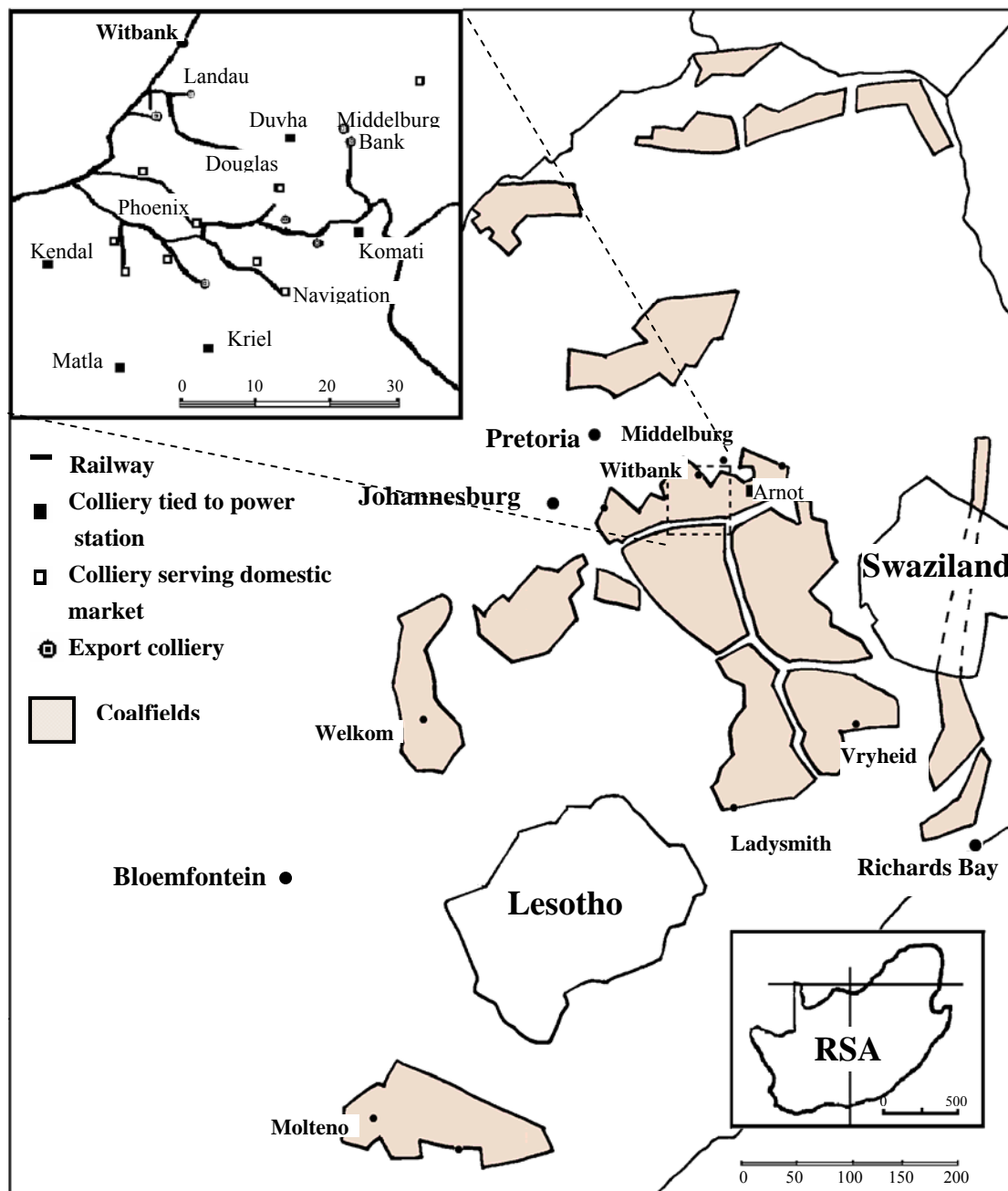


Figure 1.1: Coalfields and selected power stations of South Africa (adapted from Mehliss, 1981).

On the South African Highveld power stations are built in close proximity to the coal mines that supply them (see inset Figure 1.1). This situation results in the presence of two major environmental pollutants being disposed of adjacent to each other. The proximity of these wastes suggests that the problem of effective remediation may be

solved through co-disposal. The potential of FA for neutralising AMD is not as high as that of lime (O'Brien, 2000) but FA may be obtained at no cost with very little transport expense and the high surface areas ensures that the material need not be milled.

The neutralisation of AMD and various uses for FA have been studied extensively. Very few studies, however, have combined these two pollutants to achieve a mutual amelioration. O'Brien (2000) conducted the first of such studies in South Africa where he investigated the mineralogy of two South African fly ashes, their reaction with a synthetic AMD, the kinetics of neutralisation and the mineralogy of the precipitates. The fly ashes studied proved to have a strong neutralising capacity. The mineralogical investigations were, however hampered by the fact that solid fly ash was used for neutralisation and the ochre minerals were precipitated onto the surface of the glass spheres, making it difficult to detect the reaction products. The presence of ettringite at high pH was established, however, suggesting that this may constitute a sink for Ca, Al and SO₄ under some conditions.

McKeown (2000) investigated a soil severely contaminated by a burnt sulphur stockpile. The amelioration of this site closely followed the neutralisation procedure for acid mine drainage. The use of commercial limestone was successful in neutralising the acidity produced, but the accumulation of salts caused the development of a highly saline brine.

Azzie (2002) completed a large scale chemical classification of the waters draining collieries on the South African Highveld. This study presents comprehensive analyses of and mechanisms for the evolution of mine water. A classification scheme was developed enabling waters to be defined in terms of salinity, alkalinity or acidity and metal ion status. Despite a bimodal distribution of the pH of mine waters, being either acidic or near-neutral, the dominant anion is SO₄²⁻ with no obvious dominant cations. When assessing the treatment required for acid waters this investigation is invaluable.

Bezuidenhout (1995) investigated the dissolution characteristics of fly ash particles and the changes associated with leachate produced at the Kriel power station ash dam.

The composition of the ash water was compared to leachates of a core through the dam. The leachate composition was found to have a lower pH and decreased concentrations of Ca and SO₄. Calcium concentrations were controlled by exposure to atmospheric CO₂ and the formation of calcite. Sulphate concentrations were postulated to be controlled by the formation of ettringite and the development of a reducing environment in some areas. Metal concentrations were highest in leachates with a low pH. Elements such as Mn, Mo, Cu, I, Mg, Fe, and Ba were associated with the formation of ferrihydrite.

This investigation attempts to decrease effectively the challenging task of waste management in the coal mining industry. The hypothesis put forth in this thesis is that the reaction between AMD and FAL can be manipulated to produce mineralogical and chemically diverse precipitates which, besides sequestering environmentally excessive acidity and alkalinity, are potentially useful by-products by virtue of their surface reactivity.

Emerging from this hypothesis, the following questions concerning the nature of precipitates and the mechanism of the neutralisation reactions need to be answered.

- i. Does amelioration of AMD using fly ash effectively remove Fe and Al from solution?
- ii. What is the mineralogy of the precipitates?
- iii. What role do the precipitates play in removing salts from the polluted water?
- iv. Do the characteristics of the precipitates suggest their use as industrial adsorbents?

The aim of this study was to investigate the reactions that occur during the codisposal of fly ash leachate (FAL) and AMD, and to examine the ochre minerals that result from the neutralisation process. Four main objectives were to be achieved by means of a series of laboratory experiments using fly ash leachate and a synthetic solution of acid mine drainage.

- i. Compare fly ash to other common neutralising reagents via a series of potentiometric titrations simulating the industrial remediation of AMD.

- ii. Examine the solution chemistry to determine the effectiveness of fly ash in removing metals and other salts from acid mine water.
- iii. Synthesise the ochres formed by the neutralisation of AMD using fly ash leachate as the alkaline material.
- iv. Investigate the composition, mineralogy, properties and surface characteristics of the precipitates formed by codisposal of AMD and FAL.

Chapter 2

The genesis, remediation and environmental impacts of fly ash and acid mine drainage and the mineralogy of precipitates formed by sulphide oxidation: a literature review

2.1 Introduction

Increasingly, wastes produced by industry and mining concerns are a growing environmental issue. Many wastes are not rendered harmless with proper treatment but are simply dumped in large landfills that are unsightly time-bombs. This chapter deals with FA and AMD, describing their formation, composition and the methods used to dispose of them. A brief discussion of the common sulphide and oxide minerals that precipitate from acid mine drainage is included as the last section.

2.2 Fly ash

2.2.1 Introduction

Pulverised fuel ash results from the burning of coal in power plants. Fly ash is a fine grained material consisting largely of silicate glass beads with minor amounts of lime and mullite (Mattigod *et al.*, 1990). High concentrations of metals are present as phases that have condensed on the surface of the silica particles. Weathered fly ash cements into a hard impermeable layer as a result of the lime, and can give rise to very high pH values.

2.2.2 Products of coal combustion

The combustion of coal produces several types of waste. The different types of waste vary in particle size and mineralogy and are as follows.

2.2.2.1 Fly and bottom ashes

The physical, chemical and mineralogical properties of fly and bottom ashes depend on the composition of the parent coal, the conditions within the combustion chamber and the type of emission control devices used and their efficiency (Adriano *et al.*, 1980).

Bottom ash is a residue with a high specific gravity that remains behind in the combustion chamber. Bottom ash consists of both coarse and fine material and is a mixture between ash and slag.

Fly ash is that fraction of combustion waste that enters the flue gas stream. The ash is then collected by emission control devices or allowed to escape into the atmosphere (Adriano *et al.*, 1980).

2.2.2.2 Flue gas desulphurisation wastes

Fabric bag filters and electrostatic precipitators are required to reduce air pollution. Emission control devices remove particulates and sulphur oxides and produce flue gas desulphurisation sludges and fluidised bed boiler waste (Adriano *et al.*, 1980). A limestone slurry is added to the stack to remove sulphur oxides. This results in a mixture of calcium-sulphur salts and CaCO_3 . Particles range from 5 to 50 μm in size and contain a high concentration of soluble salts (Carlson and Adriano, 1993).

2.2.3 Mineralogy, physical characteristics and elemental composition of fly ash

The physical characteristics of combustion wastes affect the reactivity of these wastes. Factors such as the particle size and morphology, bulk density, specific gravity, permeability and etc. are all important factors when considering the geochemistry of weathering reactions and element mobilization. This review will deal chiefly with fly and bottom ash since they are very similar, with occasional mention of other types of coal combustion wastes.

Many of the physical characteristics of fly and bottom ash overlap. Table 2.1 shows a number of their characteristics. Bottom ash is coarser and as expected has a larger particle size (gravel – sand). The ranges for specific gravity and specific surface area of

bottom ash are very narrow. Fly ash has high average specific surface area and very small particle size (Mattigod *et al.*, 1990).

Table 2.1: Physical properties of fly and bottom ashes (Summers *et al.*, 1983).

Physical property	Fly ash	Bottom ash
Specific gravity	1.59 – 3.1	2.17 – 2.78
Dry bulk density (mg/m ³)	1.01 – 1.43	0.74 – 1.58
Specific surface area (m ² /kg)	200 – 3060	400
Mean particle diameter (μm)	20 – 80	500 - 7000

Fly ash is a complex heterogeneous substance composed of amorphous and crystalline phases. Particles are small, glass-like spherules ranging from 0.01 to 100 μm in size. These spherical particles are a result of the melting of silicate minerals in the combustion chamber (Carlson and Adriano, 1993). Two classes of particles are defined: cenospheres, which are hollow and plerospheres, which are filled with smaller amorphous particles and crystals. Between 70 and 90 % of fly ash consists of glassy spheres (Fisher and Natusch, 1979).

The predominant elements in FA are Al, Si, Fe, Ca, K, and Na in higher concentrations relative to those found in the parent coal. Aluminium, Ca and Fe occur in concentrations typical of soils. Sodium is present in concentrations generally exceeding those found in soil. Fossil fuel wastes are also enriched with S when compared with soil (Mattigod *et al.*, 1990).

The pH of fly ash tends to vary between 4.5 and 12 depending on the sulphur content of the parent coal. South African ashes tend be alkaline. Fresh ash contains a high concentration of soluble salts. These high concentrations can be reduced if the ash is leached or weathered. Another characteristic of ashes is that they are frequently pozzolanic. Reaction with water in the presence of lime creates a cement that leads to pore clogging, reduced infiltration and impedes root penetration in ash deposits (Carlson and Adriano, 1993; Chermak and Runnels, 1997). Campbell (1999) found that South African ashes have a tendency to display pozzolanic activity.

The most common minerals in fly ash are quartz (SiO₂) and mullite (3Al₂O₃ • 2SiO₂). The Fe-containing compounds include hematite (Fe₂O₃) and magnetite (Fe₃O₄); the Ca-compounds include anhydrite (CaSO₄) and lime (CaO). Periclase (MgO) represents the

Mg fraction and some unburned carbon makes up approximately 1 to 2% of the ash. Table 2.2 shows the transformation of minerals during coal combustion (Mattigod *et al.*, 1990). The lime occurs as particles on the surface of the glass spherules and is thought to originate from the decarbonation of limestone and/or dolomite impurities in the coal (Warren and Dudas, 1984).

Table 2.2: Thermal transformation of mineral phases (Mattigod *et al.*, 1990).

Minerals in coal	Products following combustion
Phyllosilicates	Glass, quartz (SiO_2) and mullite ($\text{Al}_6\text{Si}_2\text{O}_{13}$)
Quartz	Glass, quartz (SiO_2)
Pyrite (FeS_2), siderite (FeCO_3), iron sulphates	Hematite (Fe_2O_3) and magnetite (Fe_3O_4)
Calcite (CaCO_3)	Lime (CaO)
Dolomite ($\text{CaMg}(\text{CO}_3)_2$)	Lime (CaO), periclase (MgO)
Gypsum ($\text{CaSO}_4 \cdot 2\text{H}_2\text{O}$)	Anhydrite (CaSO_4)
Ankerite ($\text{CaMg}_{x}\text{Fe}_{(1-x)}(\text{CO}_3)_2$)	Calcium ferrite (CaFe_2O_4), periclase (MgO)

Minor elements (As, B, Pb, Ni, Se, Sr, V, and Zn) are found in higher concentrations in fly ash relative to coal and soil. The mineralogy of fly ash is a factor of the parent coal type. Anthracite, bituminous and lignite coals have mineral assemblages in different proportions. The temperature of the combustion chamber affects the degree of volatilisation of some minerals. A correlation between the concentration of trace metals and particle size has been observed. The concentration of As, Cd, Cu, Ga, Mo, Pb, S, Sb, Se, Tl and Zn increases with decreasing fly ash particle size. This concentration gradient is thought to be a result of the volatilisation of elements on combustion followed by their subsequent condensation on the fly ash spherules. The most volatile elements condense last, on the smallest particles. This partitioning is not shown in less volatile elements. The more enriched elements are on the particle surface, the more accessible they are to solution and the faster they are leached (Adriano *et al.*, 1980; Eary *et al.*, 1990; Smith, 1980).

2.2.4 The disposal of fly ash

Fly ash is transported from the power plant as slurry to a series of holding ponds where the solids are allowed to settle out of suspension and the water is recycled. The fly ash is then stockpiled and used as landfill. A small amount of fly ash is used for commercial purposes such as the cement industry. Ash wastes present an environmental

problem because of the concentration of trace elements and the increased mobility of these elements. When suspended in water fresh ash has a high pH of about 12. Stockpiled ash undergoes weathering and leaching processes that stabilise the pH and precipitate soluble minerals (Adriano *et al.*, 1980).

Alternative uses for fly ash have been investigated to facilitate its disposal and minimise negative environmental impacts. Fly ash has been somewhat successful in reclaiming areas that have been reduced to wastelands after the strip mining of coal. The spoils are acidic and infertile as a result of the oxidation of the pyritic overburden, only sparse vegetation can be cultivated and as a result extensive erosion occurs. Fresh fly ash applied to these areas greatly improved the fertility and crops were cultivated (Adriano *et al.*, 1980). Taylor and Schuman (1988) compared the effectiveness of various levels of fly ash and lime amendments in alleviating the low pH of mine spoils. Both treatments successfully raised the pH. Plant elemental concentrations were elevated but not to toxic levels. The study showed that fly ash could be used as a substitute for lime.

The disposal of fly ash in underground mine workings is a highly sought after solution to the environmental problem of fly ash. Backfilling fly ash to support the roof in order that ore pillars left unmined for that purpose may be recovered is of great value. Campbell (1999) conducted studies on the hardening of four South African fly ashes, both fresh and weathered, to assess their strength for the purpose of backfilling. The study found a strong linear relationship between total Ca content and the modulus of rupture. Other factors influencing the strength of hardened ashes include secondary minerals and particles size (Campbell, 1999).

Another method of ameliorating the effects of disposed ash is to revegetate ash-holding ponds and stockpiles. Establishing a vegetative cover prevents the wind erosion of ash sediments. A small amount of soil and organic matter greatly facilitates favourable conditions, both physical and chemical, for plant growth (Adriano *et al.*, 1980). The following section discusses the effects that fly ash have on the soil and living organisms.

2.2.5 Environmental impacts of fly ash

2.2.5.1 Plant response

Many trace elements in fly ash may benefit plant growth and improve soil properties. Plant growth on fly ash has been shown to increase the concentrations of essential nutrients S, Mo and B. The data on many other elemental concentrations in plant tissue are inconsistent. A greenhouse study, in the Western U.S. produced high yields of several agronomic crops when unweathered fly ash was added to either calcareous or acidic soils. These yield increases were attributed to increased availability of S (Page *et al.*, 1979). Increases in alfalfa yields were attributed to an alleviation of B deficiency.

Fly ash applied to acidic soils has increased yields by increasing the nutrient availability of Ca and Mg and preventing the toxic effects of Al and Mn by neutralizing soil acidity. The concentration of N, P and organic carbon is usually very low in fly ash and these nutrients need to be applied to sustain good growth. If the pH of fly ash-amended soils can be properly controlled, micronutrient deficiency may be minimized. Boron in fly ash is readily available to plants and can in many cases result in toxicity. It might take at least two to three years to reduce the phytotoxic effects of B in a fly ash treated soil to an acceptable level. When fly ash is completely weathered, it does not lead to any detectable B toxicity symptoms (Adriano *et al.*, 1980).

Tomlinson (1994) conducted studies to assess the liming potential of ettringitic waste produced from alkaline ash water and found ample evidence to support its use as an agricultural lime. Webster (1996) conducted tests with fly ash in combination with other waste products acting as ameliorants to produce a chemically inert plant growth medium. These ameliorants included sewage sludge and S, and phosphoric acid rich wastes. Pot trials with ryegrass indicated that only the sewage sludge in combination with fertiliser had a positive effect on the growth of plants (Webster, 1996).

2.2.5.2 Soil Response

Fly ash input reduces the bulk density of the soil mixture. It can significantly increase the soil mixture's water-holding capacity but does not produce a significant increase in

plant-available water. Soil hydraulic conductivities are improved at low rates of fly ash application but deteriorate rapidly when fly ash exceeds 20% by volume in calcareous soils and 10% in acidic soils. The impedance of water is caused by the pozzolanic reaction of fly ash, which tends to cement the soil particles when wetted (Campbell, 1999). This reaction is apparently more effective in acidic soils. Fly ash also reduces the cohesiveness of soil particles. Other changes to soil properties include an increase in pH, salinity and levels of certain toxic elements. Studies show that an alkaline fly ash is chemically equivalent to 20% of reagent grade CaCO_3 in reducing soil acidity and supplying plant Ca needs. This however depends on the source of fly ash and the extent to which it is weathered (Adriano *et al.*, 1980).

Hydration and carbonation play important roles in transforming the primary minerals in the fly ash into less reactive secondary mineralogical products. The reaction kinetics leading towards a chemical stabilization is probably controlled by the rate of CO_2 diffusion into the fly ash matrix. Thus pH and EC may become stabilised with time. Weathering of fly ash before application significantly reduces the salinity impact on soils, this may take several years (Adriano *et al.*, 1980).

2.2.6 Chemistry of leachates and extracts

The type and concentration of the extractant, the solid-to-solution ratio, the duration and temperature and intensity of agitation all influence the concentration of constituents and their ease of extractability from soils. However, column leaching experiments in the laboratory do not always reliably reproduce field conditions. Thus the chemistry of equilibrium extracts is studied as an indicator of the solubility-controlling solid phases in weathering wastes. Extractability is the main tool for investigating elemental mobility in fly ash. Acid extractions mobilise the largest percentage of waste constituents, whereas water extractions mobilise <10% of all major elements except Ca, Na and S. These elements can have concentrations ranging from tens to thousands of mg.l^{-1} . Potassium and Mg have elemental concentrations in fly ash reaching several hundred mg.l^{-1} . Silicon and Al concentrations do not exceed 100 mg.l^{-1} and Fe concentrations do not exceed 3 mg.l^{-1} (Ainsworth and Rai, 1987). Hydrolysis of CaO and the subsequent dissolution of Ca(OH)_2 (portlandite) are what contribute to the high degree of alkalinity in initial fly ash leachates (Warren and Dudas, 1984)

The pH of fly ash water extracts has been related to both the ratio of oxalate-extractable Fe to soluble Ca and Ca/S ratios. Alkaline fly ashes tend to have Fe/Ca ratios < 3 and Ca/S ratios > 2.5. Campbell (1999) found that the pH and Ca concentrations rose rapidly over a short period of time in the aqueous extracts of a saturated paste extract. The final solution composition of a saturated paste extract of fly ash that had been allowed to equilibrate for 24 hours was slightly supersaturated with respect to gypsum (Campbell, 1999). The variations in elemental extractability are a result of the interactions between pH, the total amount of solids, surface concentration, solid-phase forms and the type and concentrations of complexing ligands (Mattigod *et al.*, 1990).

2.3 Acid mine drainage

2.3.1 Introduction

When sulphide minerals are exposed to oxygen and water it can result in acidic waters. Any earth moving operations, such as highway construction, foundation excavation, tunnelling or mining, that expose rock strata containing sulphide minerals to accelerated weathering and oxidising conditions have the potential to create acid drainage. Acid drainage can also occur in soils containing sulphates in lagoon and estuary environments where the proximity of the sea tends to cause increased salt content and acidic conditions. Mining operations are the biggest cause of AMD production. Water infiltrates through waste rock, tailings, ore stockpiles, open pits and underground tunnels produced by mining activities and drains into rivers and wetlands. This acid mine drainage (AMD) is characterised by pH values in the range of 2 – 4 with high concentrations of metals at levels that are toxic to most organisms.

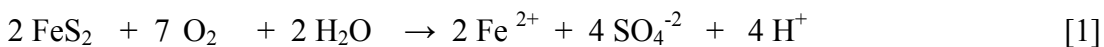
In South Africa coal mining is the chief cause of acid waters though the gold industry does also contribute to AMD production. South African coal products are mainly consumed by electricity generation and constitute a large portion of the energy reserves. As a result massive amounts of groundwater are subjected to pollution caused by the exposure of pyritic rock (Maree *et al.*, 1996). The sources of AMD, its formation, treatment and environmental effects will be discussed in further detail.

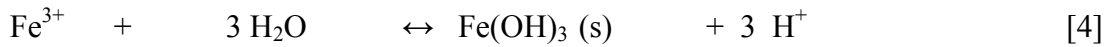
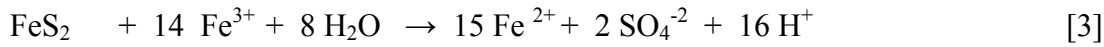
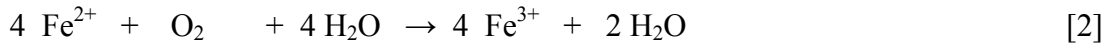
2.3.2 Sources of acid mine drainage

- Underground workings and exposed mining faces can result in a high concentration of salts, metals and acidity being released as a result of fluctuating water tables that cause the accumulation of salts during low water table and the mobilization of those salts during high water table.
- Open pits expose very large areas to the atmosphere and moisture. A fluctuating water table ensures that oxidised sulphate material is dissolved and the pyrite surface is continuously renewed and exposed to undergo further oxidation.
- Seepage and runoff from waste rock poses a large problem since these piles are generally made up of very coarse material, which results in a high permeability for water and oxygen. These dumps have the tendency to build-up oxidation products through evaporation and supersaturation processes that are released in large quantities during the following wet period.
- Process tailings stored as dumps are of finer particle size, which can restrict oxygen and moisture movement but may mean that they have a higher sulphide content. The larger surface area and greater reactivity as a result of smaller particle size, is offset by a lower permeability. Tailings tend to produce AMD at a much slower rate than waste rock (Miller and Murray, 1988; Mitchell, 2000).

2.3.3 Generation of acid mine drainage and metal mobility

The mechanism of pyrite oxidation is well understood and documented. The fact that pyrite oxidation generates acidity was recognised as far back as 315 B.C. by Theophrastus and documented by G. Agricola in *De Re Metallica* (1556). The chemistry of pyrite oxidation is summarised as follows:





This set of equations represents a cycle that is initiated by the production of ferrous iron when pyrite, or the dimorph marcasite (FeS_2), either dissociates or oxidises as shown in equation [1]. The ferrous iron produced is then oxidised to ferric iron (equation [2]), which in turn further oxidises pyrite generating more ferrous iron and acidity (equation [3]). Ferric iron can also precipitate as a hydroxide, in the process releasing acidity (equation [4]).

It can be seen from equation [1] that for every 2 moles of pyrite oxidised, 2 moles of ferrous iron and 4 moles of acidity are produced. The greatest production of acidity occurs via pyrite oxidation by ferric iron as can be seen in equation [3] where for every 1 mole of pyrite oxidised 16 moles of acidity are produced.

According to Hälbich (1997), who conducted studies on the mobility of metals in AMD, Fe mobility is controlled by pyrite oxidation and the solubility of the basic iron mineral jarosite. Aluminium solubility is controlled by the dissolution of clay minerals and adsorption to organic matter in sediments. This is evidenced by the high correlations between Al and dissolved silica and Al concentration and the acidity of AMD. The same study found that trace element concentrations are not greatly affected by precipitation at low pH values. The mobility of these elements is affected by the dissolution of minerals that contain them, and adsorption onto sediment surfaces and organic matter (Hälbich, 1997).

Azzie (1999) investigated the geochemistry and quality of five circumneutral mine waters from the South African highveld. These waters exhibited a range of electrical conductivities from 500 mSm^{-1} to below 100 mSm^{-1} and are characterised by the presence of toxic ions and high salinity and sodicity. The dominant ions in some of these waters were Na^+ , SO_4^{2-} and HCO_3^- , with one sample containing extremely high Cl. It was found that these waters were mostly supersaturated with respect to carbonate

minerals resulting in a naturally, circumneutral pH. This study concluded that some mine water could be recycled for use without extensive desalination treatment (Azzie, 1999).

2.3.3.1 Rate of AMD production

The initial abiotic oxidation of pyrite in the absence of Fe^{3+} is slow and may take weeks to occur (Singer and Stumm, 1970). The rate of oxidation of ferrous iron is a function of pH. At $\text{pH} > 4.5$ the rate is as follows:

$$\frac{-\text{d}[\text{Fe}^{2+}]}{\text{d}t} = k[\text{Fe}^{2+}][\text{O}_2][\text{OH}]^2 \quad [5]$$

where $k = 8.0 \times 10^{13}$ litre² mole⁻² atm⁻¹ min⁻¹ at 25 °C. When the pH is below 3.5 the rate of the reaction is independent of pH and proceeds via:

$$\frac{-\text{d}[\text{Fe}^{2+}]}{\text{d}t} = k'[\text{Fe}^{2+}][\text{O}_2] \quad [6]$$

where $k' = 1.0 \times 10^{-7}$ atm⁻¹ min⁻¹ at 25 °C. Singer and Stumm (1970) found this reaction to be the rate-limiting step in the pyrite oxidation cycle. But once started the reactions are self-propagating and are considered autocatalytic.

The above set of reactions ([1] – [4]) is an oversimplified account of the oxidation of pyrite. The sulphur fraction of pyrite involves the transfer of 14 electrons per mole of FeS_2 while the iron fraction involves the transfer of only one electron per mole of pyrite. Since reactions transfer only one or two electrons at a time, there are several possible sulphur intermediates that may occur. These include elemental sulphur and sulphonyanions such as thiosulphate ($\text{S}_2\text{O}_3^{2-}$), polythionates ($\text{S}_n\text{O}_6^{2-}$) and sulphite (SO_3^{2-}) but there is doubt as to whether these compounds exist in nature as they are produced in the laboratory under high stirring rates. In addition to this sulphonyanions are a source of energy for chemoautotrophic bacteria and if they do occur they may be rapidly biodegraded (Nordstrom and Alpers, 1999).

2.3.3.2 Role of bacteria

The rate of pyrite oxidisation has thus far only been discussed as occurring under abiotic conditions. Clearly acid mine drainage does not form under the sterile conditions of a laboratory. It has been known for some time that microorganisms play a large role in the formation of acid mine drainage (Chapelle *et al.*, 1993). Iron oxidising bacteria are able to catalyse the pyrite oxidation reactions so that the rate of acidity production increases by a factor of more than 10^6 (Singer and Stumm, 1970).

Waksman and Jäffe first identified the acidophilic bacteria *Thiobacillus thiooxidans* in 1921 and twenty-five years later Colmer and Hinkle (1947) isolated *Thiobacillus ferrooxidans*. Now many other iron and sulphur oxidising bacteria have been identified (Table 2.3).

Table 2.3: Bacterial genera *Thiobacillus*, *Leptospirillum* and *Sulfobacillus* and the inorganic substances that they consume. Acidophilic species are in bold (Nordstrom and Southam, 1997).

Bacteria species	Inorganic Substances
<i>Thiobacillus albertis</i>	H_2S , $\text{S}_2\text{O}_3^{2-}$
<i>Thiobacillus acidophilus</i>	* S° , $\text{S}_2\text{O}_3^{2-}$, $\text{S}_3\text{O}_6^{2-}$, $\text{S}_4\text{O}_6^{2-}$
<i>Thiobacillus denitrificans</i>	H_2S , S° , $\text{S}_2\text{O}_3^{2-}$, $\text{S}_4\text{O}_6^{2-}$
<i>Thiobacillus delicatus</i>	S° , $\text{S}_2\text{O}_3^{2-}$, $\text{S}_4\text{O}_6^{2-}$
<i>Thiobacillus ferrooxidans</i>	H_2S , sulphide minerals, S° , $\text{S}_2\text{O}_3^{2-}$, $\text{S}_4\text{O}_6^{2-}$, Fe^{2+}
<i>Thiobacillus halophilus</i>	S°
<i>Thiobacillus intermedius</i>	S° , $\text{S}_2\text{O}_3^{2-}$, $\text{S}_4\text{O}_6^{2-}$
<i>Thiobacillus neapolitanus</i>	H_2S , sulphide minerals, S° , $\text{S}_2\text{O}_3^{2-}$, $\text{S}_3\text{O}_6^{2-}$, $\text{S}_4\text{O}_6^{2-}$
<i>Thiobacillus novellas</i>	$\text{S}_2\text{O}_3^{2-}$, $\text{S}_4\text{O}_6^{2-}$
<i>Thiobacillus perometabolis</i>	S° , $\text{S}_2\text{O}_3^{2-}$, $\text{S}_4\text{O}_6^{2-}$
<i>Thiobacillus tepidarius</i>	H_2S , S° , $\text{S}_2\text{O}_3^{2-}$, $\text{S}_3\text{O}_6^{2-}$, $\text{S}_4\text{O}_6^{2-}$
<i>Thiobacillus thiooxidans</i>	S° , $\text{S}_2\text{O}_3^{2-}$, $\text{S}_4\text{O}_6^{2-}$
<i>Thiobacillus thioparus</i>	H_2S , sulphide minerals, S° , $\text{S}_2\text{O}_3^{2-}$, $\text{S}_3\text{O}_6^{2-}$, $\text{S}_4\text{O}_6^{2-}$
<i>Thiobacillus versutus</i>	H_2S , $\text{S}_2\text{O}_3^{2-}$
<i>Leptospirillum ferrooxidans</i>	Fe^{2+} , sulphide minerals
<i>Leptospirillum thermoferrooxidans</i>	Fe^{2+} , sulphide minerals
<i>Sulfobacillus thermosulfidooxidans</i>	Fe^{2+} , sulphide minerals, S°

* S° = elemental sulphur

It is still unclear as to whether bacteria catalyse pyrite oxidation through direct or indirect methods. Indirect oxidation takes place through microbial catalysis of ferrous iron in solution to ferric iron. There is evidence for direct bacterial involvement that is reflected by etch patterns on sulphide mineral grains. Bacteria attach themselves to the sulphide mineral and directly solubilise the surface through enzymatic oxidation (Nordstrom and Southam, 1997).

2.3.4 Factors affecting the production and transport of acid mine drainage

The mere fact that sulphide minerals are present in an exposed rock deposit does not mean that acid drainage will necessarily occur. There are many factors that can have an influence on acid production, possibly even mitigating ones.

What determines whether acid drainage will occur is: the quantity of carbonate minerals present in the host rock; the availability of oxygen and the degree of crystallinity, surface area and purity of the sulphide minerals present. The degree of pyrite crystallinity contributes a great deal to how reactive it is. Large euhedral pyrite cubes can be seen in display cases where they have resided for centuries without becoming tarnished. Microcrystalline, frambooidal or cryptocrystalline pyrite oxidises spontaneously on exposure to the atmosphere, with the frambooidal form being the most reactive crystal structure (Caruccio *et al.*, 1981). The surface area and grain size have a large influence on the quantity of acid drainage that is produced. The smaller the grain size, the more reactive the sulphide mineral is and the greater the surface area, which is exposed, the greater the amount of sulphide oxidation that will occur. The total surface area is however not the same as the reactive surface area since not all exposed surfaces will be in the path of water movement or available to adsorb and chemically bond with aqueous species (Nordstrom and Alpers, 1999).

Impurities in pyrite and the presence of other sulphide minerals have a large impact on sulphide oxidation because in general they are usually more reactive and can stimulate the reaction rates of other sulphides. When oxygen is restricted in the system, it prevents or slows equation [1] down. This can halt the cycle of acid production. Cementing tunnels and adits and flooding open shafts restricts the flow of oxygen.

These methods do not always prove to be helpful in restricting acid drainage (Miller and Murray, 1988). Ultimate oxidation rates in the mining environment are complicated by air and water transport processes, which are in turn affected by permeability of the host rock and existing water courses (Chermak and Runnells, 1997). Bacteria ecology and growth kinetics also affect the rate of acid production and are in turn dependant upon organic compounds and nutrients. Acid mine drainage production is further affected by climate, temperature gradients and secondary mineral precipitation (Nordstrom and Alpers, 1999).

Neutralisation resulting from reactions with carbonate minerals contained within the deposit has the greatest influence on whether water draining from a mine site will be acidic or not. The natural alkalinity within the overburden of a mine site is extremely important for predicting the acidic potential of a mine. In general materials that are sulphide-rich and carbonate-poor will produce acidic drainage. Acidity is a measure of the amount of base needed to neutralise a volume of water (Skousen *et al.*, 1996). A high degree of alkalinity in the rock, usually in the form of CaCO_3 or MgCO_3 , can raise the pH of the water and imbue it with a buffering capacity. A circumneutral pH reduces the activity of acidophilic bacteria and retards the oxidation of ferrous iron. Depending, however, on the concentration of sulphide minerals in a deposit the inherent buffering capacity may become exhausted (Doolittle *et al.*, 1993). In order to determine the acid forming potential of materials an acid-base account is performed. This involves a determination of the total sulphur content, the acid neutralising capacity and the saturated pH and EC (Miller and Murray, 1988). Caruccio *et al.* (1981) found that those mine drainages with a higher neutralizing potential (expressed as mass of CaCO_3) contained less sulphur and were not expected to produce acid leachates.

2.3.5 Environmental impacts of acid mine drainage

Acid mine drainage can have a large impact on the health of an ecosystem. Acidic waters draining into an aquatic environment can cause a reduction in species diversity and a simplification in the food chain. Both of these factors contribute to the stability of a community structure and reduce the ability of the system to withstand and recover from disturbance. This form of pollution extends its influence into the chemical, physical, biological and ecological niches. Acid mine drainage lowers the pH and

introduces toxic quantities of heavy metals into the system. The increase in acidity consumes the natural buffering capacity of the river.

As AMD comes into contact with natural waters, which are neutral and oxygenated, any ferrous iron in solution oxidises to ferric iron. The ferric iron precipitates as hydroxides or oxyhydroxides, also known simply as ochre deposits for their colour, along with many other contaminants within the AMD. This results in increased turbidity and a reduction in light penetration. River sediments provide surfaces for precipitation and the adsorption of metals. The iron precipitates coat the riverbed, which increases laminar flow and stream velocity, and decreases turbulence. The decrease in turbulence results in a loss of dissolved oxygen as iron precipitation consumes the remainder of O₂ in the water (Gray, 1997).

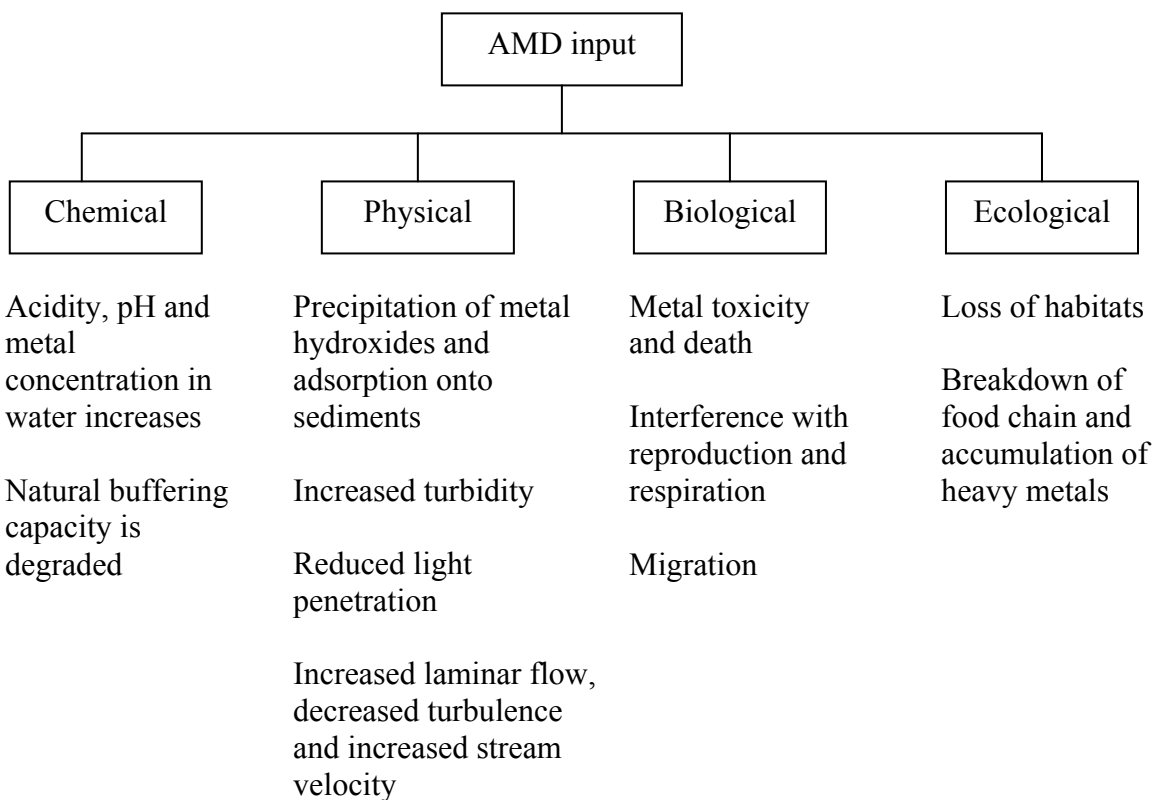


Figure 2.1: The environmental impacts of AMD on an ecosystem (adapted from Gray, 1997).

The effect these changes have on the flora and fauna is extremely detrimental. The dissolved metal concentrations cause acute and chronic toxicity in, and the death of, sensitive species. The pollution also interferes with the reproduction and respiration of

aquatic organisms, which quickly disappear from the site of disturbance. Larger fauna avoid the source of water and migrate to less polluted areas (Younger, 1995).

The overall ecological effect is a reduction of habitat, an accumulation of toxic elements in the food chain and a food chain breakdown. These effects are summarised in figure 2.1

2.3.6 Treatment of AMD

2.3.6.1 Active treatment

Conventional treatment of acid mine drainage involves the addition of neutralising reagents like NaOH (caustic soda), lime (CaO or $\text{Ca}(\text{OH})_2$), soda ash (Na_2CO_3) or limestone (CaCO_3 or MgCO_3). Skousen *et al.* (1996) provides a detailed discussion of the benefits and disadvantages of the neutralising chemicals commonly in use. The amelioration of AMD proceeds through four basic steps (Figure 2.2). Firstly the water is aerated so that ferrous iron oxidises to ferric iron. The neutralising chemicals are then added, usually concurrently with aeration, to raise the pH and to precipitate metal hydroxides. Hydrated lime is most commonly used towards this end as it is more cost effective than NaOH, and achieves a higher degree of acid neutralization than limestone.

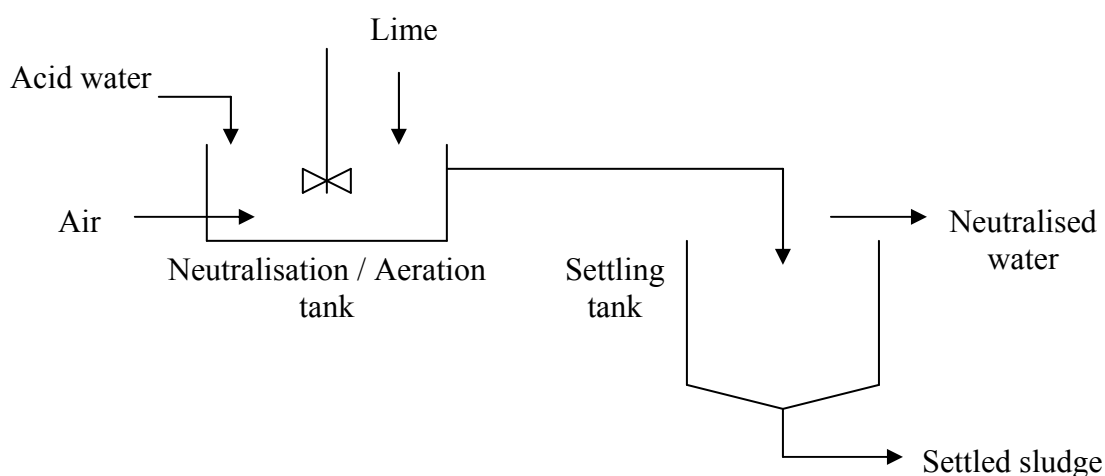
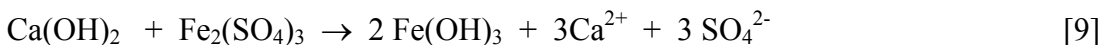


Figure 2.2: Schematic diagram for the active treatment of acid mine drainage (Maree *et al.*, 1996)

Thompson (1980) found that amelioration was best achieved with calcium hydroxide, which raised the pH and reduced total dissolved solids. The slurry then travels to a settling tank in the third step where the water is removed from the precipitated solids. Chemical coagulants and flocculants are added to remove suspended material and finally the sludge is piped to a waste disposal site (Gazea *et al.*, 1996; Mitchell, 2000).

As lime is added to the system in the second step, which may occur simultaneously with aeration, it consumes acidity in the process and produces H₂O and insoluble calcium sulphate (see equations [7], [8] and [9]) (Thompson, 1979).



Iron and other metals precipitate as hydroxides or basic sulphates. The factors that affect the chemical nature of the sludge are the rate of neutralisation, the mixing rate and the degree of aeration (Mitchell, 2000). Current models of Fe oxidation during neutralisation are based on an Fe-dependant model. This model declares that the easiest way to accelerate treatment of AMD is to increase the pH but Hustwit *et al.* (1992) found that sufficient O₂ is the rate limiting step for Fe²⁺ oxidation.

The benefit of active treatment is that treatment plants occupy a small area and it is an effective and a proven technology. Large volumes of water can be processed and the quality of the water is unaffected by variations in temperature and metal contaminants. Jenke *et al.* (1983) investigated the chemical changes, which occur in acidic, metal bearing waters when treated with lime. They indicated that the major processes controlling the chemical change in the waters was precipitation of hydroxides with co-precipitation and adsorption playing a large role.

2.3.6.2 Passive treatment

Passive treatment is considered to be a lower cost and lower maintenance option for ameliorating acid mine drainage than the addition of neutralising chemicals. A passive treatment system follows a five step process. These steps are usually accommodated via discrete cells within a constructed wetland designed to duplicate a natural system.

Since the restriction of oxygen to the pyrite propagation cycle is an important step in reducing the production of acidity, the first step in a passive treatment system is an anoxic pond to reduce the amount of dissolved oxygen in the system. This process utilises an organic-rich layer to consume oxygen. The water drains downward through this layer. Another advantage of reducing the dissolved oxygen content in the acid mine drainage is the decrease in metal deposition (Mitchell, 2000).

The second step in water treatment is to pass the drainage through an anoxic limestone drain (ALD). The ALD is constructed containing a layer of limestone that contributes to the buffering capacity of the water and adds alkalinity (Hedin *et al.*, 1994). The water is deoxygenated in the preceding step to maintain the effectiveness of the limestone layer. When the pH of the water is raised by the input of alkalinity, metals precipitate on the surfaces of the limestone and impair its neutralising capability. This process is called armouring. Armouring also affects the reactivity of chemicals during active treatment (Ziemkiewicz *et al.*, 1997). If the particle size of the reagent added is too great, it is coated by metal precipitation and prevented from further reaction, and thus most of the neutralising capacity is lost (Evangelou and Sinju, 1991).

Aerobic cells follow the anoxic limestone drains in the third step, to aerate the water and precipitate metals. Metal tolerant plant species are cultivated in order to aerate the substrate and produce alkalinity by moving carbon dioxide into the system. Many plant species have been investigated as to their metal tolerance and suitability for cultivation in a wetland. Cattail (*Typha latifolia*) and woolgrass (*Scirpus cyperinus*) have proven to have a tolerance and metal accumulation capability (Demchik and Garbutt, 1999; Gazea *et al.*, 1996). As iron precipitates, however, acidity in the form of sulphuric acid is produced.

The water then moves onto an anaerobic system in the fourth step where sulphate reducing bacteria (e.g. *Desulfovibrio desulfuricans*) remove sulphur from the water by producing hydrogen sulphide (H_2S) (Robb and Robinson, 1995). These bacteria are provided with some form of organic substrate as fuel that can consist of woodchips, manure, sewage sludge or any other form of organic waste (Kleinman *et al.*, 1991). Metals such as cadmium, zinc, copper and some iron then react with the H_2S to form insoluble precipitates.

The final step involves the provision process consists of a large rock surface area on which algae and manganese-oxidising bacteria can grow. The algae require manganese as a macronutrient and can accumulate very high concentrations (Kepler, 1986). The process of manganese removal can only occur as a final step, when pH is greater than 6 and iron concentration is low (Gazea *et al.*, 1996).

Passive treatment systems require large areas of land and long retention times to improve the quality of acid mine drainage. As a mitigation process they are not well equipped to deal with large amounts of acid mine drainage.

2.4 Mineralogy of precipitates formed through sulphide oxidation

2.4.1 Introduction

Mine waters draining pyritic sediments are typically very acidic with a high metal load resulting from primary mineral dissolution. The rate of mineral weathering is high enough that the solution reaches states of saturation and supersaturation with respect to secondary minerals. Processes such as oxidation, dilution, mixing, evaporation and neutralisation are frequently accompanied by the precipitation of metal-bearing hydroxide and hydroxysulphate minerals. These mineral precipitates, commonly referred to as “ochres”, are treated as hazardous waste as a result of the high concentrations of heavy metals. The section following is a brief description of some important secondary mineral commonly associated with acid mine waters.

2.4.2 Hydrated metal salts containing divalent cations

A brief discussion follows concerning some of the metal salts with the general formula $M^{2+}SO_4 \cdot nH_2O$. These minerals tend to dehydrate as the relative humidity decreases and as the temperature or acidity of the solution increases (Alpers, 1994). The melanterite and epsomite groups are classified as heptahydrates and are differentiated by their crystal structures. Substituting ions are accommodated in a solid solution with varying amounts of distortion. When the deformation of the crystal structure is too severe a new structure is created. The ions causing structural distortion are as follows from greatest to least distortion: $Cu^{2+} > Fe^{2+} > Co^{2+} > Mg^{2+} > Zn^{2+} > Ni^{2+}$ (Jambor *et al.*, 2000).

2.4.2.1 Melanterite group

Melanterite ($FeSO_4 \cdot 7H_2O$) is the one of the most common soluble sulphate minerals and occurs in the monoclinic crystal system. Natural melanterite can accommodate up to 8.92 wt% ZnO . Significant amounts of Mg , Cu as well as Ni can be accommodated in the structure of melanterite. Other minerals in this group include boothite ($CuSO_4 \cdot 7H_2O$), bieberite ($CoSO_4 \cdot 7H_2O$), mallardite ($MnSO_4 \cdot 7H_2O$), and zinc-melanterite ($(Zn,Cu)SO_4 \cdot 7H_2O$) (Jambor *et al.*, 2000). Melanterite can dehydrate to form any of the other sulphate minerals in this group and can oxidise to the mixed di- and trivalent Fe minerals. Upon loss of sulphate melanterite may transform to Fe oxyhydroxides (Bigham and Nordstrom, 2000).

2.4.2.2 Epsomite group

The crystal structure of this group falls into the orthorhombic system. The minerals in the epsomite-group contain one water molecule that is not bonded to the metal ion and which is readily dehydrated, much like the melanterite group. The minerals in this group are defined by the predominant cation and consist of epsomite ($MgSO_4 \cdot 7H_2O$), goslarite ($ZnSO_4 \cdot 7H_2O$) and morenosite ($NiSO_4 \cdot 7H_2O$). Fe can substitute for the Mg in epsomite up to a $Mg:Fe$ ratio of 5:1. Other elements such as Co , Cu and Mn have been shown to substitute for Mg , with a probable but unproven $Mg:Mn$ ratio of 5:2 (Jambor *et al.*, 2000).

2.4.2.3 Hexahydrite group

These sulphates are monoclinic in structure with the “hexa” referring to six structural waters. Hexahydrite, which is the Mg salt, occurs in a range of locations but the others of this group occur mainly as weathering products from sulphidic deposits. Little is known about this group of minerals but the structural similarity with the heptahydrates suggests similar levels of ion substitution. The other minerals in this group include chvaleticeite ($\text{MnSO}_4 \cdot 6\text{H}_2\text{O}$), ferrohexahydrite ($\text{Fe}^{\text{II}}\text{SO}_4 \cdot 6\text{H}_2\text{O}$), nickelhexahydrite ($\text{NiSO}_4 \cdot 6\text{H}_2\text{O}$), moorhouseite ($\text{CoSO}_4 \cdot 6\text{H}_2\text{O}$) and bianchite ($\text{ZnSO}_4 \cdot 6\text{H}_2\text{O}$) (Jambor *et al.*, 2000).

2.4.2.4 Rozenite group

The rozenite group is monoclinic in structure and consists of five minerals. The minerals in this group are not abundant and only the Mn member was known before 1960. The minerals include illesite ($\text{MnSO}_4 \cdot 4\text{H}_2\text{O}$), rozenite ($\text{FeSO}_4 \cdot 4\text{H}_2\text{O}$), starkeyite ($\text{MgSO}_4 \cdot 4\text{H}_2\text{O}$), aplowite ($\text{CoSO}_4 \cdot 4\text{H}_2\text{O}$), and boyleite ($\text{ZnSO}_4 \cdot 4\text{H}_2\text{O}$). Rozenite and starkeyite are the most common. The solid-solution data are sparse but there is an indication of extensive Mn and Ni substitution (Jambor *et al.*, 2000).

2.4.2.5 Kieserite group

The crystal system of this group is monoclinic and they are characterised as monohydrates. The cell volumes of these minerals increase in accordance with the size of the predominant cation. Large amounts of Zn have been shown to substitute into the iron member of this group, szomolnokite ($\text{FeSO}_4 \cdot \text{H}_2\text{O}$) (Jambor *et al.*, 2000).

2.4.3 Hydrated metal salts containing trivalent cations

The minerals in this category are defined by the general formula $A_2(\text{SO}_4)_3 \cdot n\text{H}_2\text{O}$ where A is either Fe^{3+} or Al^{3+} and the water content, n , ranges from 6 to 17. The Fe^{2+} sulphates may transform into more oxidised Fe^{3+} containing analogues. In this group Al may substitute for Fe but generally only to a small degree. Coquimbite ($\text{Fe}_2(\text{SO}_4)_3 \cdot 9\text{H}_2\text{O}$) has been found to have a high degree of Al substitution with an Fe:Al ratio of 58:42 mol %. The trivalent Fe minerals consist of lausenite ($\text{Fe}_2(\text{SO}_4)_3 \cdot 6\text{H}_2\text{O}$),

kornelite ($\text{Fe}_2(\text{SO}_4)_3 \cdot 7\text{H}_2\text{O}$), coquimbite ($\text{Fe}_2(\text{SO}_4)_3 \cdot 9\text{H}_2\text{O}$), ‘paracoquimbite’ ($\text{Fe}_2(\text{SO}_4)_3 \cdot 9\text{H}_2\text{O}$) and quenstedite ($\text{Fe}_2(\text{SO}_4)_3 \cdot 11\text{H}_2\text{O}$) (Jambor *et al.*, 2000).

The Al sulphates occur as alunogen ($\text{Al}_2(\text{SO}_4)_3 \cdot 17\text{H}_2\text{O}$) and meta-alunogen ($\text{Al}_4(\text{SO}_4)_6 \cdot 27\text{H}_2\text{O}$). Dehydration of alunogen can occur down to 13.5 formula waters without structural degradation. Meta-alunogen is poorly defined with variations in structural waters producing very different XRD patterns (Jambor *et al.*, 2000).

2.4.4 Mixed divalent-trivalent salts

The minerals described under the preceding headings could be considered the simple salts because SO_4^{2-} is the only anion and no OH is present. The salts containing cations of di- and trivalent states generally have the formula of $AR_2(\text{SO}_4) \cdot n\text{H}_2\text{O}$ where A is Mg^{2+} , Fe^{2+} , Mn^{2+} , Co^{2+} or Zn^{2+} , and R is Al^{3+} , Fe^{3+} or Cr^{3+} . The copiapite group, which is also included under this heading, however, contains an OH group giving them the general formula $AR_4(\text{SO}_4)_6(\text{OH})_2 \cdot 20\text{H}_2\text{O}$ (Jambor *et al.*, 2000).

2.4.4.1 Copiapite group

The general formula for the copiapite group is $A^{2+}R^{3+}_4(\text{SO}_4)_6(\text{OH})_2 \cdot 20\text{H}_2\text{O}$ where the trivalent position is dominated by Fe^{3+} . Trivalent ions (Al^{3+} and Fe^{3+}) may substitute into the A site and cause an excess of positive charge that is balanced by vacancies in the structure. The formulae for alumino- and ferricopiapite reflect the presence of vacancies in the structure and are written as $\text{Al}_{2/3}\text{Fe}_4^{3+}(\text{SO}_4)_6(\text{OH})_2 \cdot 20\text{H}_2\text{O}$ and $\text{Fe}_{2/3}^{3+}\text{Fe}_4^{3+}(\text{SO}_4)_6(\text{OH})_2 \cdot 20\text{H}_2\text{O}$ respectively (Jambor *et al.*, 2000).

2.4.5 Fe and Al hydroxysulphates

The most common efflorescent Fe sulphate minerals, melanterite, rozenite and szomolnokite can be converted to soluble hydroxysulphates such as copiapite, via partial oxidation of Fe. As the ferrous iron in solution or efflorescences oxidise, a suit of less soluble oxides, hydroxides and hydroxysulphate minerals precipitate.

2.4.5.1 Al hydroxysulphates

The major source of Al in acid waters comes from the dissolution of aluminosilicates in the country rock and from gangue material. Al hydroxysulphates are minerals with poor crystallinity and very small particle size. The minerals in this category are characterised by their Al:SO₄ mole ratios. These mole ratios reflect the composition of the aqueous solution from which the minerals precipitated and hence the pH. The Al hydroxysulphates are all white in colour except jurbanite, which is colourless (Bigham and Nordstrom, 2000).

Ettringite ($\text{Ca}_6\text{Al}_2(\text{SO}_4)_3(\text{OH})_2 \cdot 26\text{H}_2\text{O}$) is a high pH mineral whose formation in ash dams has been speculated to be the cause of a decrease in anion concentrations. If the pH is lowered ettringite will dissolve to form gypsum, calcite and gibbsite (Campbell, 1999). The early stages of pozzolanic activity in fly ash have been attributed to ettringite. The formation of ettringite in cement causes severe structural problems as it contains a large amount of structural water and has a large molecular volume. The expansion accompanying ettringite formation results in cracks and the cement becoming unstable (Hampson and Bailey, 1982).

Alunite ($\text{KAl}_3(\text{SO}_4)_2(\text{OH})_6$) occurs naturally in volcanic regions as a result of hydrothermal alteration but is not a primary component of acid mine drainage precipitates (Bigham and Nordstrom, 2000). The alunite group, which includes jarosite has the general formula $\text{AB}_3(\text{SO}_4)_2(\text{OH})_6$ where A may be K^+ , Na^+ , Pb^{2+} , NH_4^+ or Ag^+ and B is either Fe^{3+} or Al^{3+} (Brophy *et al.*, 1962). In the alunite-jarosite system there are multiple crystallographic sites for oxygen and hydrogen in the structure. Hydrogen occurs in both hydroxyl (OH^-) and hydronium (H_3O^+) crystal sites. The observed fractionation of oxygen and hydrogen suggest that that the alunite-jarosite system can be used as a geo-thermometer (Alpers *et al.*, 1992).

Basaluminitite ($\text{Al}_4(\text{SO}_4)(\text{OH})_{10} \cdot 4\text{H}_2\text{O}$) is the most common of the aluminous precipitates but is poorly crystalline. Basaluminitite and hydrobasaluminitite ($\text{Al}_4(\text{SO}_4)(\text{OH})_{10} \cdot 12\text{-}36\text{H}_2\text{O}$) have the highest Al:SO₄ mole ratios of 4:1. Basaluminitite is formed from hydrobasaluminitite, which has been dehydrated. Hydrobasaluminitite precipitates at a pH of 5 or higher from acidic mine waters that have been neutralised (Bigham and Nordstrom, 2000).

Aluminite ($\text{Al}_2(\text{SO}_4)(\text{OH})_4 \cdot 7\text{H}_2\text{O}$) and meta-aluminite ($\text{Al}_2(\text{SO}_4)(\text{OH})_4 \cdot 5\text{H}_2\text{O}$) have a Al:SO₄ mole ratio of 2:1. These minerals seem to form in a similar environment to basaluminite and hydrobasaluminate (Bigham and Nordstrom, 2000).

Jurbanite ($\text{Al}(\text{SO}_4)(\text{OH}) \cdot 5\text{H}_2\text{O}$) and rostite ($\text{Al}(\text{SO}_4)(\text{OH}) \cdot 5\text{H}_2\text{O}$) have a Al:SO₄ mole ratio of 1:1 and are well crystallised. Jurbanite is considered to be a rare and soluble efflorescent mineral (Bigham and Nordstrom, 2000). Anthony and McLean (1976) first identified jurbanite as occurring as clear colourless crystals with an assemblage of other phases (epsomite, hexahydrite, pickeringite, starkeyite and $\text{NH}_4\text{Fe}(\text{SO}_4)_2 \cdot 12\text{H}_2\text{O}$).

2.4.5.2 Fe hydroxysulphates

Schwertmannite ($\text{Fe}_8\text{O}_8(\text{SO}_4)(\text{OH})_6$) is considered to be the most common precipitate from acid mine waters. Due to its bright yellow colour schwertmannite has popularly been called “yellow boy” by miners. Schwertmannite is poorly crystalline and metastable, with 8 broad XRD peaks and occurs in the pH range of 2 to 4. The sulphate content of schwertmannite is variable so that natural samples may be best described by $\text{Fe}_8\text{O}_8(\text{SO}_4)_x(\text{OH})_{8-2x} \cdot n\text{H}_2\text{O}$ where $1 \leq x \leq 1.75$. Ferrihydrite may sorb enough sulphate to resemble schwertmannite and cause problems in differentiating the two minerals. The structure of schwertmannite is similar to that of akaganéite, $\beta\text{-FeO(OH,Cl)}$ which contains double chains of $\text{FeO}_3(\text{OH})_3$ octahedra travelling parallel to the c-axis and sharing corners to create a tunnel arrangement of connecting cavities. Akaganéite is stabilised by enclosing a Cl⁻, F⁻ or OH⁻ ion in every second cavity. It has been proposed that schwertmannite contains SO₄²⁻ in this same stabilising capacity but the large ions would cause extreme distortion of the structure (Bigham and Nordstrom, 2000). Extraction of the SO₄ destabilises the structure of schwertmannite, which then transforms to goethite (Bigham *et al.*, 1990). Schwertmannite occurs as fine needle-like crystals in rounded aggregates that resemble pin-cushions and result in a high specific surface area of 100 to 200 m²/g (Bigham, 1994).

Jarosites are formed when acid waters contain K, Na or NH₄ as well as excess sulphate and ferrous iron at a pH of 2.5. The concentration of jarosites tends to increase with decreasing pH. The morphology of jarosite crystals indicate the most common shape to

be pseudocubic (Bigham, 1994). Brophy and Sheridan (1965) found that the incorporation of the hydronium ion into the structure of jarosite indicates that it formed under low temperature and pressure whereas the incorporation of K^+ into the structure indicates formation at higher temperatures. Speciation analyses of low pH mine waters frequently give saturation indices that are supersaturated with respect to jarosite. This mineral is however, rarely detected. This suggests that some form of kinetic barrier is in place that prevents the precipitation of jarosite (Chapman *et al.*, 1983; Bigham and Nordstrom, 2000). Jarosite is assumed to be the mineral phase controlling the activity of ferric iron below a pH of 4 (Bigham and Nordstrom, 2000).

2.4.6 Fe and Al oxides and hydroxides

2.4.6.1 Fe oxides and hydroxides

All Fe^{III} oxides have the basic octahedron structural unit where each Fe atom is bounded by either six O atoms or by O and OH atoms in the case of oxyhydroxides. The O and OH atoms form layers, which approximate either hexagonal or cubic close packing. The Fe^{3+} may be replaced by another trivalent ion of similar size without modification to the structure. The different Fe oxides are distinguished by the arrangement of $Fe(O,OH)_6$ octahedra. The minerals with γ - crystal forms, such as lepidocrocite and maghemite, require a ferrous precursor to form whereas the α -polymorphs, such as goethite and hematite can develop from a ferrous *or* ferric precursor. Thus the Fe-oxides act as indicators of the type of redox conditions under which they were formed.

Goethite (α - $FeOOH$), lepidocrocite (γ - $FeOOH$) and akaganéite (β - $FeOOH,Cl$) have a structure where the octahedra are linked in double bands that share edges. Goethite is considered to be the most stable form of Fe^{III} oxides (Bigham, 1994) and forms short rod-like particles in mine drainage precipitates. The Al for Fe substitution in goethite can range from 0 – 33 mole % (Schwertmann and Cornell, 2000). In synthesised goethites, an Al substitution can reach as high as 47 mole % (Fey and Dixon, 1981). Dissolved sulphate can suppress the formation of goethite (Alpers, 1994).

Ferrihydrite ($\text{Fe}_5\text{HO}_8 \cdot 4\text{H}_2\text{O}$ or $5 \text{ Fe}_2\text{O}_3 \cdot 9\text{H}_2\text{O}$) and feroxyhyte ($\delta\text{-FeOOH}$) are considered to have a structure resembling hematite. Both these minerals have a low degree of crystallinity that is attributed to vacant Fe sites and the replacement of some oxygen with H_2O or OH (Schwertmann and Cornell, 2000). Ferrihydrite consists of highly aggregated spherical particles with a high surface area of 200 to 600 m^2/g . Ferrihydrite is always poorly crystallised and displays a range of structural order with XRD patterns of two to six lines (Bigham, 1994). Above pH 4 saturation indices indicate supersaturation with respect to ferrihydrite and this mineral is assumed to be the phase controlling ferric iron activity (Bigham and Nordstrom, 2000). The higher the rate of oxidation the more likely ferrihydrite will be favoured over goethite or lepidocrocite (Schwertmann and Fitzpatrick, 1992).

The octahedra in hematite ($\alpha\text{-Fe}_2\text{O}_3$) share both edges and faces with the layers running parallel to the c-axis. The Al analogue of this mineral is corundum ($\alpha\text{-Al}_2\text{O}_3$). Hematite has a slightly distorted structure, which leads to a compact structure of a very high density (Schwertmann and Cornell, 2000). Low temperature hematites can contain OH in the structure and aluminium can substitute for Fe up to 14 mole % (Alpers, 1994). The formation of hematite via solution requires the presence of ferrihydrite as a precursor. The presence of Ca and Mg has been found to favour the precipitation of hematite versus goethite (Alpers, 1994).

Magnetite ($\text{FeO} \cdot \text{Fe}_2\text{O}_3$) and maghemite ($\gamma\text{-Fe}_2\text{O}_3$) have a cubic structure wherein a third of the interstices are tetrahedrally coordinated with oxygen and two-thirds are octahedrally coordinated. Maghemite and magnetite can contain between 10 and 15 % Al substitution (Schwertmann and Cornell, 2000).

Green rusts are defined by the fact that anions are an essential structural component but they are not strictly oxides or hydroxides. The structure is made up of hexagonally close-packed layers of O and OH with Fe^{II} and Fe^{III} in the interstices. The Fe^{III} bestows a positive charge to the layer, which is balanced by anions such as Cl^- , SO_4^{2-} , CO_3^- etc., between the layers (Schwertmann and Cornell, 2000).

2.4.6.2 Al hydroxides

Gibbsite (Al(OH)_3) consists of Al ions coordinated between two sheets of hexagonally packed hydroxyl ions. This structure is offset slightly from the ideal packing so that gibbsite falls into the monoclinic crystal system (Schwertmann and Cornell, 2000). Bayerite (Al(OH)_3) is a dimorph of gibbsite with similar layers of octahedral, these are, however, stacked differently and yield a single-layer cell (Deer *et al.*, 1992). Above pH 5 the slow growth kinetics of diaspore ($\alpha\text{-AlOOH}$) and gibbsite control aluminium solubility (Alpers, 1994). With increasing temperature, first gibbsite, then diaspore, then corundum ($\alpha\text{-Al}_2\text{O}_3$) are the stable phases and boehmite ($\gamma\text{-AlOOH}$) is postulated to exist as a metastable phase at intermediate temperatures. The structure of boehmite is similar to that of lepidocrocite and consists of double sheets of octahedral with Al ions at their centres. Diaspore and boehmite occur principally in bauxite clay deposits, which are the main source of aluminium metal (Deer *et al.*, 1992).

2.5 Conclusions

The mineralogy of Fe and Al wastes are ultimately determined by pH, SO_4 and HCO_3 . Studies have shown that pH is the master variable that influences the speciation of secondary minerals in acid sulphate waters (Bigham *et al.*, 1996). The precipitates formed from acid mine drainage are classified as hazardous wastes because of the high concentrations of Fe, Al and other heavy metals with which they are associated. The principles and methods behind the passive and active treatment of AMD are well researched but alternative liming materials that would decrease the costs of neutralisation are constantly being sought. While small amounts of fly ash are used in cement and building industries, alternatives to dumping are continuously being sought. Many of the minerals precipitated as a result of the neutralisation of AMD are found naturally in soils and are generally not harmful.

Chapter 3

Experimental neutralisation of synthetic acid mine drainage

3.1 Introduction

The previous chapter reviewed the relevant literature concerning fly ash, acid mine drainage and the mineralogy of ochre precipitates. The literature most relevant to this chapter is that dealing with the active neutralisation of AMD. Jenke *et al.* (1983) have to date performed the most extensive investigation into the composition of mine water before, after and during neutralisation, as well as analysing the precipitates formed. They found that the transfer of O₂ and CO₂ from the atmosphere does not play a large role in the precipitation of metals, with adsorption and coprecipitation being the dominant processes facilitating the removal of metals. Their study also examined the pH of precipitation for a number of metals and found that Fe³⁺ had precipitated by pH 3.5, Al precipitation was complete by pH ~ 5 and 50 percent of Fe²⁺ had precipitated between pH values of 5 and 6. Their method of titration, however, involved only a brief reaction time of 1 minute before the reaction was quenched with acid.

Thompson (1979, 1980) has presented useful details concerning the neutralisation of mine waters in South Africa, from both coal and gold mines. Neutralisation experiments were carried out under aerobic and anaerobic conditions, using Ca(OH)₂ and CaCO₃. It was found that, although there is considerable variation in the pH and salinity of different mine waters, iron and aluminium were the dominant cations in solution.

O'Brien (2000) explored the possibilities of neutralising AMD with fly ash. Secondary precipitates were not easily identified, however, because of their admixture with a much larger quantity of unreacted fly ash.

Because the eventual aim of the present study was to discover what kind of secondary solids form as a result of reacting fly ash with AMD, it was decided that fly ash

leachate (FAL) must be used in order to isolate the precipitates in a concentrated form.

In this chapter preliminary experiments are reported with the aim of understanding the nature of the neutralisation reaction and of estimating the range of solids that can be produced. The acidic components of AMD are studied separately and in combination and different bases are employed for the neutralisation reaction in order to establish whether FAL may have specific neutralisation characteristics different from those of other liming materials.

3.2 Materials and methods

3.2.1 Sample preparation

3.2.1.1 Fly ash leachate

Two batches of fresh fly ash were obtained from Arnot power station and kept in large airtight containers during a six-month period, to minimise contact with the atmosphere. The lime in fly ash reacts with CO₂ from the atmosphere to form calcite. Thus the composition of the ash material is altered and results in Ca²⁺ and alkalinity becoming less available for reaction (O'Brien, 2000).

Fly ash leachate (FAL) was prepared as a 1:1 ratio of mass of FA to volume distilled water. The slurry was enclosed in 300 mL plastic containers, filled to approximately 90 percent capacity in order to minimise contact with air but still allow for sufficient agitation. The containers were mounted on a reciprocating shaker for 24 hours, vacuum-filtered through a Büchner funnel and the filtrate immediately stored in a sealed 1L volumetric flask. Leachate was freshly prepared in this way for each titration where it was used.

3.2.1.2 Synthetic acid mine drainage

In keeping with the rationale of O'Brien (2000) synthetic acid mine drainage (SAMD) was used for experimentation in view of the fact that real acid drainage is extremely

difficult to obtain without the samples undergoing oxidation and hydrolysis. A simplified solution containing the major ions found in acid mine waters was prepared. Based on analyses carried out on water from the Blesbokspruit catchment by Hälbich (1997) (Table 3.1) and on the composition of SAMD prepared by O'Brien (2000).

Table 3.1: Selected analyses of some acid drainage, ion concentrations in mmol/L (Hälbich, 1997).

Sample No	W1	W2	T1	T2	W13	W8	W5	W16	W22
pH	2.7	2.7	2.8	2.9	2.8	2.7	2.8	2.9	3.2
EC (mS/m)	39	40	36	37	37	36	33	48	13
Na ⁺	27	34	2.0	1.4	6.7	9.9	11	3.2	2.5
Ca ²⁺	1.1	1.0	13	12	5.4	3.4	3.5	9.0	1.3
Al ³⁺	3.0	3.2	1.2	1.4	12	7.0	3.6	8.9	1.5
Fe (tot)	1.8	2.2	3.5	13	0.35	1.3	0.53	0.18	0.029
Cl ⁻	27	28	0.51	0.14	7.2	11	14	2.8	2.5
SO ₄ ²⁻	9.5	14	34	40	8.8	16	15	23	1.3

The composition of SAMD used in this study is shown in Table 3.2. The concentrations in Table 3.2 were used to simulate an AMD with a near-equal amount of Fe and Al. In Chapter 4 this ratio is varied to better simulate real AMD. The SAMD was prepared with freshly distilled water, which was flushed with nitrogen gas, to reduce the concentration of dissolved oxygen. This ensured that the SAMD remained stable for 2 days, after which it was considered necessary to prepare a fresh solution. The Al₂(SO₄)₃, CaSO₄ and FeSO₄ were dissolved in approximately 750 mL of distilled water in a 1L volumetric flask. Prior to the addition of ferric sulphate, 2 mL/L of 1M H₂SO₄ was added to ensure a pH of less than 3, in order to prevent the immediate precipitation of ferric hydroxide. The solution was then made up to a volume of 1L.

Table 3.2: The composition of SAMD in this study.

Compound	Conc. (g/L)	Composition (mmol/L)
Al ₂ (SO ₄) ₃ •16H ₂ O	4.00	Al ³⁺ 12.7
Fe ₂ (SO ₄) ₃ •XH ₂ O	1.91	Fe ³⁺ 7.3
FeSO ₄ •7H ₂ O	1.00	Fe ²⁺ 3.6
CaSO ₄ •2H ₂ O	0.90	Ca ²⁺ 5.2
H ₂ SO ₄ (1M)	2mL/L	SO ₄ ²⁻ 40.8

3.2.2 Potentiometric titrations

A series of titrations was performed to investigate the reaction of SAMD with different bases under oxic and anoxic conditions. The latter were induced by bubbling either air or N₂ at a rapid rate through a fritted glass tube immersed in the solution. Titrations were also carried out with solutions of Al₂(SO₄)₃•16H₂O, Fe₂(SO₄)₃•XH₂O or FeSO₄•7H₂O. The basic solutions employed consisted of NaOH, either alone or in combination with CaCl₂ in order to simulate the composition of FAL. Titrations were performed upscale and downscale with an initial volume of 300 mL of solution in the titration vessel.

The equipment used to carry out these experiments consisted of a PHM 290 pH-Stat controller and an ABU 901 Autoburette, both made by Radiometer (Figure 3.1). The pH stat controller was set to deliver titrant at a constant rate of 3mL/min. The pH and EC were logged at 15-second intervals throughout the reaction. The pH meter was calibrated with standard buffers at pH values 4 and 7, while the EC meter was calibrated using a solution of 1412 mS/m and logged using a Pico ADC 16 high-resolution data logger. The reaction vessel, which was open to the atmosphere, was mounted on a magnetic stirrer. The solution underwent constant stirring throughout

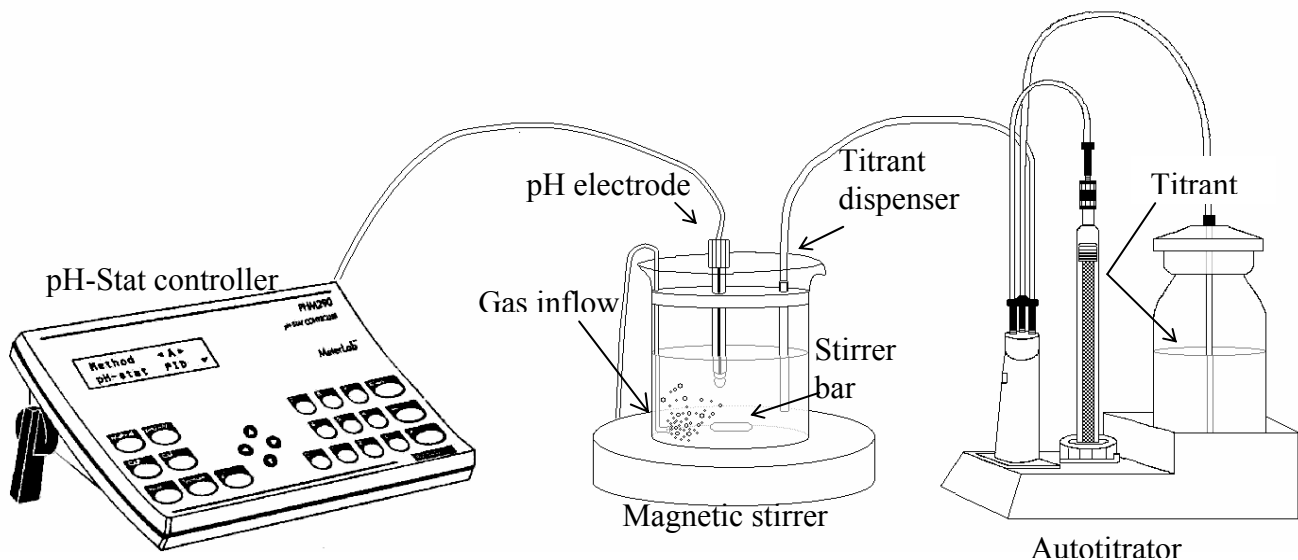


Figure 3.1: Equipment arrangement for titration experiments.

3.2.2.1 Experiment 1: Components of SAMD titrated with different bases in oxic and anoxic environments

Solutions of 11.9 mmol/L $\text{FeSO}_4 \cdot 7\text{H}_2\text{O}$, 12.0 mmol/L $\text{Al}_2(\text{SO}_4)_3 \cdot 16\text{H}_2\text{O}$ and 7.60 mmol/L $\text{Fe}_2(\text{SO}_4)_3 \cdot \text{XH}_2\text{O}$ were prepared and titrated with two different bases (Table 3.3). The concentrations were specifically chosen to ensure that a sufficient amount of precipitate would be obtained for analysis. The ferric sulphate component was the only solution requiring acidification to prevent precipitation prior to titration. However, in order to obtain the same pH starting point, 2 mL of 1M H_2SO_4 was added to all solutions prior to titration. Titration to a high pH (between 10 and 11) was achieved with 50 mmol/L NaOH or 50 mmol/L NaOH and 28.2 mmol/L CaCl_2 in either an oxic or anoxic environment. The precipitates were centrifuged and washed with distilled water three times in order to remove excess salts and dried at a temperature of 70 °C. An aliquot of the supernatant was filtered through 0.05 mm filter paper and kept for analysis by AAS and IC.

Chemical grade $\text{Fe}_2(\text{SO}_4)_3 \cdot \text{XH}_2\text{O}$ is extremely hygroscopic and in order to determine accurately the iron content of this compound, 2 g $\text{Fe}_2(\text{SO}_4)_3 \cdot \text{XH}_2\text{O}$ was heated in a furnace at 600°C overnight until all the H_2O and SO_3 was driven off and only Fe_2O_3 (Appendix 1) remained. This procedure was performed in triplicate to obtain an average value of 3.88 ± 0.016 mmol Fe^{3+} per gram of $\text{Fe}_2(\text{SO}_4)_3 \cdot \text{XH}_2\text{O}$ (where X = 7).

Table 3.3: List of titrations done for experiment 1.

Titration No.	Acid	Base	Gas
17, 45, 46	$\text{Al}_2(\text{SO}_4)_3$	NaOH	Air
18	FeSO_4	NaOH	Air
19, 49, 49b	FeSO_4	NaOH	N_2
20	$\text{Al}_2(\text{SO}_4)_3$	NaOH	N_2
21, 48	$\text{Fe}_2(\text{SO}_4)_3$	NaOH	N_2
22, 47, 58	$\text{Fe}_2(\text{SO}_4)_3$	NaOH	Air
23	$\text{Al}_2(\text{SO}_4)_3$	CaCl_2 and NaOH	Air
24, 50	FeSO_4	CaCl_2 and NaOH	Air
25	$\text{Fe}_2(\text{SO}_4)_3$	CaCl_2 and NaOH	Air
26, 51, 57	$\text{Fe}_2(\text{SO}_4)_3$	CaCl_2 and NaOH	N_2
27	$\text{Al}_2(\text{SO}_4)_3$	CaCl_2 and NaOH	N_2
28	FeSO_4	CaCl_2 and NaOH	N_2

The base solutions were prepared in order to ensure a hydroxyl concentration approximating that of fly ash leachate (Table 3.4). The alkalinity of FAL was

determined with 50 mL of 0.05M H₂SO₄, which was titrated to pH 7 with FAL. The bases used were a 50 mmol/L NaOH solution and a mixture of NaOH and CaCl₂ with concentrations of 50 mmol/L and 28.2 mmol/L, respectively. Because the solubility of Ca(OH)₂ is very low (1.85 g/L) a saturated solution could not be accurately obtained. Thus, the mixture of NaOH and CaCl₂ was chosen to simulate the lime content of FAL (Table 3.4).

Table 3.4: Composition of bases and fly ash leachate in mmol/L as determined by acid titration and AAS and IC.

FAL				NaOH (0.05M)		NaOH (0.05M) and CaCl ₂ (0.028M)	
Ca ²⁺	28.4	Cl ⁻	0.099	Na ⁺	50	Ca ²⁺	28.2
Mg ²⁺	0.092	SO ₄ ²⁻	1.10	OH ⁻	50	Na ⁺	50
Na ⁺	0.088	OH ⁻	54.8			Cl ⁻	56.4
K ⁺	0.043					OH ⁻	50

3.2.2.2 Experiment 2: Acidic solutions with differing Fe:Al mole ratios

A series of titrations of solutions of FeSO₄ and Al₂(SO₄)₃ combined in different ratios was carried out (Table 3.5). The base used was 50 mmol/L NaOH containing 28.2 mmol/L CaCl₂. These titrations were performed under oxic and anoxic conditions and were titrated to a high pH between 10 and 11.

Table 3.5: List of titrations performed with different ratios of Al:Fe^{II}.

Titration No.	Al:Fe ^{II} mmol/300mL	Al:Fe ^{II} mole ratio	Base	Gas
60	0.55 : 3.30	1 : 6	CaCl ₂ and NaOH	N ₂
29, 52	1.80 : 2.68	2 : 3	CaCl ₂ and NaOH	N ₂
30, 53	3.60 : 1.79	2 : 1	CaCl ₂ and NaOH	N ₂
31	5.40 : 0.89	6 : 1	CaCl ₂ and NaOH	N ₂
59	0.55 : 3.30	1 : 6	CaCl ₂ and NaOH	Air
32	1.80 : 2.68	2 : 3	CaCl ₂ and NaOH	Air
33	3.60 : 1.79	2 : 1	CaCl ₂ and NaOH	Air
34	5.40 : 0.89	6 : 1	CaCl ₂ and NaOH	Air

3.2.2.3 Experiment 3: The SAMD-FAL system compared with simple acids and bases

A similar series of titrations was conducted with SAMD, FAL and the Al₂SO₄ – FeSO₄ solution (molar Al:Fe ratio of 2) with the NaOH-CaCl₂ base solution described

previously, in various combinations of upscale and downscale titrations under air or N₂ as summarised in Table 3.6. In two of these titrations the base solution was spiked with sodium silicate solution to give (by analysis using ICP-AES) a Si concentration of 0.7 mmol/L in order to investigate whether the Si in FAL is likely to modify its reaction with AMD.

The silica solution was prepared by dissolving water glass, a sodium silicate liquid, in a volume of water to give a highly concentrated solution of sodium silica. One millilitre of the concentrated water glass solution was added to 200 ml distilled water. Eight millilitres of this diluted solution was then added to the 1L CaCl₂ and NaOH mixture. The sodium was determined by AAS and the silica was determined ICP-AES. Analysis by ICP-AES gave the concentration of Si in the CaCl₂ and NaOH mixture as 0.70 mmol/L.

Table 3.6: List of up- and downscale titrations performed for experiment 3.

Titration No.	Acid	Base	Gas	Direction of pH scale
35	Al ₂ (SO ₄) ₃ and FeSO ₄ (1:2)	FAL	air	down
36	Al ₂ (SO ₄) ₃ and FeSO ₄ (1:2)	FAL	N ₂	down
37	SAMD	FAL	N ₂	down
38	SAMD	FAL	air	down
55	SAMD	FAL	air	up
56	SAMD	FAL	N ₂	up
39, 54	SAMD	CaCl ₂ and NaOH	air	down
40	SAMD	CaCl ₂ and NaOH	N ₂	down
41	Al ₂ (SO ₄) ₃ and FeSO ₄ (1:2)	CaCl ₂ and NaOH	N ₂	down
42	Al ₂ (SO ₄) ₃ and FeSO ₄ (1:2)	CaCl ₂ and NaOH	air	down
43	SAMD	CaCl ₂ and NaOH with silica added	air	down
44	SAMD	CaCl ₂ and NaOH with silica added	air	up

3.2.2.4 Reproducibility of potentiometric titrations

Appendix 2 contains titrations performed under the same conditions to test the reproducibility of the titration results. The reproducibility was generally found to be good with minor exceptions.

3.3 Analysis

The alkalinity measurements were performed using a 702 SM Titrino Metrohm titrator. A small volume of supernatant from each sample, 3 mL, was rapidly titrated with 0.01M HCl down to a pH of 4.5. The method used reports alkalinity in terms of CO_3^{2-} (down to pH 8.3) and HCO_3^- (between pH 8.3 to 4.5) concentration. The total alkalinity, which is the sum of the concentrations of CO_3^{2-} and HCO_3^- , is reported in the results. For the alkalinity determination of FAL 0.1M H_2SO_4 was used. The type of acid is arbitrary as long as the concentration is known.

An aliquot of the filtered supernatant was analysed for the major cations Na^+ , K^+ , Ca^{2+} , Mg^{2+} and total Fe by atomic absorption spectrometry using a Varian Spectra AA-250 plus. The major anions Cl^- , F^- , Br^- , NO_3^{2-} and SO_4^{2-} were analysed by ion chromatography using a Dionex DX-120 ion chromatograph with an Ion Pac[®] AS14A column and AG14-4 mm guard column. The eluent was Na_2CO_3 and NaHCO_3 .

The supernatant samples were also analysed for Al^{3+} and Si^{4+} by inductively coupled plasma-atomic emission spectroscopy using a Varian Liberty Series 2 sequential ICP spectrometer. The calibration standards were prepared in a concentrated gypsum solution to minimise salt concentration effects, which can cause significant interference. A high concentration of dissolved salts can contribute to instrument drift by causing salt build-up at the tip of the nebuliser gas orifice (Eaton *et al.*, 1995). Three measurements of each sample were taken, integrating over a period of two seconds.

After grinding in an agate mortar solid precipitates in self-supporting powder mounts, prepared by backfilling and pressing against filter paper to minimise the preferred orientation, were examined in aluminium holders using a Philips 1404 diffractometer equipped with $\text{CuK}\alpha$ radiation (40 mA, 50 kV) and a graphite monochromator, by step scanning at a rate of $1^\circ 2\theta \cdot \text{min}^{-1}$ (step size $0.05^\circ 2\theta$).

3.4 PHREEQC solution modelling

The ion association model PHREEQC (Parkhurst, 1995) was used to calculate ion activities and saturation indices of mineral solids based on the pH and solution concentrations of major ions in supernatants that were analysed after titration completion. The PHREEQC thermodynamic database was employed. The software for this programme may be downloaded at <http://water.usgs.gov/software>.

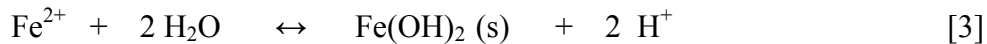
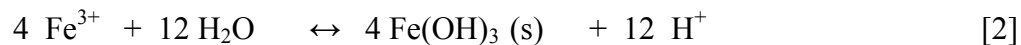
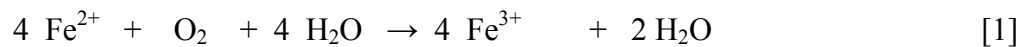
3.5 Results

3.5.1 Experiment 1: Components of SAMD titrated with different bases in oxic and anoxic environments

In Figure 3.2 the $\text{Al}_2(\text{SO}_4)_3$ graphs (a and b) show buffering at pH values 4 and 10. These buffering ranges at pH values 4 and 10 are consistent with the formation of bayerite and the re-dissolution of $\text{Al}(\text{OH})_3$, respectively. The oxidation and hydrolysis of Fe^{II} occurs at pH 6 (c and d) and the $\text{Fe}_2(\text{SO}_4)_3$ graphs (Fig 3.2 e and f) shows a buffering range at pH 3.5, which corresponds to Fe^{III} hydrolysis (Jenke *et al.*, 1983). The EC values for $\text{Al}_2(\text{SO}_4)_3$ titrated with NaOH show little variation from the starting EC, which is approximately 350 mS/m and decreases by only 35 to 45 mS/m. The EC stays constant over the buffer range because salts are being removed from solution, i.e. precipitated, at the same rate as they are being added. The EC starts to increases after the hydrolysis of Al^{3+} is complete. This trend is displayed in all the titrations. Where the base consists of the $\text{CaCl}_2/\text{NaOH}$ solution the EC is accordingly much higher and reaches values significantly greater than the starting solution. This base solution is more concentrated in terms of salt load and the rise in EC after metal precipitation is completed indicates that the salts present in solution are behaving as an indifferent electrolyte.

The $\text{Al}_2(\text{SO}_4)_3$ and $\text{Fe}_2(\text{SO}_4)_3$ (Figure 3.2) titration curves do not show any difference between oxic and anoxic environments. As there is no oxidation taking place, this is to be expected. The sawtooth pattern of the Fe^{2+} curves is a redox effect displayed as a result of the titration equipment. Each time the burette stops titrating in order to

refill (every 10mL of titrant added) oxidation continues in the beaker and the pH drops as H^+ is released. When titration resumes the pH rises again to the buffer level where it is maintained until refilling is required. This indicates that the rate of titrant addition has a large influence on the shape of the curve. It follows that, where the rate of addition is slow, the saw-toothed pattern is less pronounced as Fe^{2+} has more time to oxidise and maintain equilibrium in the solution. The pH of the Fe^{2+} equilibrium buffer range is fairly constant at a pH ~ 5 . The gaseous environment of the titration does not seem to affect the pH of the buffer range to a great extent. Where NaOH is the base there is a difference in the buffer pH in the oxic and anoxic environments. The oxic environment maintains a lower buffer pH (~ 5) than the anoxic environment (pH ~ 6). This difference is due to the release of a larger amount of acidity in the oxic environment because Fe^{2+} first undergoes oxidation (Equation 1) then hydrolysis (Equation 2). In an anoxic environment, Fe^{2+} undergoes hydrolysis but not oxidation (Equation 3).



A consistent difference between the oxic and anoxic environments in both basic solutions is, however, reflected in the EC values. In the anoxic environment, during pH buffering, the EC is higher than in the oxic environment by approximately 25 mS/m. The maintenance of a higher EC in an anoxic environment throughout the buffering reaction may be a reflection of the slower rate at which precipitation occurs when no oxygen is present.

There is a slight inflection visible in the graphs of $\text{Al}_2(\text{SO}_4)_3$ and $\text{Fe}_2(\text{SO}_4)_3$ between pH 5 and 6. This inflection may be what is termed the third buffer range by Schwertmann and Jackson (1964) on H-Amberlite-treated vermiculite. They attribute this third buffer range to the neutralisation of the excess protons of Al-OH₂ groups in positively charged, hydroxy aluminium polymers. The rate and extent to which this neutralisation process takes place is dependent upon the negative charge density of the mineral, which corresponds to the influence of different soluble anions on the pH of this third buffer range. The buffer pH is elevated with the valence of the anion, and is

thus higher for SO_4 than for Cl (Schwertmann and Jackson, 1964). This phenomenon may also apply to amphoteric Fe- and Al-hydroxides where adsorbed H^+ creates a small but noticeable buffering of the pH between 5 and 6.

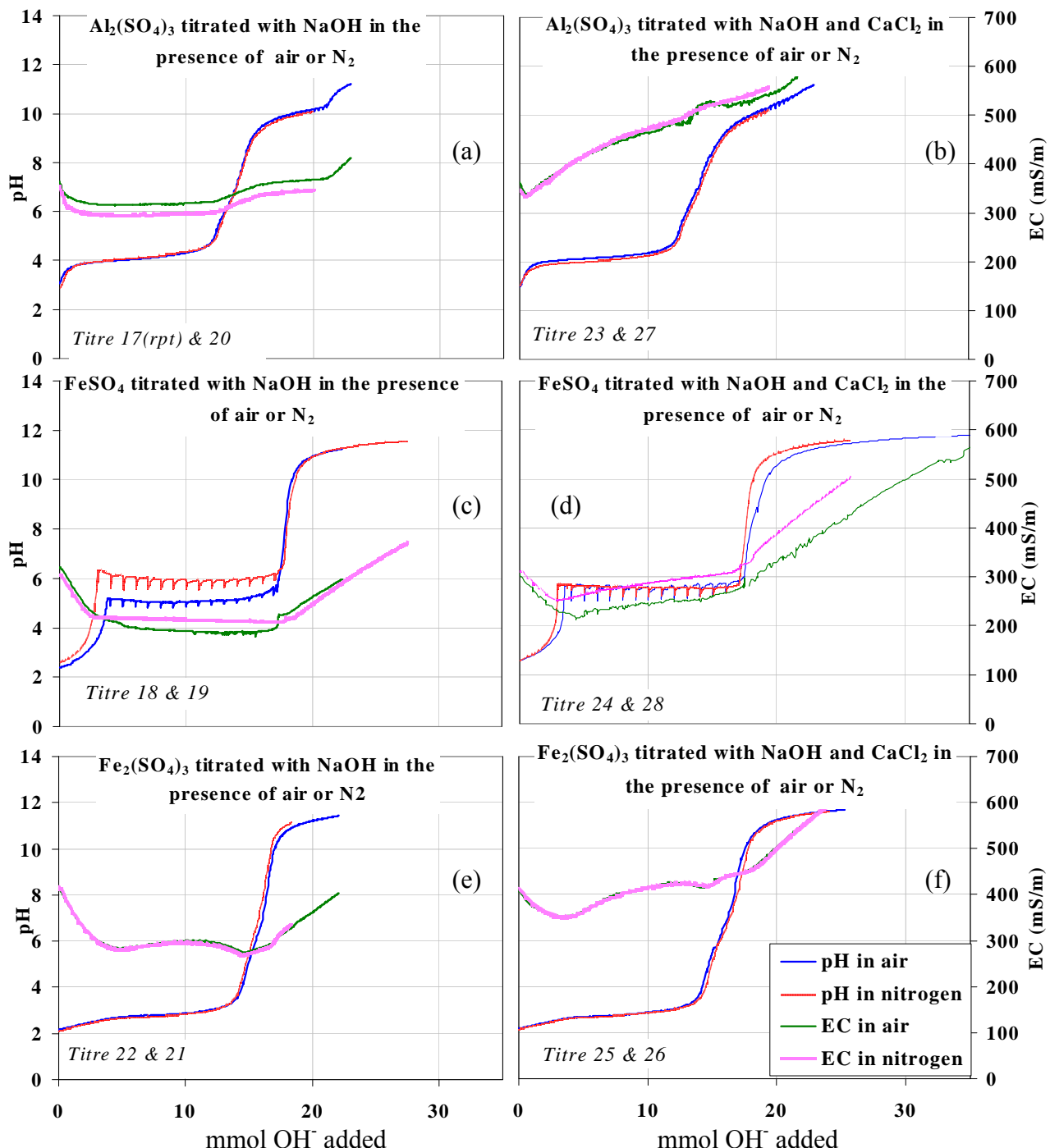


Figure 3.2: Titration graphs comparing oxic and anoxic environments in $\text{Al}_2(\text{SO}_4)_3$, $\text{Fe}_2(\text{SO}_4)_3$ and FeSO_4 acid solutions titrated with either NaOH or $\text{NaOH}-\text{CaCl}_2$. The x-axes have been normalised in order to compare the solutions at concentrations equivalent to Fe^{3+} . $\text{Al}^{3+} = 21.6 \text{ mmol}_\text{c}/\text{L}$, $\text{Fe}^{3+} = 13.7 \text{ mmol}_\text{c}/\text{L}$ and $\text{Fe}^{2+} = 7.1 \text{ mmol}_\text{c}/\text{L}$.

The only visible difference between the two different bases is a considerable difference in EC. A higher EC value for the $\text{CaCl}_2/\text{NaOH}$ solution is a result of a greater salt concentration than the NaOH solution (Appendix 3).

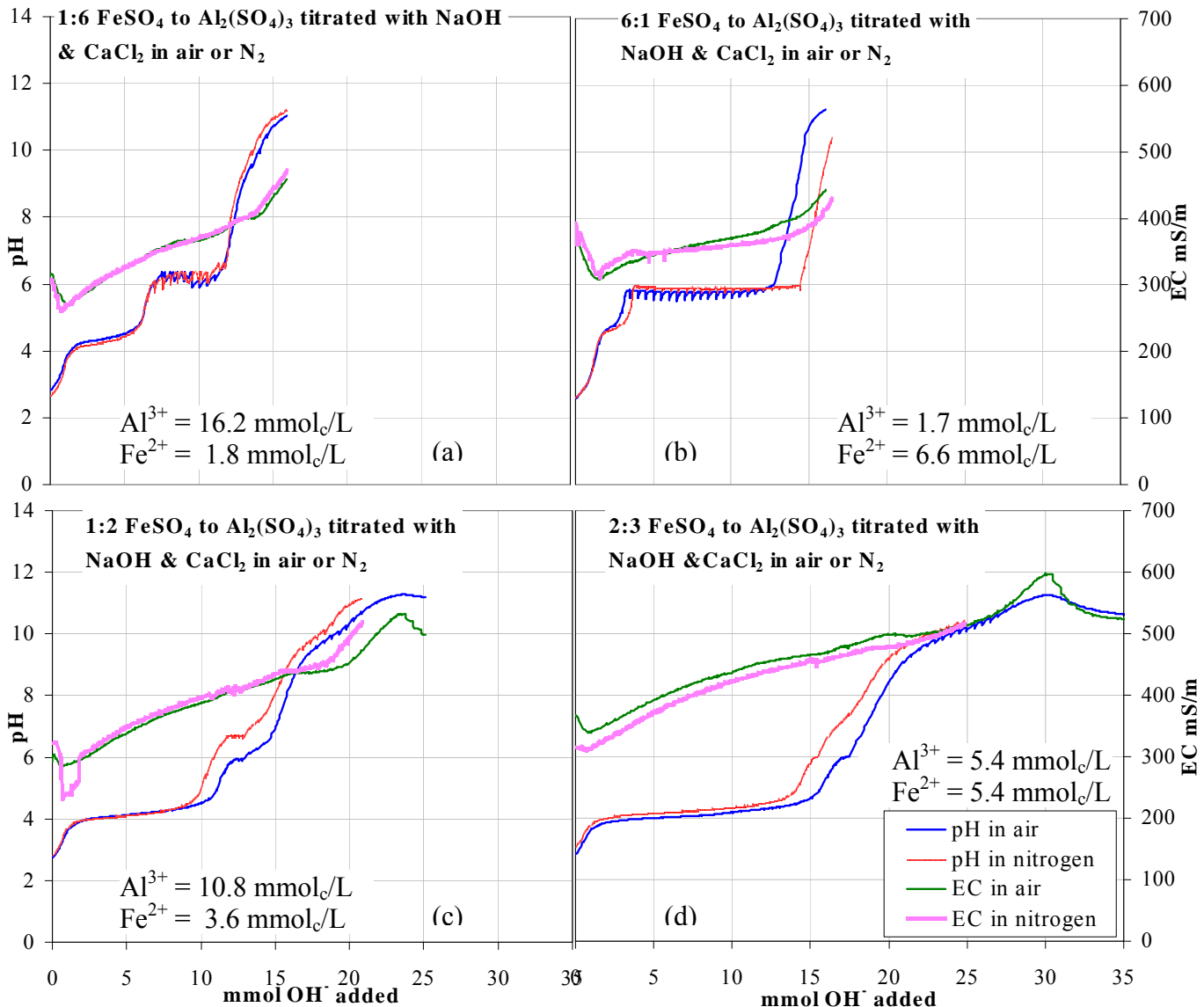


Figure 3.3: Titration graphs of Fe:Al ratios in oxic and anoxic environments: (a) 1:6 $\text{Fe}^{\text{II}}/\text{Al}$, (b) 6:1 $\text{Fe}^{\text{II}}/\text{Al}$, (c) 1:2 $\text{Fe}^{\text{II}}/\text{Al}$, (d) 2:3 $\text{Fe}^{\text{II}}/\text{Al}$.

3.5.2 Experiment 2: Different Fe:Al ratios titrated with base

Figure 3.3 displays four graphs of acidified sulphate solutions with differing ratios of Fe^{II} to Al titrated with the $\text{CaCl}_2/\text{NaOH}$ solution in oxic and anoxic environments. The graphs are labelled (a) – (d) being in order, Fe:Al ratios of 1:6, 6:1, 1:2 and 2:3.

The Al and Fe as discussed previously continue to buffer the pH at approximately 4 and 6, respectively.

The titrations under oxic conditions in graphs (c) and (d) can be seen to require more base to reach the same pH as their anoxic counterparts. The pH curves diverge at pH 4.5 where Al precipitation is nearing completion. The reason for this is unclear as no oxidation is taking place.

Purer solutions of either Fe or Al (graphs a and b) tend to keep the EC lower than more mixed solutions.

In graphs (c) and (d) there is a gradual rise and sudden fall in the EC values, at a pH of 10 in graph (c) and 11 in graph (d), for the titrations performed under oxic conditions. The anoxic titrations do not show this, as they were not titrated to a high enough pH. This is believed to be due to the precipitation of ettringite, which has been found to occur at these high pH levels (O'Brien, 2000).

3.5.3 Experiment 3: The SAMD/FAL system compared with simple acids and bases

Downscale titrations were performed to compare the $\text{CaCl}_2/\text{NaOH}$ solution with FAL, and a 1:2 Fe to Al acid sulphate solution with the synthetic AMD (Figure 3.4). There are a number of places on the curve where the pH is buffered slightly. For all reactions (a, b and c) approximately 7 mmol of acidity is added to decrease the pH to 11. At pH 11 the titration is buffered for the further addition of approximately 2 mmol of acidity. The pH decreases to 9 where there is a slight inflection. At pH 7 there is another small buffered region. When the solution has been titrated to a pH of approximately 5 – 4.5 the precipitation of $\text{Al}(\text{OH})_3$ takes place. This reaction has an extremely strong buffering capacity.

The $\text{CaCl}_2/\text{NaOH}$ solution has an EC of approximately 200 mS/m higher than that of FAL (Figure 3.4). Taking this difference into account both solutions undergo a decrease of approximately 1000 mS/m after ~ 8 mmol acidity has been added. At this

point the EC is at a minimum and does not change appreciably after the initial sharp decrease.

The FAL solution has a larger buffering zone between pH 12 and 11 than the $\text{CaCl}_2/\text{NaOH}$ solution. Because of this the reaction with FAL as the base requires slightly more acidity to reach the same pH than the $\text{CaCl}_2/\text{NaOH}$ solution. There is otherwise little difference between the two base solutions.

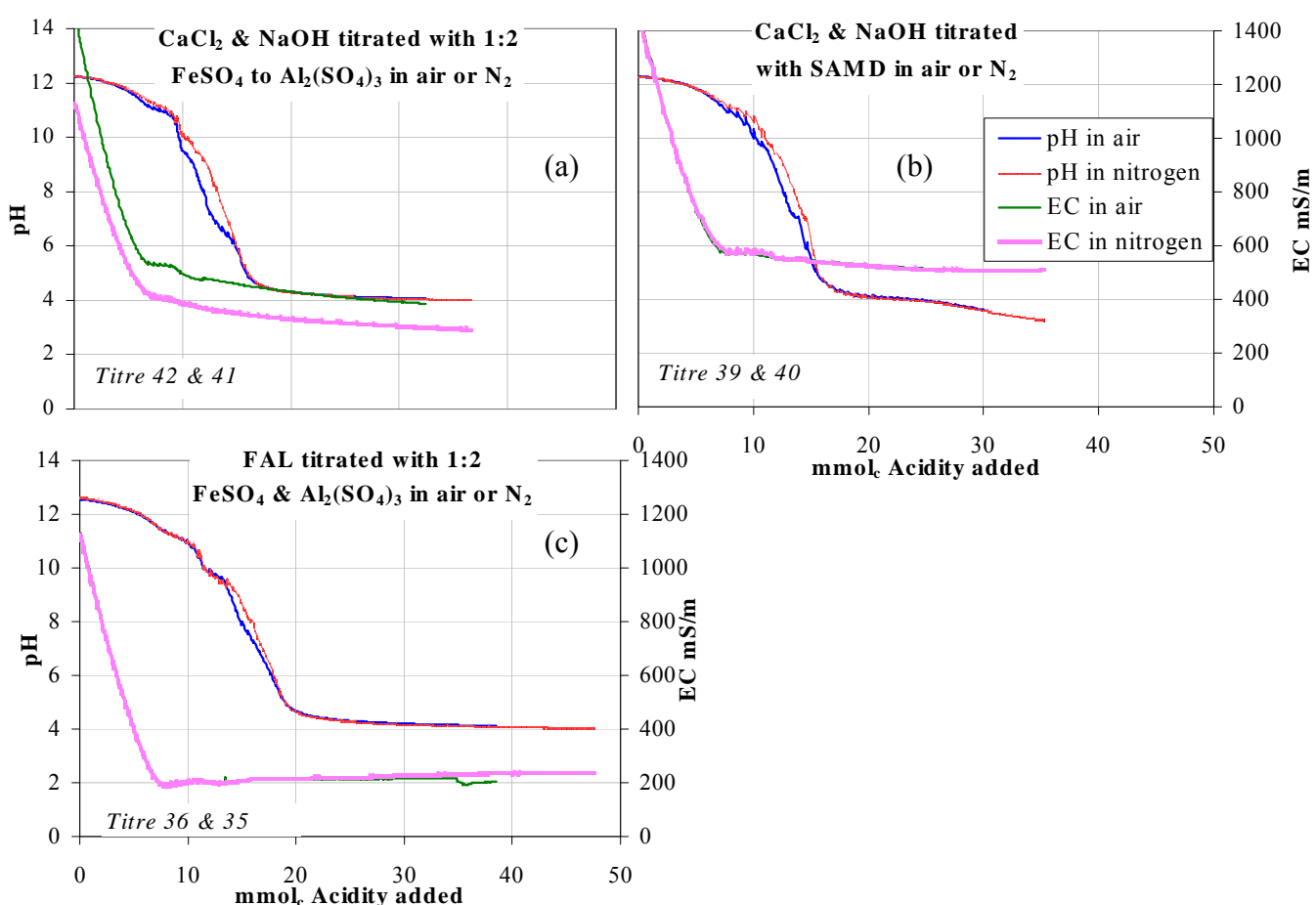


Figure 3.4: Downscale titration graphs of CaCl_2 and NaOH and FAL titrated with a 1:2 ratio of Fe:Al sulphate solution and SAMD.

In the oxic environments the pH decreases faster than in the anoxic environments (Figure 3.4). This can be seen most clearly between pH 10 and 6. In the oxic environment Fe^{2+} is oxidising and releasing more acidity than in the anoxic environment where Fe^{2+} is hydrolysing and releasing less acidity on precipitation.

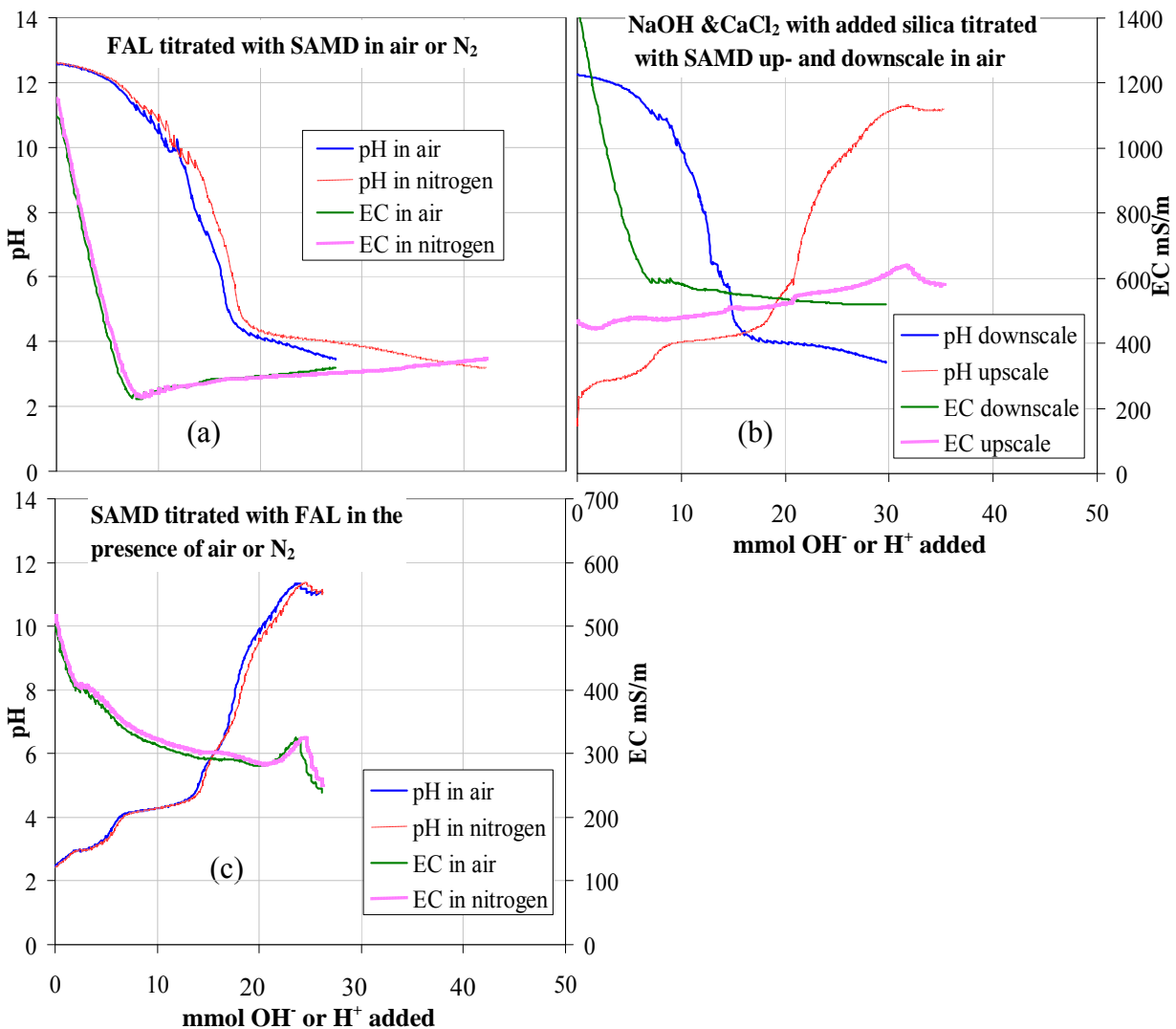


Figure 3.5: Titration graphs of FAL and a synthetic FAL with SAMD titrated upscale and downscale in air or nitrogen.

The small buffer zones at pH 11, 9 and 7 are better defined in graphs (a) and (c) where the acid is a 1:2 Fe:Al sulphate solution than in graph (b) where the acid is SAMD. This may be a result of the Fe^{III} in the SAMD precipitating as soon as it comes into contact with the base and releasing acidity as well as providing a surface to catalyse precipitation of minerals (Hansen and Taylor, 1990). The SAMD solution has a higher ionic strength approximately 200 mS/m greater than the EC for the 1:2 Fe:Al sulphate solution. This higher salt concentration may also be inducing a faster rate of precipitation.

The 1:2 Fe:Al sulphate solution has approximately twice the Al content of the SAMD solution. The influence of this can be seen in graph (b) where the buffer region at pH 4 is exceeded after approximately 30 mmol acidity has been added, whereas in graphs

(a) and (c) the pH does not show any decrease. The 1:2 Fe:Al sulphate solution contains 12 mmol/L Fe^{II} which is similar to the SAMD solution, which contains a total of 11 mmol/L Fe^{II} and Fe^{III}. Taking these differences into account there is otherwise little variation between the 1:2 Fe:Al sulphate solution and the SAMD solution.

Figure 3.5 shows the down- and upscale titrations, graphs (a) and (b) respectively, of SAMD with FAL in oxic and anoxic environments. Graph (c) shows a plot of the CaCl₂/NaOH solution containing silica titrated with SAMD in an up- and downscale reaction.

Graph (a) displays the same buffering regions as discussed above with a minimum EC of 200 mS/m. The pH decreases more rapidly in an oxic environment than in its anoxic counterpart as discussed above. Graph (b) the upscale titration of SAMD with FAL, clearly displays all three buffering regions associated with Fe³⁺, Al³⁺ and Fe²⁺ precipitation at pH 3, 4 and 5.5 respectively. The sharp drop in EC attributed to ettringite precipitation can also be seen to occur at pH 11.

The upscale titrations in graph (c) show little variation from graph (b). As concluded from experiment 1 the base makes very little difference to the titration curve. The downscale titration in graph (b) requires less titrant to reach pH 4 than the titrations in graph (a). This is not due to the greater buffering capacity of FAL at pH 12, as discussed previously, at pH 10 both reactions have consumed the same amount of acidity. There appears to be less buffering between pH 10 and 4 in graph (b) and as a consequence less acidity is consumed.

3.6 XRD data

Figure 3.6 shows FeSO₄ titrated with NaOH and the CaCl₂/NaOH solution in air and nitrogen. Several titrations were repeated, and the XRD patterns for them are also shown. For titrations 28 and 50, the base is the CaCl₂/NaOH solution and they are the only samples to have calcite present. The calcite formed after titration while the uncovered solution was equilibrating and can be considered an impurity. A magnetic product was formed in Titration 19 at pH 7 under anoxic conditions. This product

was probably originally magnetite when it was formed but oxidised to the maghemite identified by XRD. This is a result of the reaction being performed at room temperature (Schwertmann and Cornell, 2000). The final pH is critical for producing a magnetic product as above a pH of 7 the redox conditions of the solution ensure that Fe^{II} will oxidise. Titrations 49a and 49b, under the same conditions but taken to higher pH values than titration 19, did not produce a magnetic product.

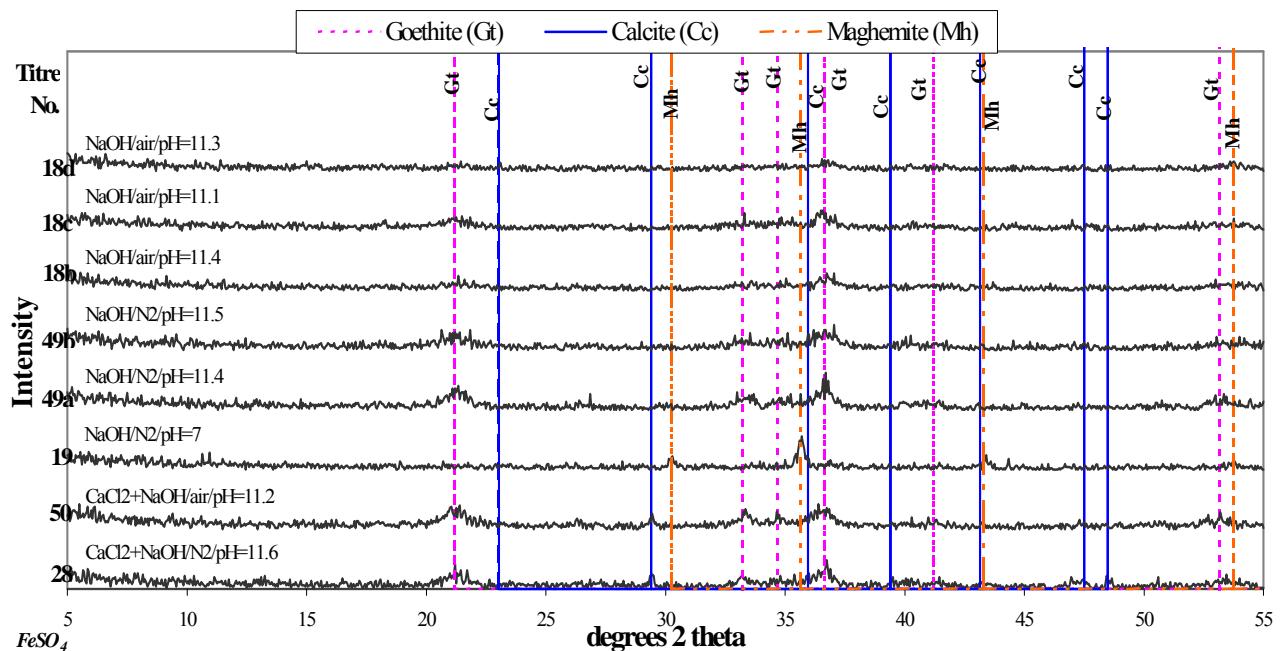


Figure 3.6: XRD patterns of the precipitates of FeSO₄ titrated with different bases in oxic and anoxic environments during experiment 1. Y-axis shows the titration number and each pattern is labelled with a summary of the conditions.

The product of titrations 49a, 49b, 18b, 18c and 18d all contain poorly crystalline goethite. The peaks are broad with a low intensity. The titrations performed under anoxic conditions show a more intense pattern than those in air. A slower rate of oxidation is more conducive to produce crystalline goethite from a Fe^{II} solution than a very rapid oxidation (Schwertmann and Cornell, 2000).

Figure 3.7 shows the XRD patterns of the products synthesised from the Fe₂(SO₄)₃ solutions. The goethite shown in Figure 3.7 has a better crystallinity than the goethite seen in Figure 3.6. The material produced in titration 51 is, however, amorphous and does not display any mineral phases with XRD. This could be a result of its lower pH.

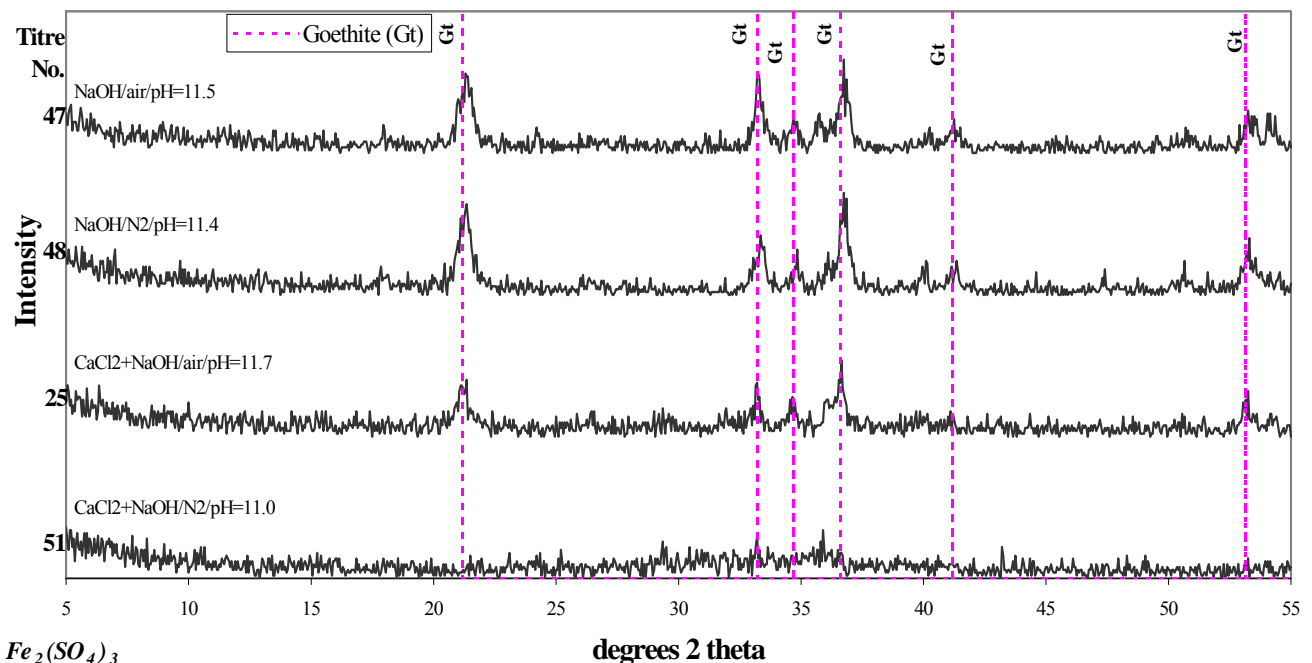


Figure 3.7: XRD patterns of the precipitates synthesised from an $\text{Fe}_2(\text{SO}_4)_3$ solution titrated with different bases in oxic and anoxic environments during experiment 1. Y-axis shows the titration number and each pattern is labelled with a summary of the conditions.

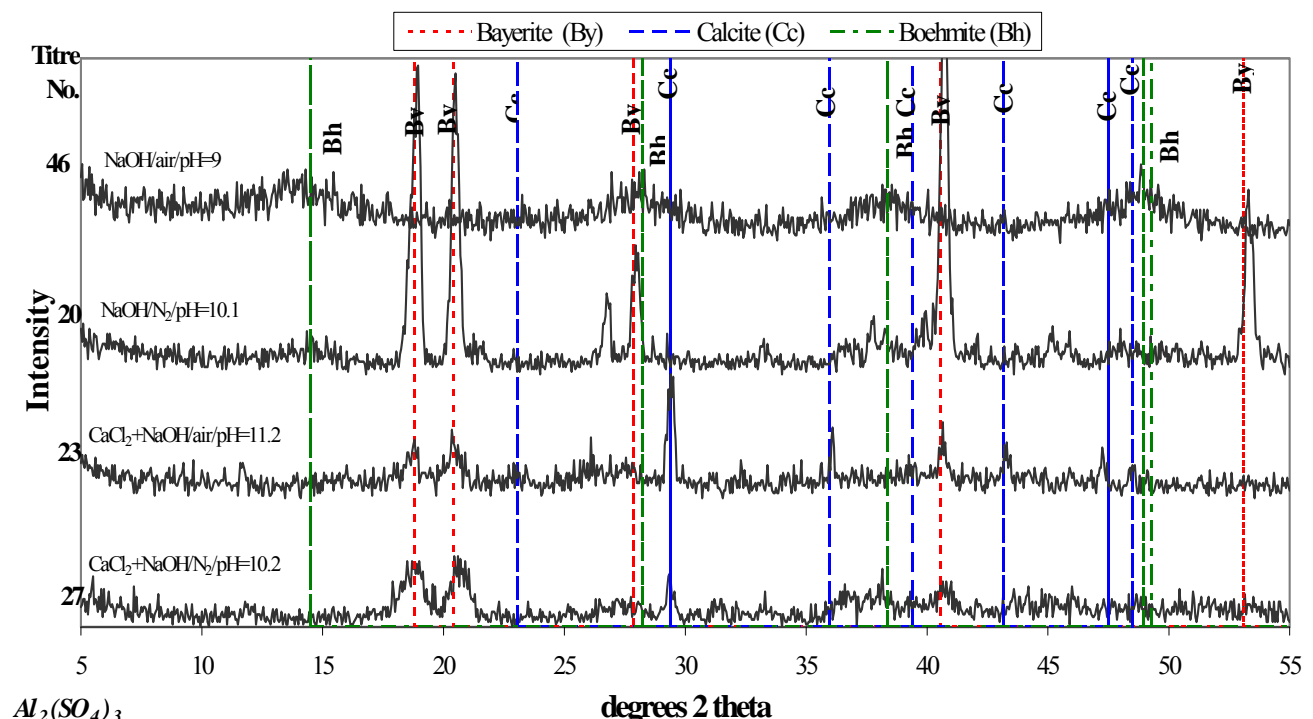


Figure 3.8: XRD patterns of the precipitates of $\text{Al}_2(\text{SO}_4)_3$ titrated with different bases in oxic and anoxic environments during experiment 1. Y-axis shows the titration number and each pattern is labelled with a summary of the conditions.

Figure 3.8 shows the XRD patterns of the products synthesised from the $\text{Al}_2(\text{SO}_4)_3$ solutions. The titrations performed with the $\text{CaCl}_2/\text{NaOH}$ solution contain calcite. Titrations 20, 23 and 27 all contain crystalline bayerite. The presence of CaCl_2 appears to inhibit the crystallinity of bayerite in the precipitates formed in titrations 23 and 27. Titration 46 was terminated at a pH of 9 and the precipitate contains a pseudo-boehmite phase.

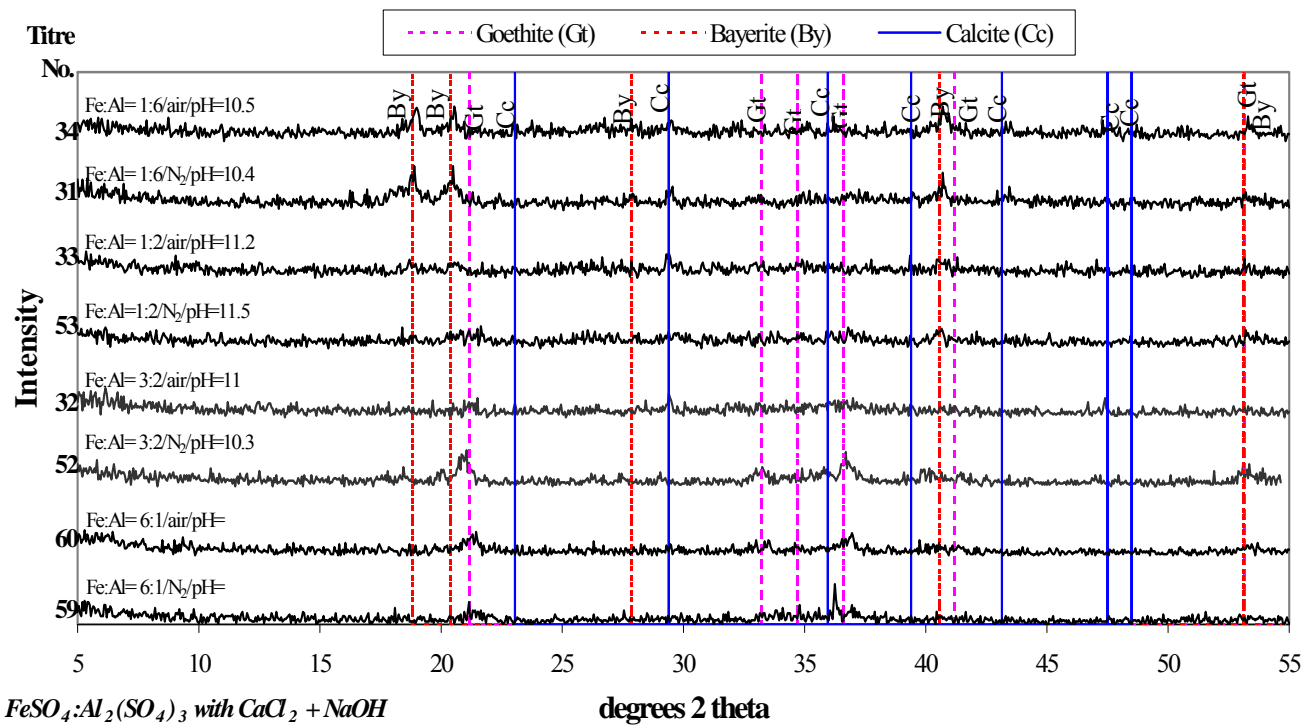


Figure 3.9: XRD patterns of the precipitates of Fe:Al ratios titrated with a base in oxic and anoxic environments during experiment 2. Y-axis shows the titration number and each pattern is labelled with a summary of the conditions.

The XRD patterns of the precipitates of solutions containing different ratios of Fe:Al are shown in Figure 3.9, with increasing amounts of Al from bottom to top. Goethite is present in the precipitates formed in titrations 59, 60, 52 and 32. Very poorly crystalline goethite and bayerite are found in the precipitate formed in titration 53 where the Fe:Al ratio is 1 to 2. The precipitates formed in titrations 33, 31 and 34 contain bayerite with a low degree of crystallinity.

Figure 3.10 shows the XRD patterns of the precipitates formed from the reactions of SAMD with the $\text{CaCl}_2\text{-NaOH}$ solution and FAL. Figure 3.11 shows the downscale reactions of a 1:2 Fe:Al sulphate solution titrated with FAL and the $\text{CaCl}_2/\text{NaOH}$ solution. None of the precipitates contain crystalline mineral phases. It is possible that the titrations proceeded too quickly to allow for crystal growth, but since this was not the case in previous titrations, it is unlikely. It is likely that the precipitates are all amorphous because of the mutual substitution of Fe and Al during hydroxide formation. It is well known that substitution of Al in the goethite structure significantly decreases the degree of crystallinity (Fey and Dixon, 1981). As a corollary to this it may be assumed that the same occurs if Fe were to be substituted for Al in the bayerite structure.

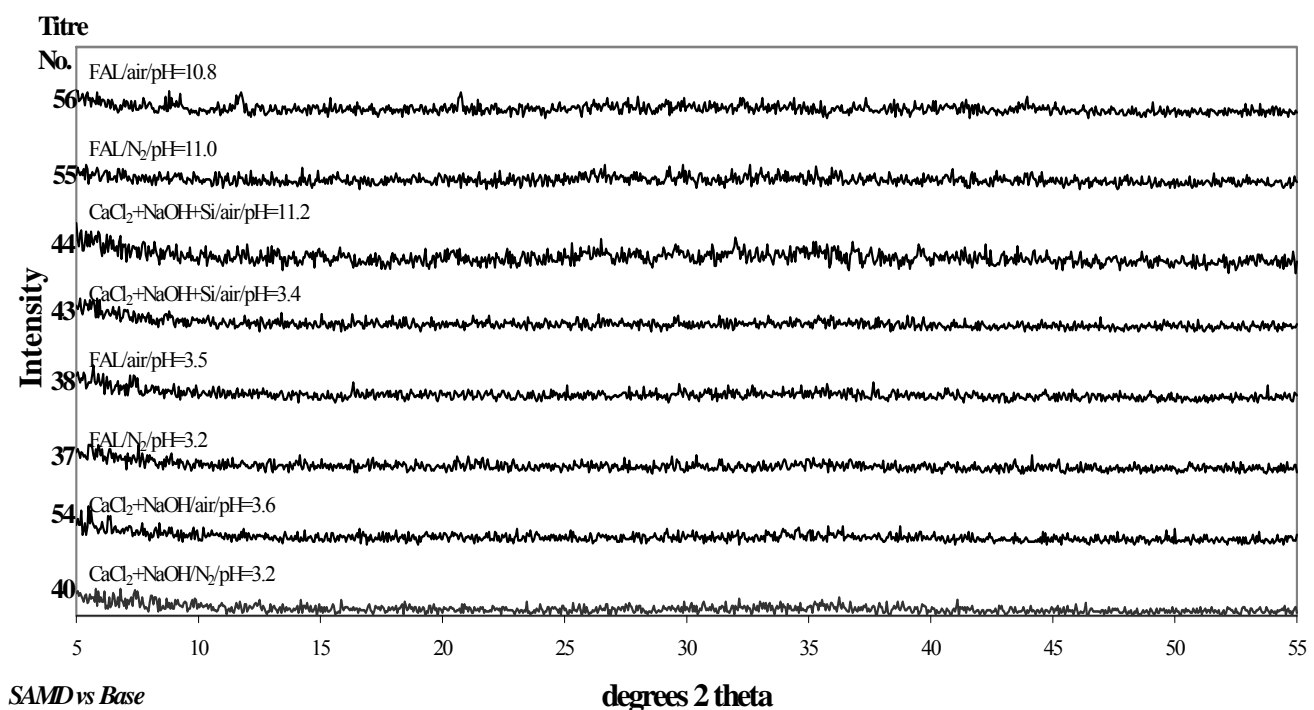


Figure 3.10: XRD patterns of the precipitates formed from the titrations of SAMD with different bases in oxic and anoxic environments during experiment 3. Y-axis shows the titration number and each pattern is labelled with a summary of the conditions.

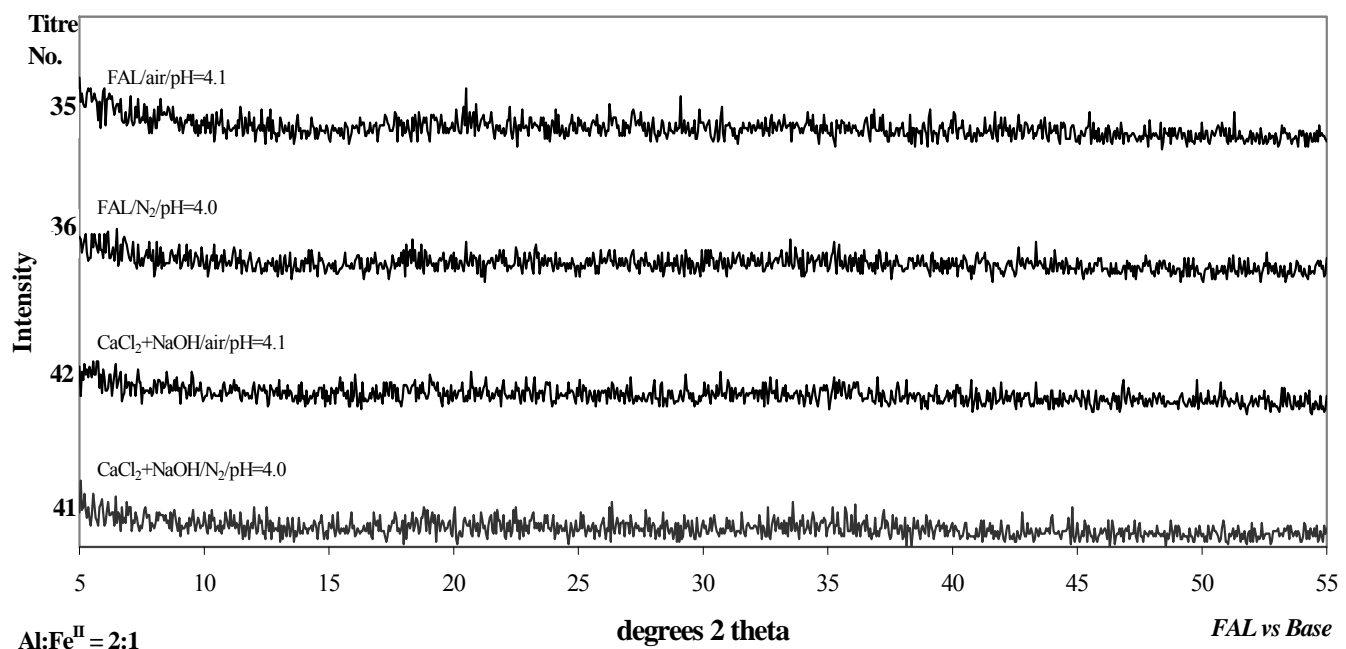


Figure 3.11: XRD patterns of the precipitates of Al:Fe = 2:1 titrated with different bases in oxic and anoxic environments during experiment 3. Y-axis shows the titration number and each pattern is labelled with a summary of the conditions.

3.7 Anion and cation data

The results presented in this section show the ions in solution before, during (Table 3.7) and after (Table 3.8) the completion of the titration experiments. The annotation BDL in Table 3.8 indicates that the ion was at concentrations below the detection limit (<0.0005 mmol/L for AAS and IC and <0.01 mmol/L for ICP) of the equipment used. Where a blank value is present it indicates that ion was not added in any of the chemical solutions that were titrated. The titration numbers in brackets indicate repeat titrations.

Table 3.7: The total amount of each ion added in mmol_c per volume of solution added before and during titration for experiment 1.

Titration No.	Reaction conditions	Al ³⁺	Tot Fe (as Fe ³⁺)	Na ⁺	Ca ²⁺	SO ₄ ²⁻	Cl ⁻	OH ⁻
17	Al ³⁺ / NaOH/ air	21.6		32.2		22.8		32.2
45 (17)	Al ³⁺ / NaOH/ air	21.6		34.4		22.8		34.4
46 (17)	Al ³⁺ / NaOH/ air	21.6		22.2		22.8		22.2
18b	Fe ²⁺ / NaOH/ air		10.8	12.6		8.4		12.6
18c	Fe ²⁺ / NaOH/ air		10.8	10.6		8.4		10.6
18d	Fe ²⁺ / NaOH/ air		10.8	11.2		8.4		11.2
19	Fe ²⁺ / NaOH/ N ₂		10.8	8.2		8.4		8.18
19b	Fe ²⁺ / NaOH/ N ₂		10.8	13.7		8.4		13.7
49a (19)	Fe ²⁺ / NaOH/ N ₂		10.8	10.8		8.4		10.8
49b (19)	Fe ²⁺ / NaOH/ N ₂		10.8	12.1		8.4		12.1
20	Al ³⁺ / NaOH/ N ₂	21.6		30.0		22.8		30.0
21	Fe ³⁺ / NaOH/ N ₂		13.7	18.3		14.9		18.3
48 (21)	Fe ³⁺ / NaOH/ N ₂		13.7	20.3		14.9		20.3
22	Fe ³⁺ / NaOH/ air		13.7	22.1		14.9		22.1
47 (22)	Fe ³⁺ / NaOH/ air		13.7	21.5		14.9		21.5
58 (22)	Fe ³⁺ / NaOH/ air		13.7	22.5		14.9		22.5
23	Al ³⁺ / NaOH, CaCl ₂ / air	21.6		34.4	40.3	22.8	38.7	34.4
24	Fe ²⁺ / NaOH, CaCl ₂ / air		10.8	17.8	20.9	8.4	20.0	17.8
50 (24)	Fe ²⁺ / NaOH, CaCl ₂ / air		10.8	18.9	22.2	8.4	21.3	18.9
25	Fe ³⁺ / NaOH, CaCl ₂ / air		13.7	25.3	29.6	14.9	28.4	25.3
26	Fe ³⁺ / NaOH, CaCl ₂ / N ₂		13.7	24.1	28.3	14.9	27.1	24.1
51 (26)	Fe ³⁺ / NaOH, CaCl ₂ / N ₂		13.7	11.1	13.1	14.9	12.5	11.1
57 (26)	Fe ³⁺ / NaOH, CaCl ₂ / N ₂		13.7	22.3	26.1	14.9	25.0	22.3
27	Al ³⁺ / NaOH, CaCl ₂ / N ₂	21.6		29.1	34.2	22.8	32.8	29.1
28	Fe ²⁺ / NaOH, CaCl ₂ / N ₂		10.8	12.9	15.1	8.4	14.5	12.9

Table 3.8: The total amount of each ion added in mmol_c per volume of solution added before and during titration for experiment 2. The base is the NaOH-CaCl₂ solution.

Titration No.	Reaction conditions	Al ³⁺	Tot Fe (as Fe ³⁺)	Na ⁺	Ca ²⁺	SO ₄ ²⁻	Cl ⁻	OH ⁻
29	Al:Fe = 6:1/ N ₂	16.2	2.70	17.8	20.8	19.2	20.0	17.8
52 (29)	Al:Fe = 6:1/ N ₂	5.40	8.10	14.0	16.4	12.0	15.7	14.0
30	Al:Fe = 2:1/ N ₂	10.8	5.40	20.8	24.4	15.6	23.4	20.8
53 (30)	Al:Fe = 2:1/ N ₂	10.8	5.40	23.1	27.1	15.6	26.0	23.1
31	Al:Fe = 2:3/ N ₂	5.40	8.10	24.8	29.1	12.0	28.0	24.8
32	Al:Fe = 6:1/ air	16.2	2.70	15.9	18.7	19.2	17.9	15.9
33	Al:Fe = 2:1/ air	10.8	5.40	25.1	29.5	15.6	28.3	25.1
34	Al:Fe = 2:3/ air	5.40	8.10	36.8	43.2	12.0	41.4	36.8
59	Al:Fe = 1:6/ air	1.66	10.0	16.4	19.2	9.5	18.4	16.4
60	Al:Fe = 1:6/ N ₂	1.66	10.0	18.9	22.1	9.5	21.3	18.9

Table 3.9: The total amount of each ion added in mmol_c per volume of solution added before and during titration for experiment 3. The shaded area indicates downscale titrations.

Titration No.	Reaction conditions	Al ³⁺	Tot Fe (as Fe ³⁺)	Na ⁺	Ca ²⁺	SO ₄ ²⁻	Cl ⁻	OH ⁻
35	Al:Fe = 2:1/ FAL/ N ₂	65.9	32.9	0.06	17.6	97.0	0.06	36.6
36	Al:Fe = 2:1/ FAL/ air	53.3	26.7	0.06	17.6	78.9	0.06	31.4
37	SAMD/ FAL/ N ₂	22.6	19.3	0.12	23.8	3.68	0.11	35.7
38	SAMD/ FAL/ air	14.7	12.6	0.08	21.6	2.39	0.07	23.2
39	SAMD/ NaOH, CaCl ₂ / air	16.3	13.9	15.0	22.0	34.8	16.9	15.0
54 (39)	SAMD/ NaOH, CaCl ₂ / air	25.1	11.4	15.0	21.2	28.4	16.9	15.0
40	SAMD/ NaOH, CaCl ₂ / N ₂	18.9	16.2	15.0	22.8	40.5	16.9	15.0
41	Al:Fe = 2:1/ NaOH, CaCl ₂ / N ₂	50.7	32.2	15.0	17.6	73.3	16.9	15.0
42	Al:Fe = 2:1/ NaOH, CaCl ₂ / air	44.9	28.5	15.0	17.6	64.8	16.9	15.0
43	SAMD/ NaOH, CaCl ₂ , Si/ air	15.9	13.6	15.0	21.9	34.0	16.9	15.0
44	SAMD/ NaOH, CaCl ₂ , Si/ air	11.4	9.80	35.3	44.5	24.5	39.7	35.3
55	SAMD/ FAL/ air	21.6	9.80	0.11	33.9	27.7	0.10	24.8
56	SAMD/ FAL/ N ₂	21.6	9.80	0.12	37.8	28.1	0.11	26.8

Tables 3.10 to 3.12 show the ions in the supernatant solutions that were analysed by IC and AAS. Discrepancies between the amount of ion put in and that found in the supernatant solution can be seen for some ions, especially those of high concentrations such as SO₄. Where the supernatant solutions contain more of an ion than was originally put in it is assumed that no amount of that ion has been removed from solution. This error is a result of the large dilution of the samples in order that they could be analysed on the sensitive AAS and IC equipment.

The titrations performed for experiment 1 (Table 3.10) show very low concentrations of Al and Fe. Titration 19 was not titrated to a high pH and therefore not all the Fe precipitated. A fraction of the ferrous iron in solution oxidised and lowered the pH so that the remainder could not precipitate. The titrations containing no Ca 17 – 22 have high SO₄ concentrations, indicating that no SO₄ has been removed. The titrations performed with the CaCl₂-NaOH solution contain Ca and SO₄ in equimolar concentrations in the supernatant solution, which is in equilibrium with gypsum (see following section). A considerably larger amount of Ca than SO₄ has been removed from the supernatant solution. Some of the Ca that has been removed from solution may have formed calcite as the solutions were titrated to high pH (Jenke *et al.*, 1983). The calcite was however filtered out of the supernatant and does not always appear in

the XRD patterns. There is a further possibility that Ca may be being included in the structure of the material precipitating as a $\text{CaAl}(\text{OH})_2\text{SO}_4$ compound similar to the pyroaurite and hydrotalcite minerals (Thevenot *et al.*, 1989). Where Al was the metal cation a higher amount of SO_4^{2-} tends to be removed out of solution (titrations 23 and 27). An average of 36% of Cl has also been removed from solution. This may also be included in the structure of the material precipitating. Sodium tends largely to stay in solution but a greater amount is removed when a high proportion of Fe stays in solution.

Table 3.10: Ion concentrations in mmol_c/L in the supernatant solutions upon completion of titrations performed for experiment 1. Final pH measured immediately prior to analysis.

Titration No.	pH	Reaction conditions	Al ³⁺	Tot Fe (as Fe ³⁺)	Na ⁺	Ca ²⁺	SO ₄ ²⁻	Cl ⁻	OH ⁻
17	8.50	Al ³⁺ / NaOH/ air	0.014		26.2	24.2			5.43
45 (17)	10.30	Al ³⁺ / NaOH/ air	0.91		30.8	21.1			14.6
46 (17)	6.10	Al ³⁺ / NaOH/ air	BDL		21.4	18.1			0.74
18b	8.78	Fe ²⁺ / NaOH/ air		BDL	11.5	8.9			3.60
18c	8.52	Fe ²⁺ / NaOH/ air		BDL	10.4	9.3			2.52
18d	8.60	Fe ²⁺ / NaOH/ air		0.0036	11.3	9.5			2.60
19	3.20	Fe ²⁺ / NaOH/ N ₂		9.68	4.61	10.5			BDL
19b	3.82	Fe ²⁺ / NaOH/ N ₂		1.16	9.18	10.7			BDL
49a (19)	8.40	Fe ²⁺ / NaOH/ N ₂		0.0025	10.3	8.9			2.22
49b (19)	8.72	Fe ²⁺ / NaOH/ N ₂		BDL	12.9	10.3			4.09
20	8.40	Al ³⁺ / NaOH/ N ₂	0.31		29.4	25.5			6.95
21	7.60	Fe ³⁺ / NaOH/ N ₂		0.024	17.3	17.6			1.57
48 (21)	8.53	Fe ³⁺ / NaOH/ N ₂		0.0042	19.5	16.8			3.71
22	8.90	Fe ³⁺ / NaOH/ air		BDL	23.3	20.2			9.65
47 (22)	9.12	Fe ³⁺ / NaOH/ air		0.011	20.2	16.6			0.69
58 (22)	10.20	Fe ³⁺ / NaOH/ air		0.00040	22.7	14.5			9.27
23	6.45	Al ³⁺ / NaOH, CaCl ₂ / air	0.028		34.0	14.1	17.7	29.8	0.86
24	6.94	Fe ²⁺ / NaOH, CaCl ₂ / air		BDL	17.0	5.85	7.9	14.4	0.41
50 (24)	6.45	Fe ²⁺ / NaOH, CaCl ₂ / air		BDL	14.1	9.2	1.02	1.08	0.26
25	7.12	Fe ³⁺ / NaOH, CaCl ₂ / air		BDL	23.2	12.9	13.9	19.3	0.75
26	7.10	Fe ³⁺ / NaOH, CaCl ₂ / N ₂		BDL	21.7	12.3	14.0	19.2	0.60
51 (26)	6.40	Fe ³⁺ / NaOH, CaCl ₂ / N ₂		BDL	13.6	9.7	11.0	10.3	0.21
57 (26)	10.91	Fe ³⁺ / NaOH, CaCl ₂ / N ₂		BDL	21.7	13.2	13.3	15.7	1.49
27	8.30	Al ³⁺ / NaOH, CaCl ₂ / N ₂	0.57		26.3	14.9	16.9	22.1	0.86
28	7.42	Fe ²⁺ / NaOH, CaCl ₂ / N ₂		BDL	13.4	6.55	8.0	10.5	0.41

Table 3.11: Ion concentrations in mmol_c/L in the supernatant solutions upon completion of titrations performed for experiment 2. Final pH measured immediately prior to analysis.

Titration No.	pH	Reaction conditions	Al ³⁺	Tot Fe (as Fe ³⁺)	Na ⁺	Ca ²⁺	SO ₄ ²⁻	Cl ⁻	OH ⁻
29	6.67	Al:Fe = 6:1/ N ₂	BDL	BDL	18.3	7.5	10.5	14.0	0.23
52 (29)	6.50	Al:Fe = 6:1/ N ₂	BDL	BDL	14.2	10.3	11.6	10.6	0.32
30	6.19	Al:Fe = 2:1/ N ₂	BDL	0.0019	21.3	10.0	13.5	16.1	0.29
53 (30)	10.20	Al:Fe = 2:1/ N ₂	0.97	BDL	22.5	10.4	11.3	17.2	1.77
31	7.70	Al:Fe = 2:3/ N ₂	BDL	BDL	23.9	13.2	16.6	18.5	0.69
32	6.50	Al:Fe = 6:1/ air	BDL	BDL	15.4	7.70	9.30	12.2	0.49
33	7.05	Al:Fe = 2:1/ air	BDL	BDL	24.7	7.70	11.5	20.0	0.46
34	6.60	Al:Fe = 2:3/ air	BDL	BDL	33.8	11.2	16.0	30.0	0.88

The titrations performed for experiment 2 (Table 3.11) have metal concentrations all below detectable limits except for solutions 30 and 53, which have very low concentrations of Fe and Al, respectively. An average of 60% of the Ca added has been removed from solution and the amount remaining is less than equimolar with SO₄. Again, more SO₄ is removed from solution when the Al concentration is high, and close to zero SO₄ is removed when the Fe concentration is high. There is again a fairly large amount of Cl that has been removed from solution, approximately 31%. The highest amounts of Cl are removed from solution when Fe concentrations are high and very little SO₄ has been removed from solution.

The downscale titrations (35 – 43 and 54) in Table 3.12 show a very different pattern from the upscale titrations. There is a high concentration of metal still in solution. Titrations 35, 36, 41 and 42 with the 2:1 Al:Fe sulphate solution as the acid, show a considerable decrease in metal concentration, with greater Al and Fe removal occurring in an anoxic environment. Where SAMD is the acid however very little Al is removed and only slightly more Fe is removed.

The type of base does not seem to make a difference to metal removal. Where only a small amount of Al is removed (titrations 37 – 40 and 43), no SO₄ is removed from solution. Where a considerable amount of Al is removed a correspondingly large amount of SO₄ is also removed. Less SO₄ is removed when FAL is the base (titrations 35 and 36) than when CaCl₂/NaOH is the base. Repeat titration 54 replicates the

corresponding Al and SO₄ removal from solution and also shows a considerable decrease in the Cl concentration.

Table 3.12: Ion concentrations in mmol_c/L in the supernatant solutions upon completion of titrations performed for experiment 3. Final pH measured immediately prior to analysis.

Titre No.	pH	Reaction conditions	Al ³⁺	Tot Fe (as Fe ³⁺)	Na ⁺	Ca ²⁺	SO ₄ ²⁻	Cl ⁻	OH ⁻
35	4.00	Al:Fe = 2:1/ FAL/ N ₂	18.8	13.5	0.39	15.8	48.2	0.40	BDL
36	6.53	Al:Fe = 2:1/ FAL/ air	12.5	8.92	0.17	15.5	39.4	0.20	0.57
37	3.42	SAMD/ FAL/ N ₂	22.8	5.85	0.18	27.2	68.6	0.27	BDL
38	3.61	SAMD/ FAL/ air	8.33	2.22	0.12	20.5	38.3	0.38	BDL
39	3.84	SAMD/ NaOH, CaCl ₂ / air	10.3	2.67	14.1	15.3	37.0	11.3	BDL
54 (39)	4.22	SAMD/ NaOH, CaCl ₂ / air	5.98	1.55	13.8	15.3	BDL	BDL	BDL
40	3.36	SAMD/ NaOH, CaCl ₂ / N ₂	12.4	3.13	14.3	15.9	41.6	11.3	BDL
41	4.12	Al:Fe=2:1/NaOH, CaCl ₂ / N ₂	6.97	5.87	8.16	6.47	21.7	6.46	BDL
42	4.12	Al:Fe=2:1/NaOH, CaCl ₂ / air	5.19	5.29	9.43	7.7	19.0	7.02	BDL
43	3.69	SAMD/NaOH, CaCl ₂ , Si/air	9.88	2.74	15.5	16.5	35.4	11.6	BDL
44	7.55	SAMD/NaOH, CaCl ₂ , Si/air	0.46	BDL	32.4	13.8	17.8	27.0	0.55
55	6.30	SAMD/ FAL/ air		BDL	0.30	15.2	BDL	BDL	0.30
56	9.12	SAMD/ FAL/ N ₂		0.58	0.0064	0.23	9.2	BDL	BDL
									0.85

The upscale titration of SAMD and FAL in air (titration 55) shows complete metal and SO₄ removal with Ca the only ion remaining in solution. The upscale titration of SAMD and FAL in N₂ (titration 56) has a very small amount of Al and Fe still in solution

3.8 Mineral saturation indices

The results of the saturation index (SI) calculations using the PHREEQC model are presented in Tables 3.13, 3.14 and 3.15 for experiments 1, 2 and 3, respectively. How the calculations are achieved is described as following. The PHREEQC programme calculates single ion activities based upon pH and ion concentration input data measured for the supernatant solutions from each titration. The calculation makes use of a thermodynamic database (PHREEQC) of ion association constants that allow for the speciation of the solution to be calculated by a method of iterative convergence such that a constant ionic strength criterion is employed to determine the outcome of ion activity and ion pair calculations involving all possible species in solution. These

single ion activities relating to possible mineral solids of interest are then employed to calculate the ion activity product (IAP), which is then compared with the corresponding solubility product (K_{sp}) to determine the saturation index of each mineral solid by:

$$SI = \log IAP - \log K_{sp}$$

Consequently, a SI of 0 represents equilibrium between the solution and the mineral in question. Positive and negative SI values indicate that the solution is undersaturated or oversaturated with respect to the mineral in question. The closer the SI is to 0, the greater is the likelihood that near-equilibrium has been achieved between the solution and the mineral in question. Although the SI cannot be used to prove that a particular mineral has formed and/or exerts a controlling influence on solution composition, it can provide valuable combinations of expected equilibria based on other evidence (e.g. mineralogical existence from XRD). One important qualification should be made in such interpretations, however, relating to the Guy-Lussac-Ostwald (GLO) step rule (Sposito, 1984), which dictates that if a solution is supersaturated with respect to more than one solid phase with the same stoichiometry (e.g. bayerite and gibbsite), then the least stable of these solids is the one most likely to form and, subsequently, to control solution composition until such time as it has dissolved significantly allowing the formation of a more stable (i.e. more crystalline) solid. The metastable character of the solid phase may dictate that this recrystallisation will take much longer than the normal period of experimental observation. The most stable phase of an assemblage of competing solids is therefore the least likely to form.

Where Al or Fe are detectable in the supernatant solution (Table 3.13) gibbsite and amorphous $Al(OH)_3$ or goethite and amorphous $Fe(OH)_3$ appear as phases in solution, respectively. From the XRD data it is evident that amorphous $Fe(OH)_3$ is kinetically favoured in titrations 18d and 51, whereas all titrations containing Al alone result in crystalline bayerite, and pseudo-boehmite in the case of titration 46. Those solutions containing Fe with a pH between 8 and 9 are close to being in equilibrium with respect to natrojarosite. Below a pH of 8 the solution is supersaturated with respect to natrojarosite. Since goethite is the predominant phase precipitating it is more than likely that it alone is controlling the solubility of Fe where it exists in solution. The supernatant solutions approach equilibrium with gypsum in all titrations containing $CaCl_2$.

Table 3.13: The saturation indices for selected phases in the supernatant solutions for each titration in experiment 1. The (a) designates amorphous material.

Titration No.	pH	Reaction conditions	Al(OH) ₃ (a)	Fe(OH) ₃ (a)	Gbb*	Gth	Gyp	Jrb	Na-jrs
17	8.50	Al ³⁺ / NaOH/ air	-2.03	0.65				6.67	-
45 (17)	10.3	Al ³⁺ / NaOH/ air	-2.06	0.63				-9.91	
46 (17)	6.10	Al ³⁺ / NaOH/ air							
18b	8.78	Fe ²⁺ / NaOH/ air							
18c	8.52	Fe ²⁺ / NaOH/ air							
18d	8.60	Fe ²⁺ / NaOH/ air		1.91	7.80				-2.22
19	3.20	Fe ²⁺ / NaOH/ N ₂		-7.00	-1.11				-11.5
19b	3.82	Fe ²⁺ / NaOH/ N ₂		-6.16	-0.27				-10.3
49a (19)	8.40	Fe ²⁺ / NaOH/ N ₂		1.79	7.68				-2.07
49b (19)	8.72	Fe ²⁺ / NaOH/ N ₂							
20	8.40	Al ³⁺ / NaOH/ N ₂	-0.62	2.07				-4.61	
21	7.60	Fe ³⁺ / NaOH/ N ₂		2.71	8.60				3.85
48 (21)	8.53	Fe ³⁺ / NaOH/ N ₂		1.99	7.89				-1.09
22	8.90	Fe ³⁺ / NaOH/ air							
47 (22)	9.12	Fe ³⁺ / NaOH/ air		1.88	7.77				-2.29
58 (22)	10.2	Fe ³⁺ / NaOH/ air		-0.47	5.42				-12.7
23	6.45	Al ³⁺ / NaOH, CaCl ₂ / air	0.06	2.75		-0.53	-0.86		
24	6.94	Fe ²⁺ / NaOH, CaCl ₂ / air				-1.04			
50 (24)	6.45	Fe ²⁺ / NaOH, CaCl ₂ / air				-1.64			
25	7.12	Fe ³⁺ / NaOH, CaCl ₂ / air				-0.60			
26	7.10	Fe ³⁺ / NaOH, CaCl ₂ / N ₂				-0.61			
51 (26)	6.40	Fe ³⁺ / NaOH, CaCl ₂ / N ₂				-0.73			
57 (26)	10.9	Fe ³⁺ / NaOH, CaCl ₂ / N ₂				-0.60			
27	8.30	Al ³⁺ / NaOH, CaCl ₂ / N ₂	-0.25	2.44		-0.50	-4.76		
28	7.42	Fe ²⁺ / NaOH, CaCl ₂ / N ₂				-0.97			

*Gbb = Gibbsite, Gth = Goethite, Gyp = Gypsum, Jrb = Jurbanite and Na-jrs = Natrojarosite.

The saturation indices for the titrations performed during experiment 2 (Table 3.14) do not contain very much information as only solutions from titrations 30 and 53 contain metals in detectable concentrations. All solutions are undersaturated with respect to gypsum but the saturation indices for gypsum are close enough to 0 to assume a near-equilibrium state. It can be assumed from experiment 1 that goethite controls the solubility of Fe in titration 30 and ettringite is controlling the solubility of Al in titration 53. All the precipitates formed from this experiment displayed very poor crystallinity with XRD analysis. Only titration 52 can clearly be seen to contain goethite and only titrations 31 and 34 contain bayerite. Calcite is present in titrations 31, 32, 33 and 34.

Table 3.14: The saturation indices for selected phases in the supernatant solutions for each titration in experiment 2. The (a) designates amorphous material and the base is the NaOH-CaCl solution in all cases.

Titration No.	pH	Reaction conditions	Al(OH) ₃ (a)	Fe(OH) ₃ (a)	Ett*	Gbb*	Gth*	Gyp*
29	6.67	Al:Fe = 6:1/ N ₂						-0.86
52 (29)	6.50	Al:Fe = 6:1/ N ₂						-0.69
30	6.19	Al:Fe = 2:1/ N ₂			-1.98		4.00	-0.69
53 (30)	10.2	Al:Fe = 2:1/ N ₂	-1.90	-1.36		0.79		-0.74
31	7.70	Al:Fe = 2:3/ N ₂						-0.54
32	6.50	Al:Fe = 6:1/ air						-0.87
33	7.05	Al:Fe = 2:1/ air						-0.85
34	6.60	Al:Fe = 2:3/ air						-0.65

*Ett = Ettringite, Gbb = Gibbsite, Gth = Goethite and Gyp = Gypsum.

From the XRD results, the Fe and Al solubility is likely to be controlled in all titrations in Table 3.15 by amorphous Fe(OH)₃ and Al(OH)₃, respectively, since no crystalline material is present in the precipitate. All titrations are near equilibrium with respect to gypsum. In the downscale titrations (35 – 43, 54) the solubility of SO₄ may be controlled by jurbanite, with respect to which every solution is supersaturated except that from titration 54.

Table 3.15: The saturation indices for selected phases in the supernatant solutions for each titration in experiment 3. The (a) designates amorphous material and the shaded area indicates downscale titrations.

Ttn No.	pH	Reaction conditions	Al(OH) ₃ (a)	Fe(OH) ₃ (a)	Gbb*	Gth*	Gyp*	Jrb*	Na-jrs*
35	4.00	Al:Fe = 2:1/ FAL/ N ₂		-2.52	-4.75	0.17	1.14	-0.25	1.87 -8.32
36	6.53	Al:Fe = 2:1/ FAL/ air		2.72	2.59	5.41	8.48	-0.21	2.18 5.86
37	3.42	SAMD/ FAL/ N ₂		-4.38	-6.99	-1.69	-1.10	0.04	1.17 -13.3
38	3.61	SAMD/ FAL/ air		-4.04	-6.72	-1.35	-0.81	0.14	1.13 -13.6
39	3.84	SAMD/ NaOH, CaCl ₂ / air		-3.33	-6.01	-0.64	-0.12	0.30	1.40 -10.2
54 (39)	4.22	SAMD/ NaOH, CaCl ₂ / air		-1.51	-4.87	1.18	1.02		
40	3.36	SAMD/ NaOH, CaCl ₂ / N ₂		-4.48	-7.16	-1.79	-1.27	0.27	1.09 -12.3
41	4.12	Al:Fe=2:1/NaOH, CaCl ₂ / N ₂		-2.42	-4.72	-0.32	1.23	-0.76	1.49 -7.62
42	4.12	Al:Fe=2:1/NaOH, CaCl ₂ / air		-2.50	-4.68	-0.19	1.22	-0.72	1.37 -7.75
43	3.69	SAMD/NaOH, CaCl ₂ , Si/air		-3.62	-6.28	-0.93	-0.39	0.29	1.29 -10.7
44	7.55	SAMD/NaOH, CaCl ₂ , Si/air	0.33			3.02		-0.53	-2.75
55	6.30	SAMD/ FAL/ air							
56	9.12	SAMD/ FAL/ N ₂		-0.99	1.64	1.68	7.54		

* Gbb = Gibbsite, Gth = Goethite, Gyp = Gypsum, Jrb = Jurbanite and Na-jrs = Natrojarosite.

3.9 Discussion

The potentiometric titrations define the buffering ranges for metal hydroxide precipitation to be at pH values 3.5, 4, 6, and 10 for upscale titrations. Downscale titrations show buffering ranges at 12 – 11, 9, 7 and 4.5. The downscale buffering regions are not as pronounced as those for the upscale titrations. This is because the precipitation and oxidation of Fe releases more acidity per unit volume and as a result the pH decreases at a much faster rate than titrant addition could account for. These buffering regions are an important aspect of the neutralisation process as each buffer must be surpassed in order to achieve complete metal removal from the waste water. Although upscale titrations were taken to high pH values (> 10) during the experiment, the equilibrium pH is much lower. For many of the titration solutions the pH is close to 8.3, which is the equilibrium pH of CaCO_3 . The formation of CaCO_3 probably has the largest influence on the decrease in pH and the removal of Ca from solution. Some titration solutions however, have a pH that has been decreased to 6 or less. This indicates that an amount of unoxidised Fe was still present in solution, which on oxidising released enough acidity to decrease the pH to circumneutral values. The titration solutions that have maintained a high pH have small amounts of Fe remaining in solution indicating that oxidation was not complete. Thus the rate of oxidation of the reaction is an important factor in determining metal removal. This is evidenced in the sawtooth pattern of the Fe^{2+} curves, which is a redox effect, displayed as a consequence of the titration equipment used. The $\text{Al}_2(\text{SO}_4)_3$ and $\text{Fe}_2(\text{SO}_4)_3$ titration curves do not show any difference between oxic and anoxic environments is to be expected as there is no oxidation taking place. The rate of the reaction was not specifically investigated during the course of these experiments but a slower reaction rate and efficient aeration can be seen to promote maximum metal removal.

The amount of base required to surpass the buffered area for each titration is inversely proportional to the concentration of each metal in the acidic solution for all the solutions except for a Fe:Al ratio of 6:1. Put simply, the less of each metal in solution the greater the buffer region for that metal. This suggests that the higher concentration of the acid solution has an impact on how quickly metal precipitation occurs, more so for Al than for Fe. Another reason for this trend could be surface induced

precipitation. As a metal hydroxide precipitates its surface acts as a catalyst for further precipitation, much as a seed crystal does. This surface induced precipitation is a much overlooked phenomenon (Hansen and Taylor, 1990).

The XRD patterns of simple solutions show the precipitate to contain goethite and bayerite with poor crystallinity. When the precipitate results from more complicated solutions, i.e. SAMD and FAL, no phases can be identified with XRD. The fact that the precipitated material is amorphous indicates that there are processes interfering with the ordered arrangement and the formation of the kinetically favoured metastable phase (Sposito, 1984). The lack of crystallinity is likely to be a result of the 1:1 Al:Fe ratio in SAMD because the XRD patterns for experiment 2 show the precipitates to be amorphous when the Al:Fe ratio is high. The formation of an amorphous precipitate may also be a result of SO₄ being incorporated into the structure of the material and deforming the lattice enough to prevent an ordered arrangement.

From the anion and cation data it can be seen that a large amount of Ca is being removed from solution. This could be a result of the formation of calcite, as discussed above, but there is a possibility that Ca may be being included in structure of the material precipitating as an Al hydroxysulphate compound similar to the pyroaurite and hydrotalcite-like minerals, which have the general formula [M_{1-x}²⁺M_x³⁺(OH)₂]^{x+}[X_{x/m}^{m-}•nH₂O], where M²⁺ = Mg²⁺, Ni²⁺, Zn²⁺ ...; M³⁺ = Al³⁺, Fe³⁺ ...; X^{m-} = OH⁻, Cl⁻, NO₃⁻, CO₃²⁻ ..., and 0.25 ≤ x ≤ 0.33 (Bigham and Nordstrom, 2000; Thevenot *et al.*, 1989; Allman, 1968).

Where Al and not Fe was the metal cation a higher amount of SO₄, as much as 6 times, has been removed out of solution. There is also a small amount of Cl that has been removed from solution, which may also be being included in the structure of the material precipitating. Another reason for SO₄ removal could be the adsorption of this anion on a positively charged surface. The minor inflection visible between pH 5 and 6 in the graphs of Al₂(SO₄)₃ and Fe₂(SO₄)₃, which is attributed to the neutralisation of excess protons of Al-OH₂ groups, could instead be the adsorption of SO₄ onto the surface to balance the excess positive charge. It seems however, likely that SO₄ adsorption would occur on both Al- and Fe-hydroxides and that SO₄ removal would not be so closely linked with Al removal.

This pattern of Al and SO₄ being coincidentally removed is displayed in all the titrations where a large amount of Al is removed. Where no or very little Al is removed no SO₄ has been removed from solution.

Very little SO₄ is removed when there is no Ca is present in the titration. The coinciding removal of Ca and SO₄ may simply be as a result of the precipitation of gypsum. This reason does not seem likely, however, because the number of moles of each ion being removed is not equivalent. The ion data for the titrations in experiment 1 and 2 show a much higher amount of Ca being removed from solution than SO₄. The ion data for the downscale titrations show a much higher amount of SO₄ removed than Ca, this is because there was a fixed volume of base and the acid was the titrant, so that there was a finite amount of Ca at the start.

3.10 Conclusions

Upscale potentiometric titrations of SAMD show buffer zones at pH values 3.5, 4, 6 and 10 corresponding to Fe³⁺ precipitation, Al³⁺ precipitation, Fe²⁺ hydrolysis and oxidation and Al(OH)₃ re-dissolution, respectively.

Downscale potentiometric titrations with SAMD show buffer zones at pH values 12 – 11, 9 and 4.5, which correspond to Fe³⁺ precipitation and Fe²⁺ oxidation and hydrolysis, Al³⁺ precipitation and Al(OH)₃ re-dissolution, respectively. A sharp decrease in EC values occurs in downscale potentiometric titrations, so that the minimum EC is slightly lower than the minimum EC for upscale titrations.

Goethite, bayerite, calcite and maghemite are the only crystalline phases identifiable by XRD while solutions with a high Al:Fe molar ratio in the acidic sulphate solution results in material in which no phase can be identified.

Anion and cation data indicate that an aluminium sulphate phase is precipitating because more SO₄ is precipitated from solution when a high amount of Al is precipitated from solution. This aluminium sulphate phase is, however, not crystalline and cannot be identified by XRD. No sulphate is removed from solution when Ca is

absent from the reaction. A higher concentration of Fe and Al are precipitated from solution during upscale reaction than during downscale titration. In the supernatant solutions of the upscale titration of SAMD with FAL in air Fe, Al and SO₄ are all below detectable limits.

Chapter 4

Characterisation of reaction solids

4.1 Introduction

The previous chapter dealt with the neutralisation of mixed Al:Fe acid solutions in detail. Buffer zones for Fe^{II} oxidation and Fe^{III} and Al precipitation were clearly established. The results indicated that in a reaction involving mixed Al:Fe solutions the product was amorphous. The anion and cation data indicated that along with goethite, bayerite and gypsum an Al-sulphate mineral was also precipitating although it was not crystalline and could not be identified by XRD.

This chapter deals in greater detail with the nature of the neutralisation product. This material is expected to be predominantly composed of an iron hydroxide, either ferrihydrite or goethite. The most significant investigations in the literature deal with the co-precipitation of Fe and Al (Bigham *et al.*, 1990; Bigham, 1994; Brophy *et al.*, 1962; Brophy and Sheridan 1965; Schwertmann and Fitzpatrick, 1992), and the potential substitution of Al for Fe in the iron hydroxides that precipitate (Fey and Dixon, 1981; Schwertmann and Cornell, 2000). Another important consideration is the influence of SO₄, either included in the structure (Alpers, 1994; Jambor *et al.*, 2000; Bigham and Nordstrom, 2000), or adsorbed onto the surface of the material.

Precipitates were produced at different pH values using FAL and SAMD with different Fe:Al ratios. The products were then characterised using a range of instrumental methods and the solution chemistry and surface charge of the products were also investigated.

4.2 Materials and methods

4.2.1 Fly ash leachate

Large quantities of FAL were used. Two kg of fly ash were placed in plastic containers with a volume of 5 L. To this was added 2 L of distilled water. The jar was

sealed and agitated on a reciprocating shaker for 24 hours, and the mixture was then filtered using a Büchner suction funnel and kept in a sealed container.

4.2.2 Simulated acid mine drainage

The SAMD was made by the same method as that described in Chapter 3, but with different amounts of Al added. The concentrations of $\text{Fe}_2(\text{SO}_4)_3 \cdot \text{XH}_2\text{O}$, $\text{FeSO}_4 \cdot 7\text{H}_2\text{O}$, $\text{CaSO}_4 \cdot 2\text{H}_2\text{O}$ and H_2SO_4 (1M) were the same as specified in Chapter 3. The amount of $\text{Al}_2(\text{SO}_4)_3 \cdot 18\text{H}_2\text{O}$ added was decreased to give Fe:Al molar ratios 2.5, 0.8 and 7.3. The Fe^{3+} and Fe^{2+} concentrations were 7.3 and 3.6 mmol/L, respectively, for all ratios. For the molar ratios 2.5, 0.8 and 7.3 the Al concentration was 4.4, 13.3 and 1.5 mmol/L, respectively. Table 4.1 shows the initial volume of SAMD or FAL used and its pH and EC. The volume of acid or base added to achieve the final pH is given as well as the final EC. All but one of the products was precipitated under oxic conditions.

4.2.3 Preparation of products for analysis

Precipitates were stored in 150 mL plastic containers in the solution from which they precipitated. In preparation for analysis the bulk of the supernatant was poured off and stored. The products were washed several times by pouring out the excess liquid, adding distilled water, allowing the precipitate to settle and repeating the procedure until the precipitate was free of salts. The products were then dried at 70°C. The dried product was ground in an agate mortar in preparation for analysis.

Table 4.1 shows the reaction conditions for the precipitates numbered 1 – 12. The molar ratios of Fe:Al in the SAMD are shown as well as the initial volume of solution present in the beaker to which the titrant was added. In the upscale reactions the initial volume refers to SAMD and in the downscale reactions the initial volume refers to FAL. The initial (before titration) and final pH and EC are shown as well as the nature of the gas bubbled through the solution during titration.

Table 4.1: Reaction conditions for precipitation products showing the different SAMD molar ratios. Samples 6-10 are downscale reactions and the initial volume is that of FAL.

Sample No	Fe:Al molar ratio in SAMD	Initial Vol mL	pH	EC (mS/m)	Final pH	Gas
1	7.3	1500	2.36	409	3.03	299 air
2	0.8	1500	2.48	487	3.24	394 air
3	0.8	1500	2.61	472	4.19	328 air
12	0.8	1500	2.46	520	4.27	362 air
4	2.5	1500	2.37	405	4.48	271 air
5	7.3	1500	2.39	409	6.97	245 air
11	7.3	1500	2.38	416	9.20	281 N ₂
6	7.3	900	12.60	1221	6.75	261 air
7	7.3	900	12.65	1172	8.42	260 air
8	0.8	1000	12.60	1222	7.52	303 air
9	0.8	900	12.60	1264	8.14	212 air
10	7.3	900	12.62	1295	11.24	221 air

4.3 Analysis

The analytical methods used for the experiments outlined in this chapter not described here can be found in Chapter 3, these are XRD for the solid product and IC, AAS and ICP for the supernatant solutions.

The surface area of the precipitates was determined through the Brunauer-Emmett-Teller method of analysis using a Micromeritics Accelerated Surface Area and Porosimetry (ASAP) 2010 system. An amount of product of approximately 250 mg, was subjected to degassing at 120 °C for approximately 24 hours. This degassing stage rids the product of adsorbed gases and H₂O. The product was then placed in a N₂ stream and the mass change of the solid due to gas adsorbed was measured relative to the change in partial pressure of N₂.

For analysis by infrared spectroscopy approximately 2 mg of precipitate was milled with 200 mg of KBr in an agate mortar, the powdered mixture was placed in an steel die used for the purpose of pressing the powder into discs. A vacuum pump was attached to the die and a vacuum was applied for approximately 2 minutes. Ten tonnes of pressure were applied, three times, to the die for periods of 2 minutes at a

time. The die was opened and the product, now pressed into a small transparent disc was loaded into the spectrometer. A background spectrum was first obtained using a blank KBr disc before the precipitates were run. The spectra were recorded as transmittance spectra.

Thermal gravimetric and differential thermal analysis (TGA/DTA) was performed using a Stanton Redcroft Simultaneous Thermal Analyser (STA 780). Approximately 50 mg of product was heated in air from room temperature to about 600 °C at a rate of 10.3 °C·min⁻¹.

The surface charge of the products was determined using a similar approach to that described by Hunter (1981). Three solutions of KCl were made up in concentrations of 1.00, 0.10 and 0.01 M. These solutions were titrated with HCl or NaOH to obtain a correction curve, indicating the buffering capacity of each KCl solution. A total of 15 suspensions of each product were prepared using a 20 mg of sub-sample and 10 mL of KCl solution. To each suspension a acid or base was added to give a pH value within a range of 3.0 and 9.0. The suspensions were agitated overnight on a reciprocating shaker and the final pH was measured. The volume of acid or base required to reach a particular suspension pH was corrected by subtracting the volume required to reach the same pH in KCl solution without the suspended solid. A family of curves was plotted for each solid at the different KCl concentrations

4.4 Results

The results presented in this chapter characterise the precipitates produced at different pH values from SAMD and FAL. These reaction products are labelled 1-12 and the reaction conditions are summarised in Table 4.1. Sample 13 is waste sludge produced by neutralising AMD with lime and was obtained from Landau colliery.

4.4.1 Anion and cation data

Table 4.2 shows the total amount of all ions in the solutions used to precipitate products 1-12. Table 4.3 shows the ion data for the supernatant solutions after the

products 1 – 12 were prepared and removed from solution. Samples 6 – 10 were prepared by downscale reaction. The K, Mg, Na and Cl ions were introduced into solution by the FAL and occur in only small amounts. Of the Ca present only 5 mmol/L was added with the SAMD and approximately 3.6 mmol/L of SO₄ was added with the FAL.

Table 4.2: Quantities (mmol_c) of ionic reactants used in preparing products of different Fe:Al molar ratios.

No.	Fe:Al	K ⁺	Mg ²⁺	Na ⁺	Ca ²⁺	Fe tot	Al ³⁺	SO ₄ ²⁻	Cl ⁻	OH ⁻
1	7.3	0.09	0.0031	0.15	59.3	49.1	59.9	129	0.090	18.1
2	0.8	0.05	0.0019	0.11	49.6	49.1	6.75	76.0	0.061	14.2
3	0.8	0.12	0.0045	0.23	81.6	49.1	6.75	78.7	0.26	33.9
12	0.8	0.11	0.0040	0.17	81.7	49.1	6.75	83.4	0.26	30.5
4	2.5	0.13	0.0037	0.24	62.7	49.1	19.8	85.2	0.22	24.9
5	7.3	0.17	0.0025	0.30	63.6	49.1	59.9	125	0.37	26.5
11	7.3	0.11	0.0040	0.17	81.7	49.1	59.9	137	0.26	30.5
6	7.3	0.075	0.0060	0.17	72.2	45.8	55.9	124	0.13	33.0
7	7.3	0.075	0.0045	0.17	64.0	39.2	47.9	107	0.11	28.0
8	0.8	0.11	0.0025	0.23	61.0	21.1	2.90	34.1	0.51	36.0
9	0.8	0.057	0.0030	0.14	64.3	14.0	1.92	31.4	0.16	29.9
10	7.3	0.057	0.0030	0.14	65.7	18.5	22.5	58.1	0.16	29.9

The supernatant data show that none of the K, Mg, Na and Cl was removed from solution and was, therefore, not involved in product precipitation. There is 94% Al removal in solution 1 because the starting Al concentration is low. Solutions 2 and 3 show no Al removal because the pH is very low and the Al concentration is high. Solutions 4 and 5 both have 70 and 76% Al removal, respectively. This is possibly a result of the higher Fe concentration in solution. Solutions 6 – 11 show complete Al removal. For Solutions 1 – 5 Fe removal is not complete but is still quite high at 74%, 58%, 71%, 70% and 76% respectively. Solutions 6 – 12 show complete Fe removal from solution. Only solutions 11 and 12 show significant Ca and SO₄ removal. Calcium removal for solutions 11 and 12 is 61% for both and SO₄ removal is 65% and 78% respectively. It is probable that a large amount of Ca removed is due to calcite precipitation. Sulphate concentrations in the supernatant correlate quite well with the molar ratio of Fe:Al. When the Fe:Al ratio is low very little to no SO₄ is removed, while low Fe:Al ratios correspond with significant SO₄ removal from solution. The

one exception of this correlation is in solution 1 where the small amount of Al originally added has precipitated out along with a significant amount of SO₄. More SO₄ is removed in the circumneutral pH range than Ca.

Table 4.3: Ion concentrations in mmol/L in the supernatant solutions upon completion of titration. Final pH measured immediately prior to analysis.

No.	Fe:Al	pH	K ⁺	Mg ²⁺	Na ⁺	Ca ²⁺	Fe tot	Al ³⁺	SO ₄ ²⁻	Cl ⁻	OH ⁻
1	7.3	3.20	0.18	0.15	0.26	62.3	12.5	3.45	81.9	1.59	BDL
2	0.8	3.26	0.11	0.21	0.20	56.6	20.6	49.8	143	0.31	BDL
3	0.8	4.27	0.16	0.20	0.33	85.6	14.2	23.0	133	1.98	BDL
12	0.8	4.23	0.081	0.16	0.30	87.0	14.6	4.71	145	1.18	BDL
4	2.5	4.30	0.29	0.21	0.31	67.8	11.7	3.24	84.1	0.73	BDL
5	7.3	6.45	0.39	0.14	0.36	68.6	0.021	BDL	70.7	0.46	1.68
11	7.3	6.57	0.088	0.073	0.18	83.1	BDL	BDL	83.4	BDL	0.60
6	7.3	6.00	0.13	0.12	0.23	73.3	BDL	BDL	71.9	1.18	0.48
7	7.3	6.25	0.26	0.096	0.27	66.4	0.0011	BDL	62.7	0.53	0.78
8	0.8	6.88	0.14	0.038	0.28	60.9	BDL	BDL	58.6	0.22	1.37
9	0.8	7.11	0.09	0.023	0.19	31.8	BDL	BDL	30.1	0.15	1.05
10	7.3	10.7	0.35	0.0073	0.16	31.6	BDL	0.11	29.2	0.75	3.08

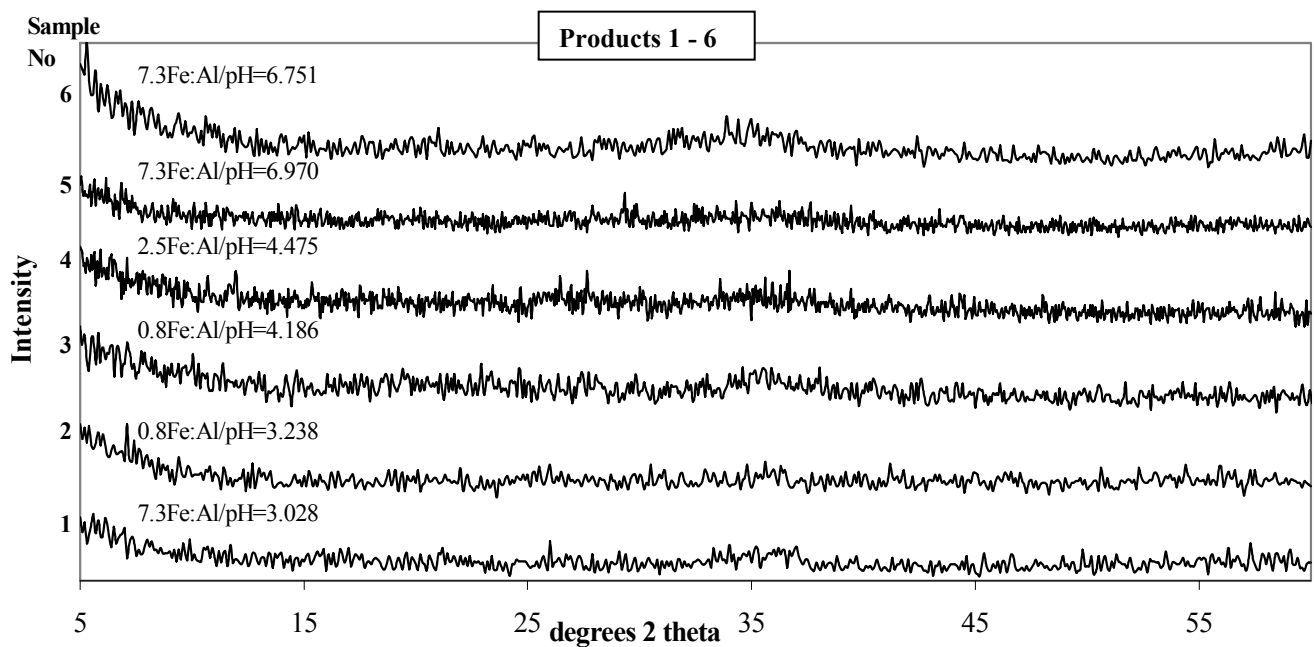


Figure 4.1: XRD spectra for products 1 – 6, showing Fe:Al ratios and final solution pH.

4.4.2 X-ray diffractometry

Products from titrations 1 – 6 are shown in Figure 4.1. The diffractograms in Figure 4.1 display a single broad, shallow halo in the region of 30 to 40° 2θ . This is an indication that the products have very poor crystallinity.

Figure 4.2 shows the XRD spectra for products 7 – 12. Samples 8 and 9 contain bayerite of very poor crystallinity. These products were produced by downscale addition of acid and have a larger proportion of Al than products 6, 7 and 10.

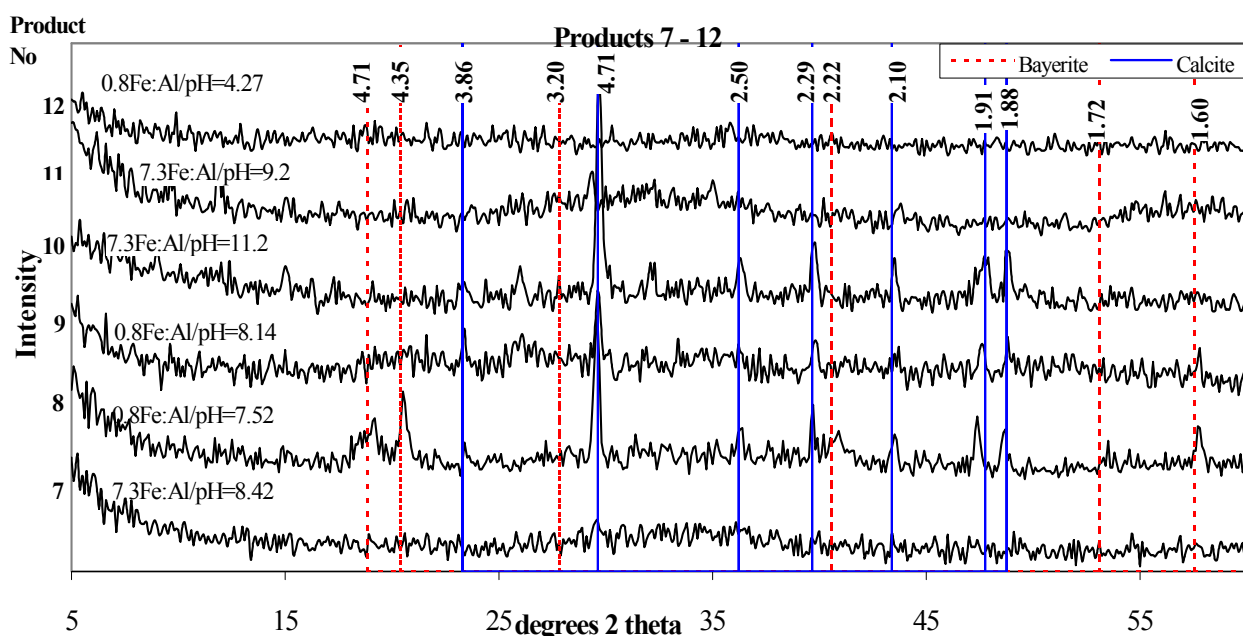


Figure 4.2: XRD spectra for products 7 – 12 (y-axis), showing Fe:Al ratios and final solution pH. Bayerite and calcite lines are labelled.

Products 8, 9 and 10 also contain calcite. The calcite pattern for product 10 has the greatest intensity and its solution pH was much higher than those of the other solutions. Calcite formation in products 9 and 10 accounts for the significant Ca removal discussed above. The diffractogram for product 11 exhibits only broad, shallow halos in the ranges of 30 - 35° 2θ and 52 - 60° 2θ , indicating very low crystallinity. This may be due either to the fact that the reaction was carried out under nitrogen or that it was taken to a relatively high pH of 9.2 as compared to the other upscale titrations. The only mineral clearly identifiable by XRD in the Landau waste (Sample 13) is gypsum (Figure 4.3).

Sample 13

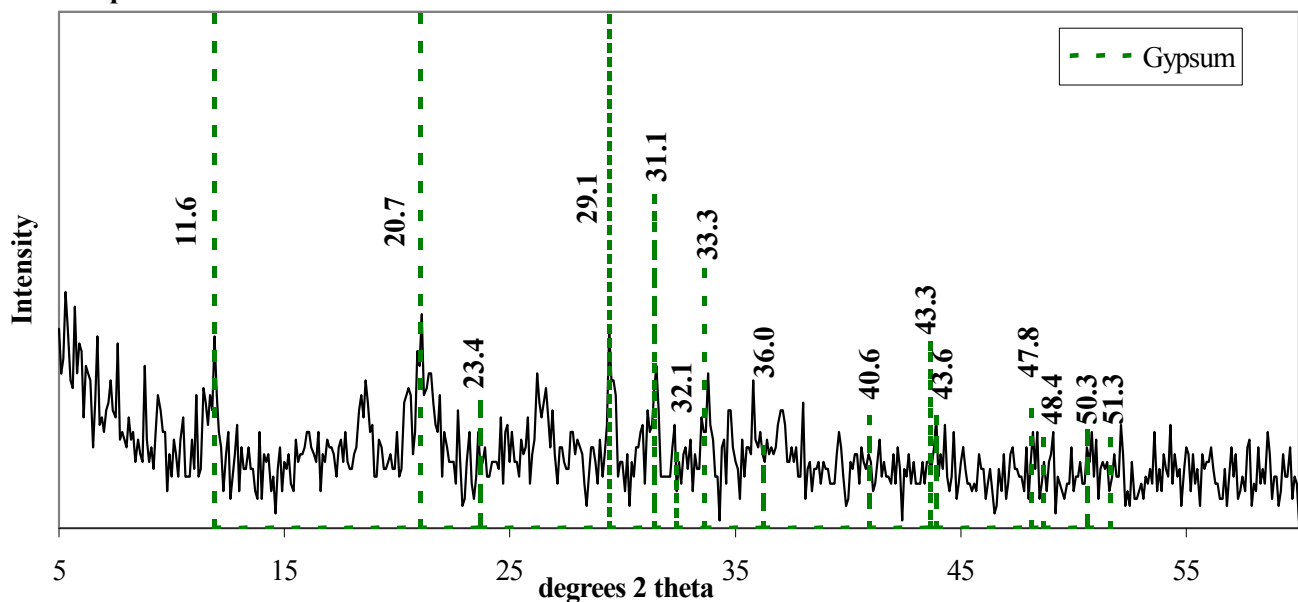


Figure 4.3: XRD pattern of waste sludge produced by the neutralisation of AMD with lime from Landau colliery.

4.4.3 Thermal gravimetric and differential thermal analysis

The TGA and DTA curves for all products, including the waste sludge from Landau colliery, are shown in Figure 4.4. Although the products were heated to 600 °C, Figure 4.4 only has a scale to 320 °C because very little change in the thermographs is observed after this temperature, with one exception mentioned in the text. Product 1 shows a large endotherm at 165°C with a slight shoulder at 140°C. Product 3 has a peak of similar shape except it occurs at 150°C and the shoulder, which is larger than for product 1, occurs at 125°C. This small peak at 125°C can also be seen in products 2, 7 and 13. After the initial endotherm for products 1, 2, 3, 7 and 13 there is a broad exotherm that gradually flattens off. The exotherm for product 7 occurs at a lower temperature, 150°C, than for products 1, 2, 3, and 13. For product 13 there is a further small exotherm at 170°C.

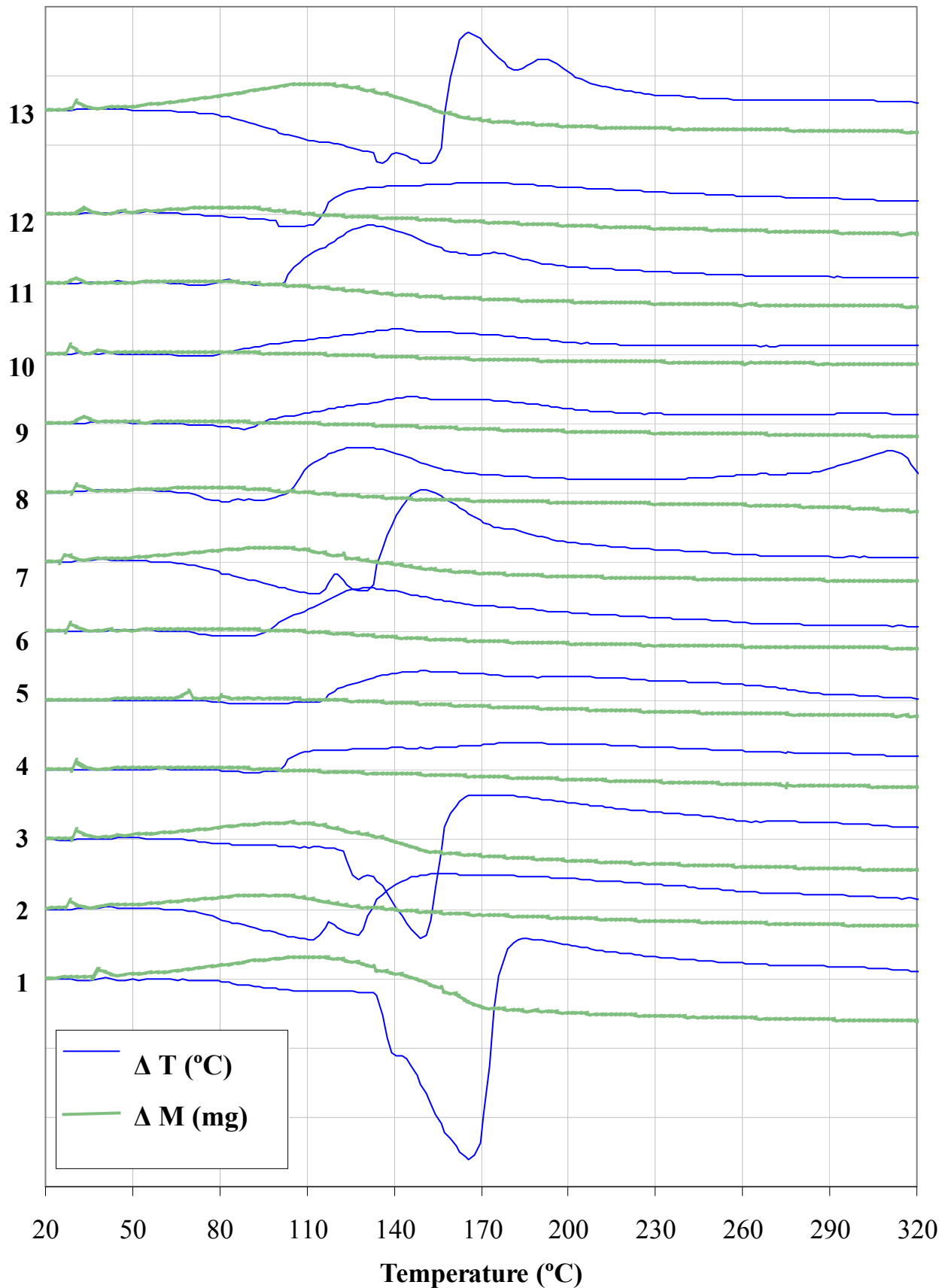


Figure 4.4: DTA and TGA curves for all products, horizontal divisions are equivalent to 20 °C and 20 mg.

The mass for products 1, 2, 3, and 13 shows a gradual increase peaking between 100 and 120 °C and then a gradual loss coinciding with the corresponding exotherm. Products 4, 5 and 12 show very small mass and thermal changes. Products 4 and 12 show a small, broad exothermic peak and a very small mass change, while product 5 shows no thermal reactions and only a small mass change. Products 6, 8, and 11 have very similar spectra with a broad exotherm, peaking at 130°C, and a very small loss in mass. Products 9 and 10 are virtually identical with a small broad exotherm peaking between 140 and 150°C.

Mackenzie and Berggren (1970) discuss the DTA patterns for what they term ferric oxide gels, given the formula $\text{Fe}_5\text{OH}_8 \cdot 4\text{H}_2\text{O}$. These gels are now known to be the poorly crystalline mineral ferrihydrite. Freshly prepared ferrihydrite shows a large, low temperature ($\sim 150^\circ\text{C}$) endothermic peak followed by a strong, sharp exothermic peak. The temperature and shape of these peaks depend on the final solution pH and the temperature of precipitation. An increase in the pH results in a marked broadening and a change in temperature of the exothermic peak, generally an increase. The low temperature endotherm is attributed to adsorbed water while the exotherm represents the final crystallization of hematite ($\alpha\text{-Fe}_2\text{O}_3$). The presence of Al and Si in ferrihydrite weakens and broadens the transformation peak and shifts it to higher temperatures ($>600^\circ\text{C}$) (Cornell and Schwertmann, 1996). Product 8 is the only product that displays this transformation exotherm at $\sim 300^\circ\text{C}$. It is likely that the other products have Al substitution in their structure and therefore this transformation peak may occur at temperatures above 600°, which is beyond the range of this analysis, and therefore cannot be confirmed. A ferrihydrite which has been aged, yields much smaller and broader endo- and exotherms (Mackenzie and Berggren, 1970). For patterns 1 and 3 the endotherm is large, suggesting that the amount of sorbed water must be large. The exotherm is, however, small and very broad.

The endotherm peaks for products 2, 7 and 13 bear a strong resemblance to those of $\delta\text{-FeOOH}$ (Mackenzie and Berggren, 1970), showing a low temperature endotherm at just over 100°C and two more small endotherms at 275°C and 320°C with an exothermic component thereafter. The second endothermic peak at 130°C and the

exothermic component for product 2 are at much lower temperatures. The endothermic peak may be attributed to the transformation of δ -FeOOH to hematite and the exotherm could be the result of either direct transformation to hematite or to the transformation of fine-grained to better crystallized hematite (Mackenzie and Berggren, 1970).

Transformations are thought to be diffusion controlled since peak temperature varies with particle size. Mackenzie found in 1958 (Mackenzie and Berggren, 1970) that the transformation from α -FeOOH (goethite) to α -Fe₂O₃, which occurs at 380°C for highly crystalline material, can occur at temperatures as low as 190°C for very poorly crystalline material. This could explain the lower temperature exotherms of products 2 and 7 at 150°C. The higher temperature exotherm at 165°C for product 13 may indicate a slightly higher degree of ordering in this largely amorphous material.

Not shown on Figure 4.4 is a broad endotherm between 500°C and 550°C for product 13. This is an indication that a poorly crystalline material similar to γ -AlOOH, also called pseudo-boehmite, is present. This material also displays a low temperature endotherm, which is probably due to sorbed water. The dip in the exotherm at 195°C could be a result of the γ -AlOOH sorbed water endotherm (Mackenzie and Berggren, 1970).

It has been established from the XRD patterns that with the exception of calcite and a small amount of bayerite, there is only very poorly crystalline material in the precipitates. Ferrihydrite is very difficult to identify by XRD and thus its presence as suggested by TGA is unconfirmed.

4.4.4 Infrared spectroscopy

Figures 4.5 – 4.8 show the infrared spectra for products 1 – 13. Table 4.4 lists some common molecules and functional groups and their infrared assignments. The major peaks are labelled on the spectra and subsequently listed in Table 4.5 with their assigned vibrational modes.

Table 4.4: The infrared active bands for some common molecules (Nakamoto, 1963 and 1997; Smith 1999)

Molecule	ν_1 (stretch, sym, low int.)	ν_2 (bend, sym, low int.)	ν_3 (stretch, asym, v. int.)	ν_4 (bend, asym, med int)
O-H	3700 - 3400			
H-O-H	3657	~1600	3756	
CaCO ₃		880 - 860	1510 – 1410	~ 700
SO ₄	983	450	1140 - 1080	680 - 610
CaSO ₄	1018	415, 499	1108, 1115, 1128, 1160	609, 628, 674

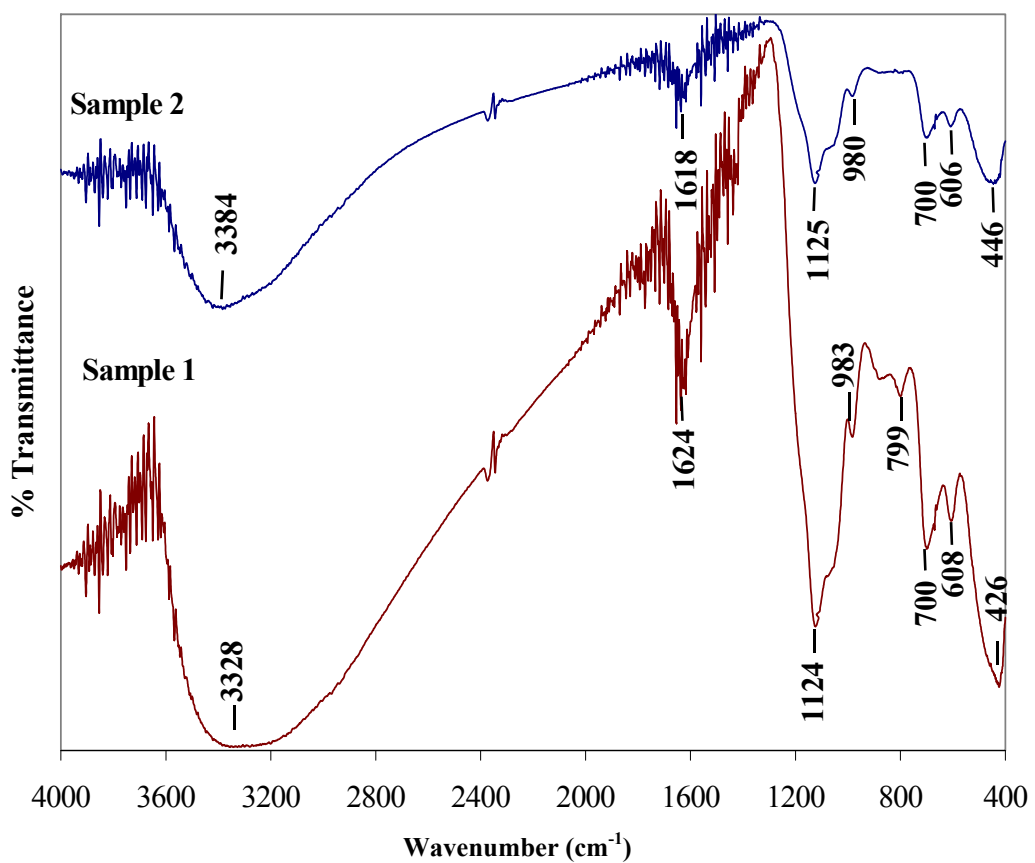


Figure 4.5: Infrared spectra for products 1 and 2.

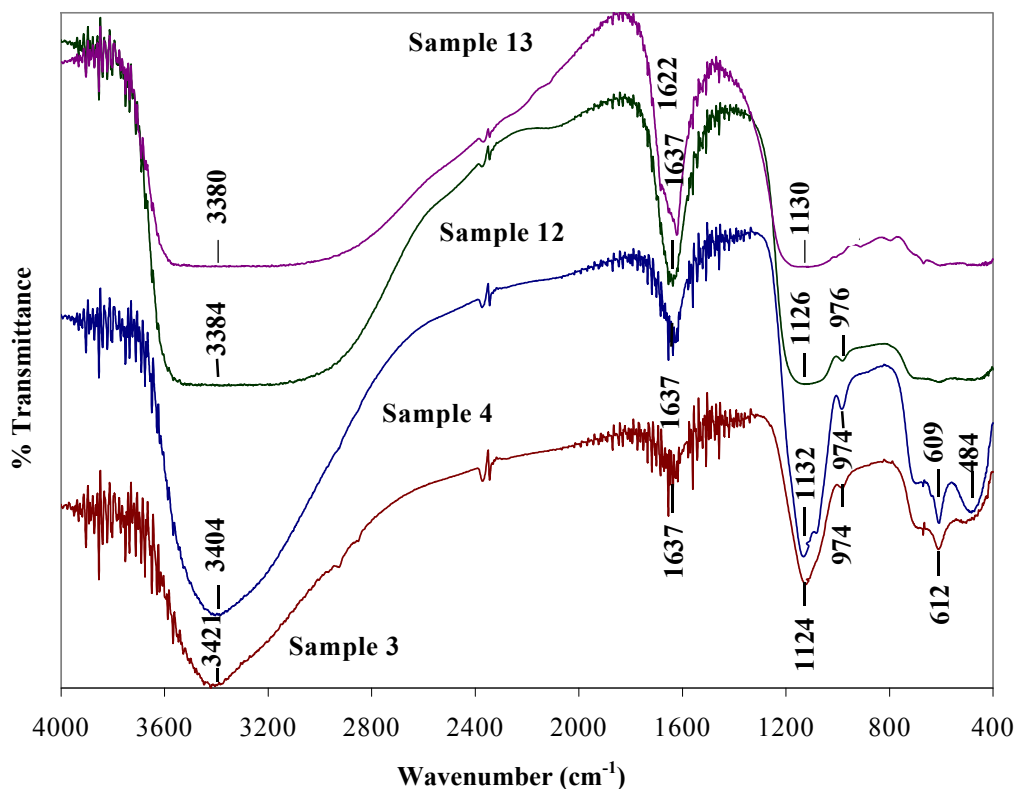


Figure 4.6: Infrared spectra for products 3, 4, 12 and 13.

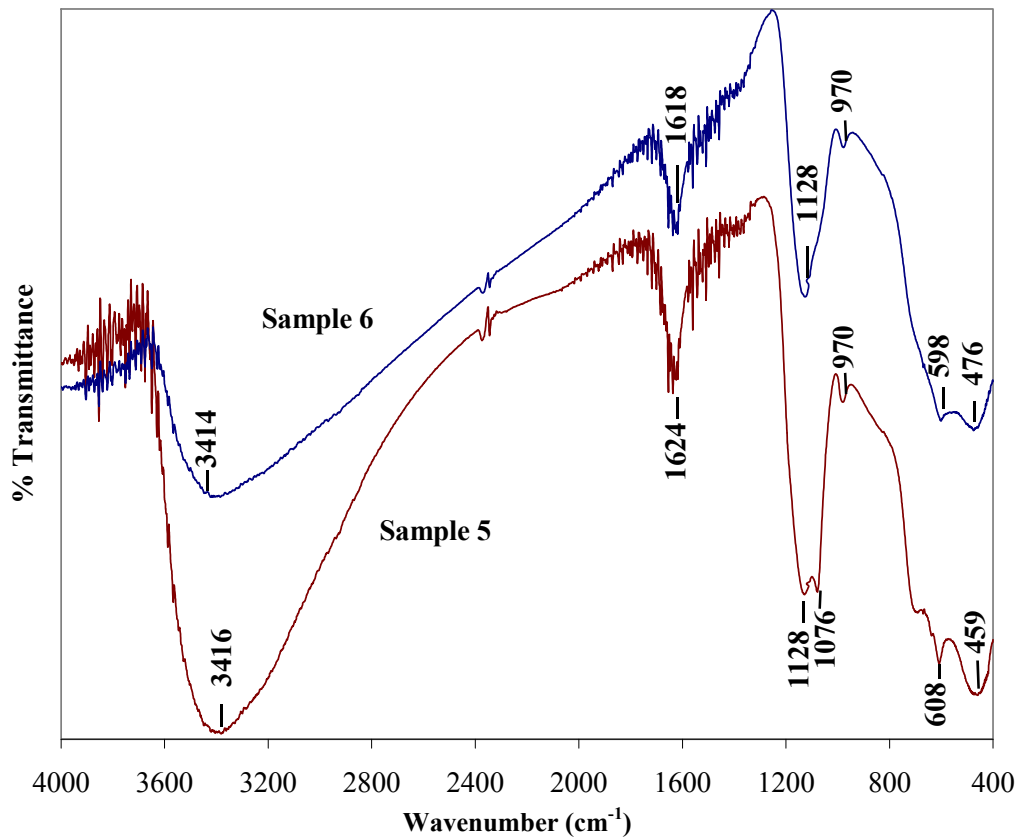


Figure 4.7: Infrared spectra for product 5 and 6.

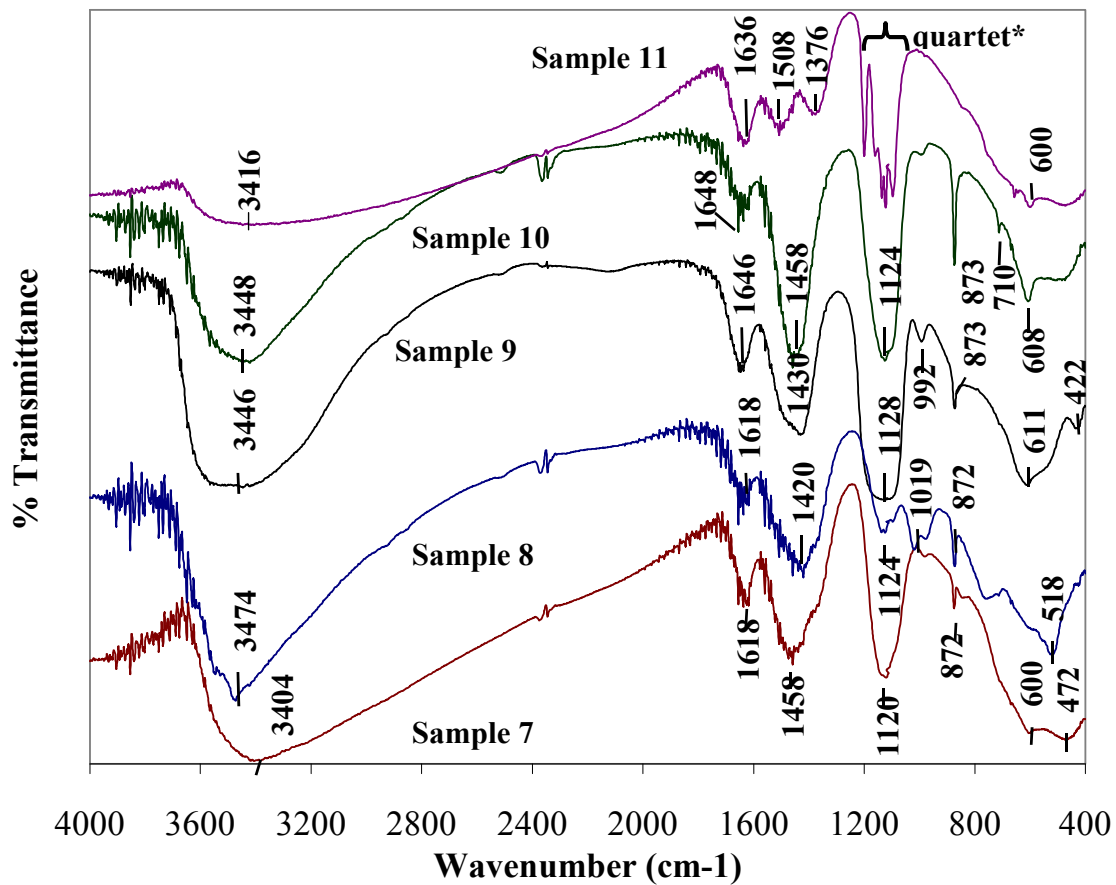


Figure 4.8: Infrared spectra for products 7 – 11. *The quartet is labelled in Table 4.5.

Table 4.5: The major infrared peaks for each product and their assignments. Titrations 6-10 are downscale.

No	pH	Fe:Al ratio	OH ⁻	H ₂ O	CO ₃ ²⁻	SO ₄ ²⁻	SO ₄ ²⁻	CO ₃ ²⁻	SO ₄ ²⁻	M-O
			v ₁	v ₂	v ₃	v ₃	v ₁	v ₂	v ₄	
1	3.0	7.3	3328	1624		1124	983		608	426
2	3.2	0.8	3384	1618		1125	980		606	446
3	4.2	0.8	3421	1637		1124	974		612	494
12	4.3	0.8	3384	1637		1126	983			
4	4.5	2.5	3404	1637		1132	974		609	484
5	7.0	7.3	3416	1624		1076	970		608	459
						1128				
11	9.2	7.3	3415	1636	1508	1199	Quartet		652	
						1136			640	
						1123			599	
						1097				
13	neutral	-	3380	1622		1130			652	580
6	6.8	7.3	3414	1618		1128	970		598	476
7	8.4	7.3	3404	1618	1458	1120		874	608	428
8	7.5	0.8	3474	1618	1420	1124	1019	873		518
9	8.1	0.8	3446	1646	1430	1128	992	873	611	422
10	11.2	7.3	3448	1648	1458	1124	982	873	608	452

All the products display strong sulphate peaks showing asymmetric stretching vibrations and both asymmetric and symmetric bending vibrations. The fact that there is sulphate in all the products, including those synthesised at pH values higher than 5, suggests that it is structural and not merely adsorbed. When the pH is high, the surface of the metal hydroxide will negatively charged and the sulphate anion could not be adsorbed (Hunter, 1981). Products 7 – 10, which were prepared from downscale titrations, have strong CO_3^{2-} peaks present. The presence of CO_3^{2-} in the products is most likely due to the formation of calcite in the FAL early in the reaction when the FAL is exposed to the atmosphere. There is also a possibility that there is CO_3^{2-} in the structure of the precipitate, thus forming a hydrotalcite-like mineral (Thevenot *et al.*, 1989).

The degeneration of the sulphate bands in product 11 may be attributed to the presence of gypsum but this degeneration is apparently also caused by the formation of a bridged bidentate complex with C_{2v} symmetry (Figure 4.9) (Nakamoto, 1963).

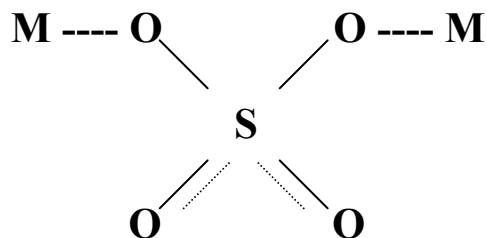


Figure 4.9: A bridged bidentate metal sulphate complex.

There are two bands for OH differentiated as “free” and “bonded”. Free OH denotes that it is free from hydrogen bonding and has a higher frequency (3700 cm^{-1}) while bonded OH occurs at a frequency of 3510 cm^{-1} . Thus the 3510 cm^{-1} band can be assigned to “free H_2O ” i.e. adsorbed onto the surface. Inner and outer bonded hydroxyls have absorption peaks at even higher frequencies (3700 and 3625 cm^{-1}) (Lyon, 1964).

The OH stretching bands for all products occur at wavenumbers less than 3500 cm^{-1} . The OH stretching mode for goethite occurs at $\sim 3150 \text{ cm}^{-1}$. Thus a portion of the OH stretching mode is a result of an M – OH bond, possibly goethite or ferrihydrite.

Goethite shows a symmetric Fe – O stretching in the *a*-*b* plane at \sim 630 cm⁻¹ which corresponds to a transition moment parallel to the *a* axis. The M – O absorption bands for goethite show a shoulder at \sim 495 cm⁻¹, a peak at 449 and a large peak at 397. For hematite these bands are shifted to 528, 436 and 295 (Cambier, 1986). Exact identification of the metal-oxygen bond is difficult, and the peaks in that range have, therefore simply been labelled as the M – O stretch. The higher M – O bands in products 13 and 8 are probably a result of the Al minerals. It has been established from XRD that product 8 contains bayerite and TGA data suggests that product 13 contains pseudo-boehmite.

4.4.5 Surface area

Surface area data are presented in Table 4.6. The specific surface area for the precipitates varies widely. There is no clear explanation as to why products 5, 6, 8 and 11 have such a high surface area and the remaining precipitates do not. There is a possibility that the surface area of the material may alter when the product is degassed and dried during preparation for analysis. In addition, N₂, being a relatively large molecule may not be able to enter small pores (Cornell and Schwertmann, 1996). This possibility is further suggested by the fact that the largest surface areas also tend to have the highest pore volume, suggesting that in these cases the gas has penetrated the structural interstices.

Particle size and thus surface area and porosity of iron oxides depend strongly on the conditions of crystal formation. High rates of crystal growth and low temperatures result in the formation of small, poorly ordered crystals with surface areas of several hundred m²/g (Cornell and Schwertmann, 1996). Goethite can have a range of surface areas between 8 – 200 m²/g for both natural and synthetic products. Aluminium reduces both the rate of growth and the crystal size of goethites. Schwertmannite has high surface areas ranging from 240 to 320 m²/g. There is considerable uncertainty about the surface area of ferrihydrite. Various methods report conflicting results. It is reported that the surface area for ferrihydrite may vary between 100 and 700 m²/g (Cornell and Schwertmann, 1996).

Table 4.6: Surface areas and pore volume and diameters for precipitates.

No.	pH	Fe:Al ratio	Product mass (mg)	Single point BET (m ² /g)	BET (m ² /g)	Pore volume (cm ³ /g)	Average pore diameter (Å)
1	3.0	7.3	164	7.42	7.70	0.026	132.4
1Rpt	3.0	7.3	195	4.19	4.35	0.019	174.9
2	3.2	0.8	188	25.7	26.5	0.123	186.4
3	4.2	0.8	192	19.2	19.8	0.098	197.6
12	4.3	0.8	179	19.4	19.8	0.113	229.4
4	4.5	2.5	179	42.8	44.0	0.197	178.9
5	7.0	7.3	189	200.4	205.5	0.359	69.9
13	neutral	-	182	13.3	13.6	0.045	132.5
11	9.2	7.3	182	218.4	225.7	0.177	31.4
6	6.8	7.3	186	235.7	241.7	0.174	28.8
7	8.4	7.3	184	36.6	37.8	0.030	31.7
8	7.5	0.8	182	180.8	186.8	0.264	56.4
9	8.1	0.8	192	11.8	12.2	0.064	211.6
10	11.2	7.3	205	24.9	25.3	0.101	159.5

From the results in Table 4.6 it can be seen that in general the more circumneutral precipitates have the highest surface areas. This may be a result of the fact that the rate of precipitation is high.

4.4.6 Surface charge

The relative surface charge of the precipitates is presented in Figures 4.10 and 4.11. To convert the relative surface charge to absolute surface charge the curve must be shifted so that the point of zero charge (pzc) falls on the x-axis at 0 cmol/kg (Hunter, 1981). The net surface charge (Q_p) may then be converted (Stumm, 1992) to σ_p (Coulombs.m⁻²) by: $\sigma_p = Q_p * F/s$ where F is the Faraday constant (96490 C.mol⁻¹) and s is the specific surface area in m²/g. The pzc is influenced by many factors (McBride, 1994). The most important of these are temperature and the presence of other ions in the system. Dehydration of an iron oxide reduces the number of hydroxyl groups and induces an acid shift in the pzc. The specific adsorption of ions other than protons often causes a shift in the pzc. Adsorbed cations cause the pzc to shift to a lower pH while adsorbed anions cause the pzc to shift to a high pH. Adsorbed CO₃²⁻ can cause a dramatic reduction in the pzc on oxide surfaces, particularly goethite.

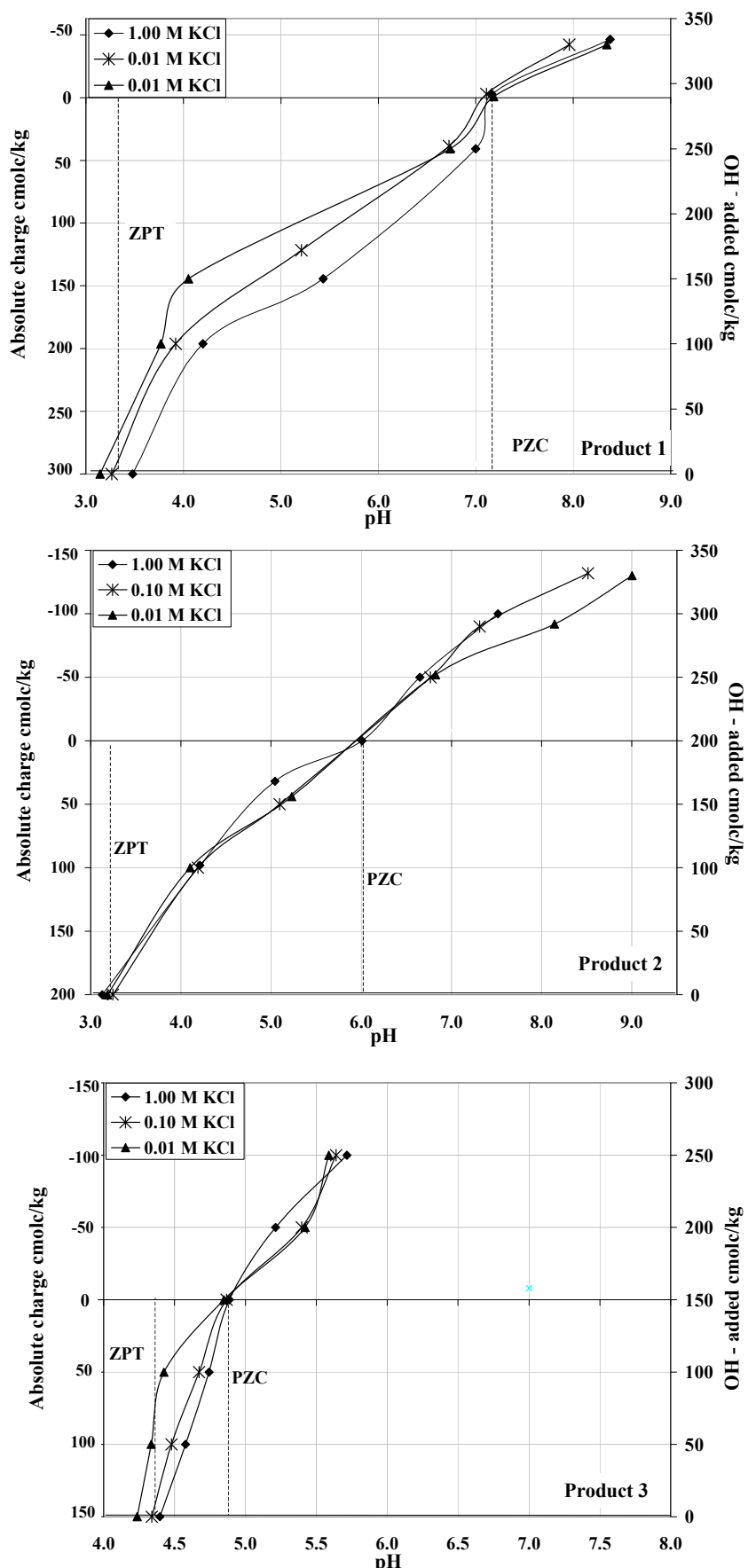


Figure 4.10: Surface charge graphs for products 1 – 3, where the point of zero charge (pzc) and the zero point of titration (zpt) are shown.

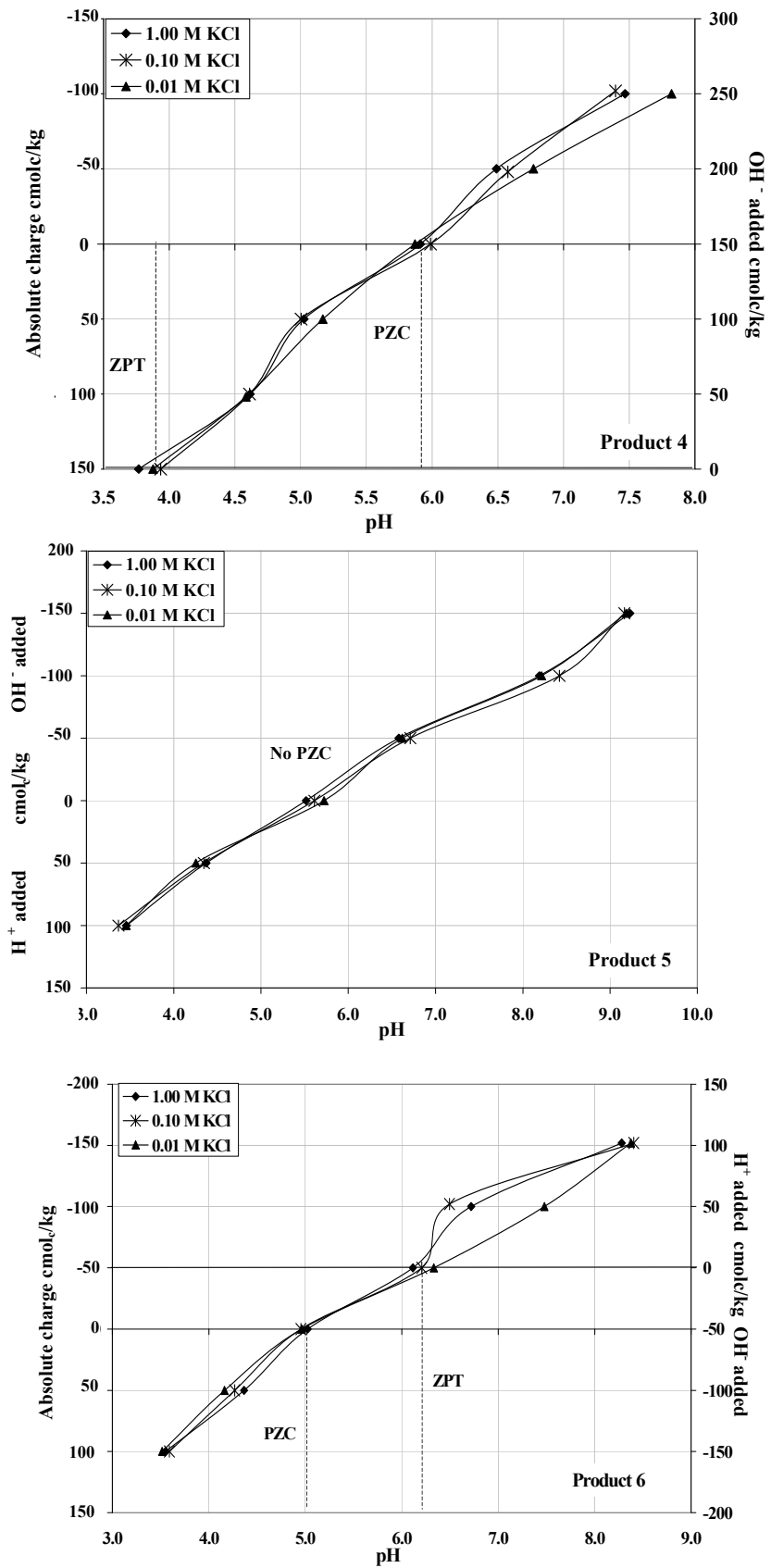


Figure 4.11: Surface charge graphs for products 4 – 6.

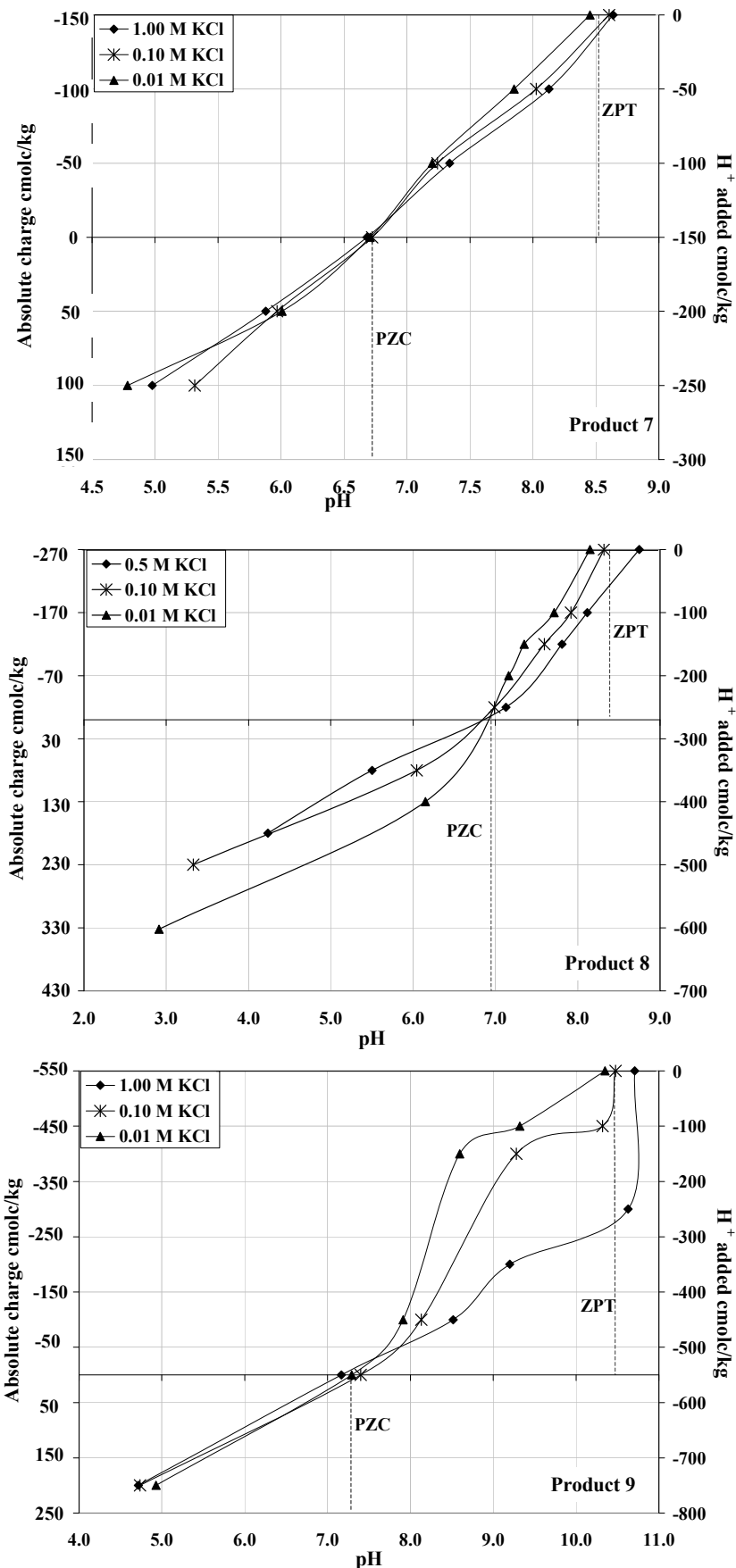


Figure 4.12: Surface charge graphs for products 7 – 9, where the point of zero charge (pzc) and the zero point of titration (zpt) are shown.

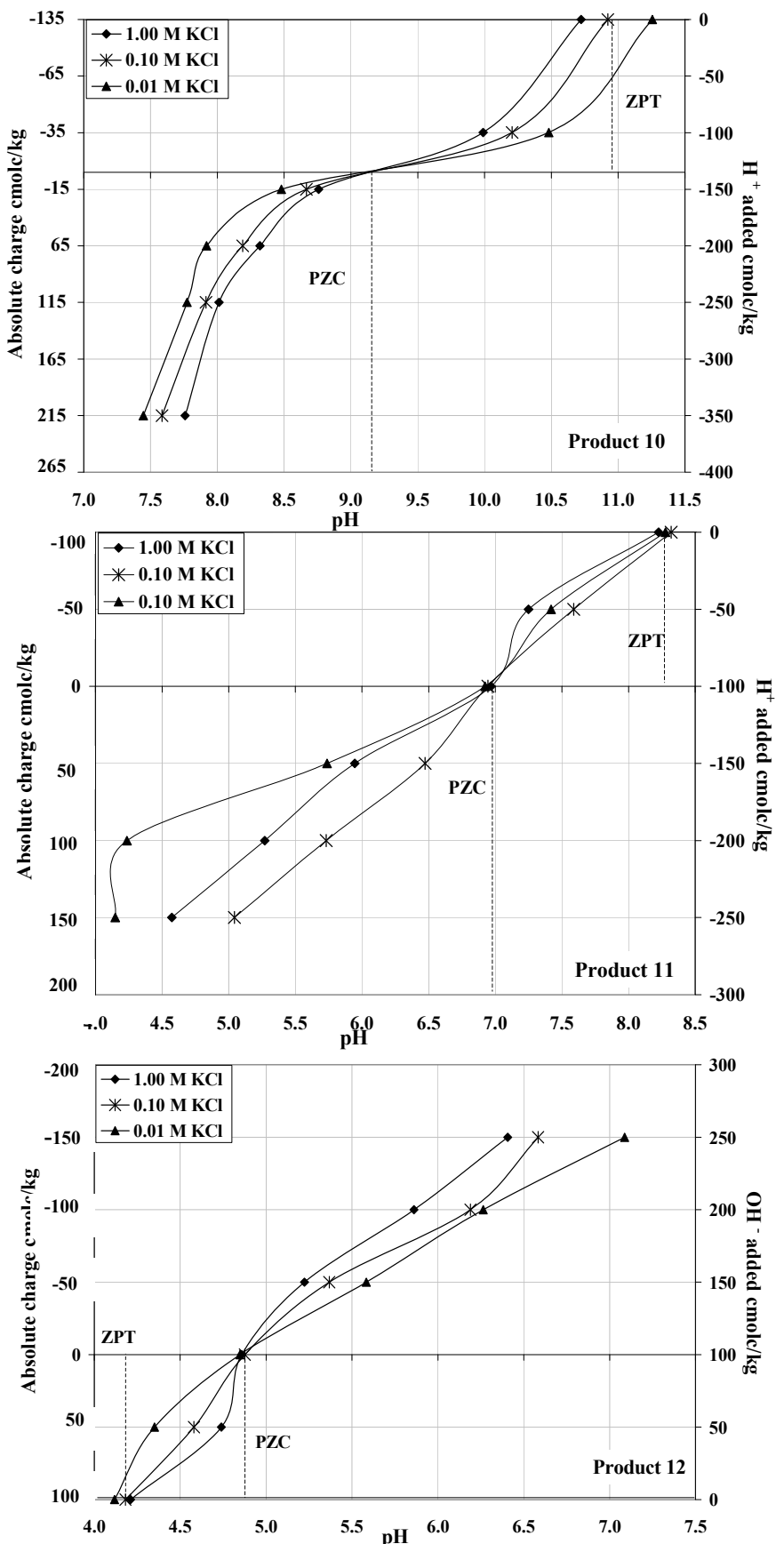


Figure 4.13: Surface charge graphs for products 10 – 12, where the point of zero charge (pzc) and the zero point of titration (zpt) are shown.

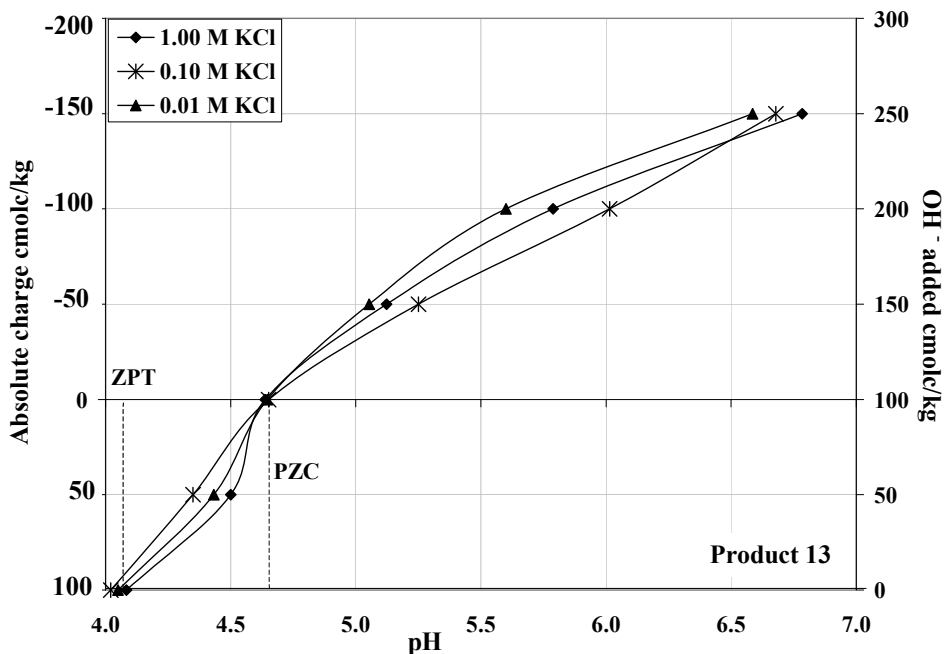


Figure 4.14: Surface charge graph for product 13, where the point of zero charge (pzc) and the zero point of titration (zpt) are shown.

Product 5 does not show a large difference amongst the different ionic strengths used and a point of zero charge cannot be determined. From Table 4.7, which summarises the data presented in Figures 4.10 - 4.14, it is evident that products 1 and 2, formed at pH values where only ferric compounds are precipitating, have neutral pzc's. Product 11, which was titrated to a high pH, also displays a pzc of 5. This information supports the statements made by other researchers concerning the optimum pH of formation of minerals with pH-dependant charge, for maximum sulphate adsorption (Jenke *et al.*, 1983). For the downscale reactions (6 – 10) the pzc's all tend to be at circumneutral pH values except for product 10 that was formed at very high pH values. The amount of charge occurring on these precipitates is very high. Over the pH range of 4 – 8 there is an average of approximately 250 cmol/kg. This high value suggests that the use of these ochres as cheap low-grade adsorbents is very feasible.

Table 4.7: pH of formation and point of zero charge shown with SAMD composition.

Product no	pH of formation	Fe:Al ratio	pH of pzc
1	3.0	88/12	7.2
2	3.2	45/55	6
3	4.2	45/55	4.9
12	4.3	45/55	4.8
4	4.5	71/29	5.9
5	7.0	88/12	none
13	neutral	-	4.6
11	9.2	88/12	5
6	6.8	88/12	5
7	8.4	88/12	6.7
8	7.5	45/55	7
9	8.1	45/55	7.5
10	11.2	88/12	9.2

4.4.7 PHREEQC modelling of anion and cation data

The saturation indices in Table 4.8 indicate that all solutions are saturated or very close to being saturated with respect to gypsum. Samples 3, 4 and 12 indicate slight supersaturation with respect to gibbsite and a higher degree of supersaturation with respect to goethite. The saturation index for goethite in solution 5 indicates a high degree of supersaturation. The saturation indices for products 2 – 4 and 12 indicate that these solutions are supersaturated with respect to alunite ($KAl_3(SO_4)_2(OH)_6$). All solutions were highly undersaturated with respect to jarosite, the Fe analogue of alunite, and the SI values are, therefore, not presented in Table 4.8. Solutions 1 – 4 and 12 are all supersaturated with respect to jurbanite. The SI for jurbanite in solution 1 is very close to 0 suggesting near-equilibrium with this mineral. Solution 7 is supersaturated with respect to goethite. Solution 10, at high pH, is supersaturated with respect to ettringite and slightly undersaturated with respect to gibbsite.

Table 4.8: List of phases and their saturation indices in the product supernatant solutions*.

No	pH	Fe:Al ratio	Alunite Ettringite Fe(OH) ₃ Gibbsite Goethite Gypsum Jurbanite					
			Alunite	Ettringite	Fe(OH) ₃	Gibbsite	Goethite	Gypsum
1	3.0	7.3	-1.4	-46.3	-7.3	-3.2	-1.4	0.4
2	3.2	0.8	2.0	-43.9	-7.0	-2.0	-1.1	0.4
3	4.2	0.8	7.2	-31.4	-4.1	0.7	1.8	0.6
12	4.3	0.8	6.4	-32.1	-4.2	0.5	1.7	0.6
4	4.5	2.5	5.3	-33.0	-4.0	0.1	1.9	0.4
5	7	7.3			-0.3		5.6	0.4
11	9.2	7.3						0.5
6	6.8	7.3						0.5
7	8.4	7.3			-2.2		3.7	0.4
8	7.5	0.8						0.4
9	8.1	0.8						0.0
10	11.2	7.3	-16.2	1.9		-0.6		0.0
								-12.3

*The dissolution reactions used and the log K_{sp} values not found in the PHREEQC database are as follows:

Ettringite (Myeni *et al.*, 1998): Ca₆Al₂(SO₄)₃(OH)₁₂ • 26 H₂O → 6 Ca²⁺ + 2 Al³⁺ + 3 SO₄²⁻ + 12 OH⁻ + 26 H₂O; log K_{sp} = -111.6

Jarosite (Parkhurst and Appelo, 1999): KFe₃(SO₄)₂(OH)₆ + 6 H⁺ → 3 Fe³⁺ + 6 H₂O + K⁺ + 2 SO₄²⁻; log K_{sp} = -9.21

Natrojarosite (Parkhurst and Appelo, 1999): NaFe₃(SO₄)₂(OH)₆ + 6 H⁺ → Na⁺ + 3 Fe³⁺ + 2 SO₄²⁻ + 6 H₂O; log K_{sp} = -11.2

Jurbanite (Nordstrom, 1982): Al(OH)(SO₄) • 5 H₂O → Al³⁺ + OH⁻ + SO₄²⁻ + 5 H₂O; log K_{sp} = -17.8

4.5 Discussion

The cation and anion data indicate that the optimum pH for metal removal is > 6. At this pH, upscale Fe and Al buffer ranges have been transcended. Downscale reactions also show complete metal removal, but in the instance of a fixed amount of basic solution (FAL) the contribution of acidity via the oxidation of Fe^{II} results in a rapid drop of the pH to a level where Fe does not precipitate but remains in solution. High concentrations of sulphate remain in all supernatant solutions. This may be a result of the high amount of Ca in solution. The tendency for Ca²⁺ and SO₄²⁻ ions to associate very strongly in solution, it is likely that a higher degree of sulphate removal was not achieved because a saturated gypsum solution is more thermodynamically favoured than the precipitation of jarosite or jurbanite. The results in Chapter 3 suggest that greater sulphate removal can be achieved with a high Al concentration. This conclusion is supported by the solution modelling data, which indicates that jurbanite

is supersaturated in solution at low pH values. Infrared data indicating the presence of SO₄ in the low pH precipitates also suggests the formation of an Al-sulphate phase although this conclusion is unsupported as the SO₄ found in these precipitates may be adsorbed onto the surface of the product.

X-ray diffraction data show mostly amorphous material. Only products 8 and 9 definitely show a poorly crystalline bayerite. Calcite was present in all downscale reactions except for product 6 (this is confirmed by infra-red). A phase with very poor crystallinity can be detected in product 11 showing a diffractogram consisting of two broad halos at 30 – 35 and 52 – 60 °2θ. Two-line ferrihydrite has peaks at approximately 40 and 75 °2θ. Thus the XRD pattern may indicate that the material in product 11 is ferrihydrite. If this were the case the shift in the position of the peaks could be due to Al substitution.

DTA suggest quite strongly that the material in products 1, 2, 3, 7 and 13 contains ferrihydrite, while products 6, 8, 9, 10, 11 and 13 seem to contain some poorly crystalline goethite. Samples 2, 3 and 12 do not show a large exotherm indicating ferrihydrite transformation. This could be a result of the high ratio of Al in these products, indicating a retardation of the ferrihydrite structure and the formation of a larger amount of amorphous material. The waste sludge from Landau colliery (sample 13) may also contain pseudo-boehmite.

The surface charge is consistently high for all the products. The surface areas of the products are similar to the range of goethite surface areas and have the same degree of variation. Poorly crystalline iron oxide can be used to adsorb unwanted elements as a result of its high surface area and affinity for many ions. Other researchers have found that a natural ferrihydrite, with a high surface area is extremely effective in removing P and heavy metals such as Zn, Cd, Co, Ni, and Cr from contaminated water (Cornell and Schwertmann, 1996).

4.6 Conclusions

The jurbanite-alunite system controls the composition of solutions at low pH. While solutions that have a pH > 4 are controlled by the solubility of goethite and gibbsite. The solubility of ferrihydrite controls the composition of solutions at circumneutral pH. Solutions with a high pH are controlled by the solubility of ettringite and solutions with a low pH are controlled by jurbanite.

High surface charges and the potential for high surface areas indicate that these precipitates have potential to act as low-grade environmental adsorbents.

XRD, IR, and TGDTA data indicate that the precipitates consist of poorly crystalline highly Al-substituted goethite and ferrihydrite with large amounts of SO₄ included in the structure. Bayerite appears in product 8 and calcite is present in 3 products precipitated through downscale reaction.

Chapter 5

General discussion

The aim of this study was to investigate the products formed during the co-disposal of fly ash leachate (FAL) and synthetic acid mine drainage (SAMD) and to examine the sesquioxidic minerals that result from the neutralisation process. It was hypothesised that the ochre precipitates formed would have great usefulness as low-grade industrial adsorbents for water purification by reason of their high surface area and amphoteric properties. In order to determine whether FAL was a suitable reagent for the neutralisation of AMD it was compared with several other neutralising agents. The final titration solutions were analysed for anions and cations to determine the capacity for FAL to remove salts from solution. Precipitates prepared from large quantities of FAL and SAMD were described in terms of mineralogy, composition and surface characteristics.

The literature reviewed in Chapter 2 concerning the glassy nature of fly ash and its frequently high concentrations of lime and trace metals is extensive. Many researchers have investigated alternative uses for fly ash as a lime amendment, to improve soil properties and as a source of trace metals for plants to facilitate its disposal. Very few studies have investigated the potential of fly ash to act as an ameliorant for other wastes. Similarly, the sources and causes of acid mine drainage are well known and documented. The literature reviewed in Chapter 2 concerning the amelioration of AMD deals extensively with passive treatment and the established active treatments using $\text{Ca}(\text{OH})_2$ and CaCO_3 but alternative liming treatments have not been investigated.

The buffering displayed during the experimental neutralisation of synthetic acid mine drainage concurs with the results of related studies (O'Brien, 2000; Jenke *et al.*, 1983). The precipitates formed during these experiments with SAMD and FAL displayed a distinct lack of crystallinity. It was concluded that high concentrations of Al in the SAMD had a considerable inhibiting effect on the crystallinity of the precipitates (Fey and Dixon, 1981). A significant correlation between the amount Al

and SO₄ removed from solution suggests that an amorphous jurbanite-like phase is forming (Anthony and McLean, 1976). It was proven by up-scale titration that FAL was indeed a suitable neutralising agent for SAMD as it resulted in near-complete metal and substantial SO₄ removal.

The SAMD used to synthesise the reaction solids had different amounts of Al in solution and the reactions were terminated at a range of different pH values. The crystallinity of the samples was very poor with a great portion of the samples displaying only broad halos, possibly indicating poorly crystalline goethite or ferrihydrite (Schwertmann and Cornell, 2000). Several downscale reactions produced calcite and one product where the SAMD had a high Al concentration contained bayerite with a poor degree of crystallinity. Infra-red analysis determined that all the samples contained SO₄ even those formed at high (>7) pH values where the anion could not be adsorbed onto the surface and was thus part of the structure (Nakamoto, 1997; McBride, 1994). Thermal analysis indicated water loss and the transformation of metal hydroxides to metal oxides. The low temperatures of these transformations indicated that the material was very similar to ferrihydrite. It was concluded that the precipitates not identified by XRD were composed of poorly crystalline, highly Al-substituted goethite and ferrihydrite with large amounts of SO₄ included in the structure, which inhibited the crystallinity (Mackenzie, 1970). It was determined that as a result of the potentially high surface areas and the high, pH-dependant surface charge, these sesquioxides would have great potential as low-grade adsorbents for industrial use and for the clean-up of contaminated waters.

The experiments carried out in this study do not represent a definite procedure of synthesis. The titrations were designed in an attempt to emulate current neutralisation procedures. The lack of significant trends in the data suggest that variations in factors such as oxidation rates, ion adsorption and surface catalysis can have a large impact on the characteristics of the precipitated product. If these syntheses were to be performed in the field, the variations in AMD and FA composition would result in inconsistent products. Despite this unpredictability, ochre precipitates have potentially high surface areas and very high pH-dependant charge. There is also the possibility of producing novel or magnetic products by further manipulating the reaction conditions.

Further research conducted, pertaining to this study should investigate the adsorption capacity of these sesquioxides. Several samples of waste ochres from various neutralisation plants across the Highveld should be analysed for their capacity to adsorb various metals and common environmental pollutants. The development of novel products (e.g. magnetite and green rusts) should be attempted by experimenting with reaction conditions such as temperature and oxidation rate

Further investigation needs to be carried out concerning how the speed of titration and the availability of O₂ affect the product that is precipitated. This is especially important, as real AMD is likely to have a great deal more unoxidised Fe than the synthetic mixtures used in this study. The much overlooked phenomenon of surface induced precipitation (Hansen and Taylor, 1990) must also be more thoroughly investigated as this could result in a reduction in the amount basic material needed for neutralisation and ion removal.

The stability of these ochres and how they weather is also of great importance. The degree to which ions adsorbed onto the surface of the sesquioxides are exchanged for ions in solution is critical for the determination of their effectiveness as environmental ameliorants.

Chapter 6

References

1. Adriano, D.C., Page, A.L., Elseewi, A.A., Chang, A.C. and Straughan, A. **1980**: Utilization and disposal of fly ash and other coal residues in terrestrial ecosystems: A review. *Journal of Environmental Quality*, 9, 333 – 334.
2. Ainsworth, C.C. and Rai, D. **1987**: Chemical characterisation of fossil fuel wastes. EPRI EA-5321, *Electric Power Research Institute*, Palo Alto, CA.
3. Allman, R **1968**: The crystal structure of pyroaurite. *Acta Crystallographica*, B24, 972 – 977.
4. Alpers, C.N., Rye, R.O., Nordstrom, D.K., White, L.D. and King, B-S. **1992**: Chemical, crystallographic and stable isotopic properties of alunite and jarosite from acid-hypersaline Australian lakes. *Chemical Geology*, 96, 203 – 226.
5. Alpers, C.N. **1994**: Secondary minerals and acid mine water chemistry. Chapter 9, In: Short course handbook on environmental geochemistry of sulphide mine-wastes, Jambor, J.L. and Blowes, D.W. (Eds), Mineralogical Association of Canada, Waterloo, Ontario.
6. Anthony, J.W. and McLean, W.J. **1976**: Jurbanite, a new post-mine sulphate mineral from San Manuel. Arizona, *American Mineralogist*, 61, 1 – 4.
7. Azzie, B. A-M. **1999**: The geochemistry and quality of waters from selected collieries on the South African highveld. Masters Thesis, University of Cape Town, S.A.
8. Azzie, B. A-M. **2002**: Coal mine waters in South Africa: Their geochemistry, quality and classification. PhD Thesis, University of Cape Town, S.A.

9. Bezuidenhout, N. **1995**: Chemical and mineralogical changes associated with leachate production at Kriel power station ash dam. Masters Thesis, University of Cape Town, S.A.
10. Bigham, J.M, Schwertmann, U., Carlson, L. and Murad, E. **1990**: A poorly crystallised oxyhydroxysulphate of iron formed by bacterial oxidation of Fe(II) in acid mine waters. *Geochimica et Cosmochimica Acta*, 54, 2743 – 2758.
11. Bigham J.M. **1994**: Mineralogy of ochre deposits formed by sulphide oxidation. Chapter 4, In: Short course handbook on environmental geochemistry of sulphide mine-wastes, Jambor, J.L. and Blowes, D.W. (Eds), Mineralogical Association of Canada, Waterloo, Ontario.
12. Bigham, J.M, Schwertmann, U. and Pfaff, G. **1996**: Influence of pH on mineral speciation in a bioreactor simulating acid mine drainage. *Applied Geochemistry*, 11, 845 – 849.
13. Bigham, J.M. and Nordstrom, D.K. **2000**: Iron and aluminium hydroxysulphates from acid sulphate waters. Chapter 7, In: Reviews in mineralogy and geochemistry: Sulphate Minerals – Crystallography, geochemistry and environmental significance, Alpers, C.N., Jambor, J.L. and Nordstrom, D.K. (Eds), Vol. 40, Mineralogical Society of America, Washington, D.C.
14. Brophy, G.P., Scott, E.S. and Snellgrove, R.A. **1962**: Sulphate studies II: Solid solution series between alunite and jarosite. *American Mineralogist*, 47, 112 – 126.
15. Brophy, G.P. and Sheridan, M.F. **1965**: Sulphate studies IV: The jarosite-natrojarosite-hydronium jarosite solid solution series. *American Mineralogist*, 50, 1595 – 1607.
16. Cambier, P. **1986**: Infrared study of goethites of varying crystallinity and particle size: I. interpretation of OH and lattice vibration frequencies. *Clay Minerals*, 21, 191 – 200.
17. Campbell, A.E. **1999**: Chemical, physical and mineralogical properties associated with the hardening of some South African fly ashes. University of Cape Town, S.A.

18. Carlson, C.L. and Adriano, D.C. **1993**: Environmental Impacts of Coal Combustion Residues. *Journal of Environmental Quality*, 22, 227 – 247.
19. Caruccio, F.T., Geidel, G. and Pelletier, M. **1980**: Occurrence and prediction of acid drainages. *ASCE National Convention*, October, Hollywood, Fla., 167 – 178.
20. Chapelle, F.H., Bradley, P.M. and McMahon, P.B. **1993**: Subsurface microbiology. Chapter 8, In: Regional Groundwater Quality, Alley, W.M. (Ed.), Van Nostrand Reinhold, New York.
21. Chapman, B.M., Jones, D.R. and Jung, R.F. **1983**: Processes controlling metal ion attenuation in acid mine drainage streams. *Geochimica et Cosmochimica Acta*, 47, 1957 – 1973.
22. Chermak, J.A. and Runnels, D.D. **1997**: Development of chemical caps in acid rock drainage environments. *Mining Engineering*, June, 93 – 97.
23. Colmer, A.R. and Hinkle, M.E. **1947**: The role of microorganisms in acid mine drainage. *Science*, 106, 253 – 256.
24. Cornell, R.M. and Schwertmann, U. **1996**: The iron oxides: Structure, properties, reactions occurrence and uses. VCH, Weinheim, Germany.
25. Deer, W.A., Howie, R.A. and Zussman, J. **1992**: An introduction to the rock-forming minerals. 2nd Edition, Longman, England.
26. Demchik, M and Garbutt, K. **1999**: Wetlands and aquatic processes: Growth of woolgrass in acid mine drainage. *Journal of Environmental Quality*, 28, 243 – 249.
27. Doolittle, J.J., Hossner, L.R. and Wilding, L.P. **1993**: Division S-5 – Soil Genesis, morphology and classification: Simulated aerobic pedogenesis in pyritic overburden with a positive acid-base account. *Soil Science of America Journal*, 57, 1330 – 1336.

28. Eary, L.E., Dhunpat Rai, D., Mattigod, S.V. and Ainsworth, C.C. **1990**: Geochemical factors controlling the mobilization of inorganic constituents from fossil fuel combustion residues: II. Review of the minor elements. *Journal of Environmental Quality*, 19, 202 – 214.
29. Eaton, A.D., Clesceri, L.S. and Greenberg, A.E. (Eds) **1995**: Standard methods for the examination of water and wastewater. American Public Health Association, American Water Works Association and Water Environment Federation, Washington.
30. Evangelou, V.P. and Sinju, U.M. **1991**: Evaluation and Qualification of Armouring Mechanisms of Calcite, Dolomite and Rock Phosphate by Manganese. In: Proceedings Second International Conference on the Abatement of Acidic Drainage, September, 16 – 18, Montreal, MEND, 363 – 382.
31. Fey, M.V. and Dixon J.B. **1981**: Synthesis and properties of poorly crystalline hydrated aluminous goethites. *Clays and Clay Minerals*, 29, 91 – 100.
32. Fisher, G.L. and Natusch, F.S. **1979**: Size dependence of the physical and chemical properties of coal fly ash. In: Analytical methods for coal and coal products, Karr, C. Jr (ed), Vol. III, p 489 – 541, Academic Press, New York.
33. Gazea, B., Adam, K. and Kontopoulos, A. **1996**: A review of passive systems for the treatment of acid mine drainage. *Minerals Engineering*, 9, 1, 23 – 42.
34. Gray, N.F. **1997**: Environmental impact and remediation of acid mine drainage: a management problem. *Environmental Geology*, 30, (1/2), 62 – 71.
35. Hälbich, T.F.J. **1997**: The mobility of metals in acid mine drainage. University of Cape Town, South Africa.
36. Hampson, C.J. and Bailey, J.E. **1982**: On the structure of some precipitated calcium alumino-sulphate hydrates. *Journal of Matter Science*, 17, 3341 – 3346.

37. Hansen, H.C.B. and Taylor, R.M. **1990**: Formation of synthetic analogues of double metal hydroxy carbonate minerals under controlled pH condition: I. The synthesis of pyroaurite and reevesite. *Clay Minerals*, 25, 161 – 179.
38. Hedin, R.S., Watzlaf, G.R. and Nairn, R.W. **1994**: Passive treatment of acid mine drainage with limestone. *Journal of Environmental Quality*, 23, 1338 – 1345.
39. Hunter R.J. **1981**: Zeta potential in colloid science: principles and applications. Academic Press, Sydney.
40. Hustwit, C.C., Ackman, T.E. and Erikson, P.E. **1992**: The role of oxygen transfer in acid mine drainage (AMD) treatment. *Water Environmental Research*, 54, 6, 817 – 823.
41. Jambor, J.L., Nordstrom, D.K and Alpers, C.N. **2000**: Metal-sulphate salts from sulphide mineral oxidation. Chapter 6, In: Reviews in mineralogy and geochemistry: Sulphate Minerals – Crystallography, geochemistry and environmental significance, Alpers, C.N., Jambor, J.L. and Nordstrom, D.K. (Eds), Vol. 40, Mineralogical Society of America, Washington, D.C.
42. Jenke, D.R., Pagenkopf, G.K. and Diebold, F.E. **1983**: Chemical changes in concentrated, acidic, metal-bearing wastewaters when treated with lime. *Environmental Science Technology*, 17, 4, 217 – 223.
43. Kepler, D.A. **1986**: Manganese removal from mine drainage by artificial wetland construction. In: Proceedings of the 8th Annual National Abandoned Mine Lands Conference, Billings, MT, 74 – 80.
44. Kleinmann, R.L.P., Edenborn, H. and Hedin, R.S. **1991**: Biological treatment of mine water – An Overview. p 27 – 42, In: Proceedings of the 2nd International Conference on the Abatement of Acidic Drainage, 16 – 18 September, Mine Environment Neutral Drainage Program, Montreal, Canada.
45. Lyon, R.J.P. **1964**: Infrared analysis of soil minerals. Chapter 6 In: Soil Clay Mineralogy: A Symposium, Longman, 171 – 199.

46. Mackenzie, R.C. **1970**: Differential thermal analysis. Volume 1, John Wiley and Sons, London.
47. Mackenzie, R.C. and Berggren, G. **1970**: Oxides and hydroxides of higher valency elements. Chapter 9, In: Differential thermal analysis, Mackenzie, R.C., Volume 1, Academic Press Inc, London.
48. Maree, J.P., van Tonder, G.J. and Millard, P. **1996**: Underground neutralisation of mine water with limestone. *Water Research Commission Report No. 609/1/96*, Pretoria, South Africa.
49. Mattigod, S.V., Dhanpat Rai, Eary, L.E. and Ainsworth, C.C. **1990**: Geochemical factors controlling the mobilisation of inorganic constituents from fossil fuel combustion residues: I. Review of the major elements. *Journal of Environmental Quality*, 19, 188 – 201.
50. McBride, M.B. **1994**: Environmental chemistry of soils. Oxford University Press. U.K.
51. McKeown, S. **2000**: The geochemistry and amelioration of a sulphur-contaminated environment near Somerset West, South Africa. Masters Thesis, University of Cape Town, S.A.
52. Mehliss, A.T.M. **1981**: Operating and developing coal mines in the RSA, Department of mineral and energy affairs, Minerals Bureau, SA.
53. Miller, S. and Murray, G. **1988**: Prediction of time dependant factors in acid mine drainage. In: The Third International Mine Water Congress, October, 165 – 172, Melbourne, Australia.
54. Mitchell, P. **2000**: Prediction, prevention, control and treatment of acid rock drainage. Chapter 7, In: Environmental policy in mining: corporate strategy and planning for closure, Warhurst, A. and Noronha, L. (Eds.), CRC Press.

55. Myeni, S.C.B., Trania, S.J. and Logan, T.J. **1998**: Ettringite solubility and geochemistry of the $\text{Ca}(\text{OH})_2 - \text{Al}_2(\text{SO}_4)_3 - \text{H}_2\text{O}$ system at 1 atm pressure and 298 K. *Chemical Geology*, 148, 1 -19.
56. Nakamoto, K. **1963**: Infrared spectra of inorganic and coordination compounds. John Wiley and Sons Inc., New York.
57. Nakamoto, K. **1997**: Infrared and Raman spectra of inorganic and coordination compounds, Part A: Theory and application in inorganic chemistry. 5th edition, John Wiley and Sons Inc., New York.
58. Nordstrom, D.K. **1982**: The effect of sulphate on aluminium concentration in natural waters: some stability relations in the system $\text{Al}_2\text{O}_3 - \text{SO}_3 - \text{H}_2\text{O}$ at 298 K. *Geochimica et Cosmochimica Acta*, 46, 681 – 692.
59. Nordstrom, D.K. and Southam, G. **1997**: Geomicrobiology of sulphide mineral oxidation. Chapter 11, In: Geomicrobiology: Interaction Between Microbes and Minerals, Banfield, J.F. and Nealson, K.H. (Eds.), Rev. Mineral., 35, 361 – 390.
60. Nordstrom, D.K. and Alpers, C.N. **1999**: Geochemistry of acid mine waters. In: The environmental geochemistry of mineral deposits Part A: Processes, techniques and health issues, Plumlee, G.S. and Logsdon, M.J. (Eds), Reviews in Economic Geology Vol 6A, SEG Inc., Michigan.
61. O'Brien, R.D. **2000**: The neutralisation of acid mine drainage by fly ash. Masters Thesis, University of Cape Town, South Africa.
62. Page A.L., Elseewi, A.A. and Straughan, I. **1979**: Physical and chemical properties of fly ash from coal-fired power plants with reference to environmental impacts. *Residue Review*, 71, 83 – 120.
63. Parkhurst, D.L. and Appelo, C.A.J. **1999**: User's guide to PHREEQC (Version 2): A computer program for speciation, batch-reaction, one-dimensional transport, and

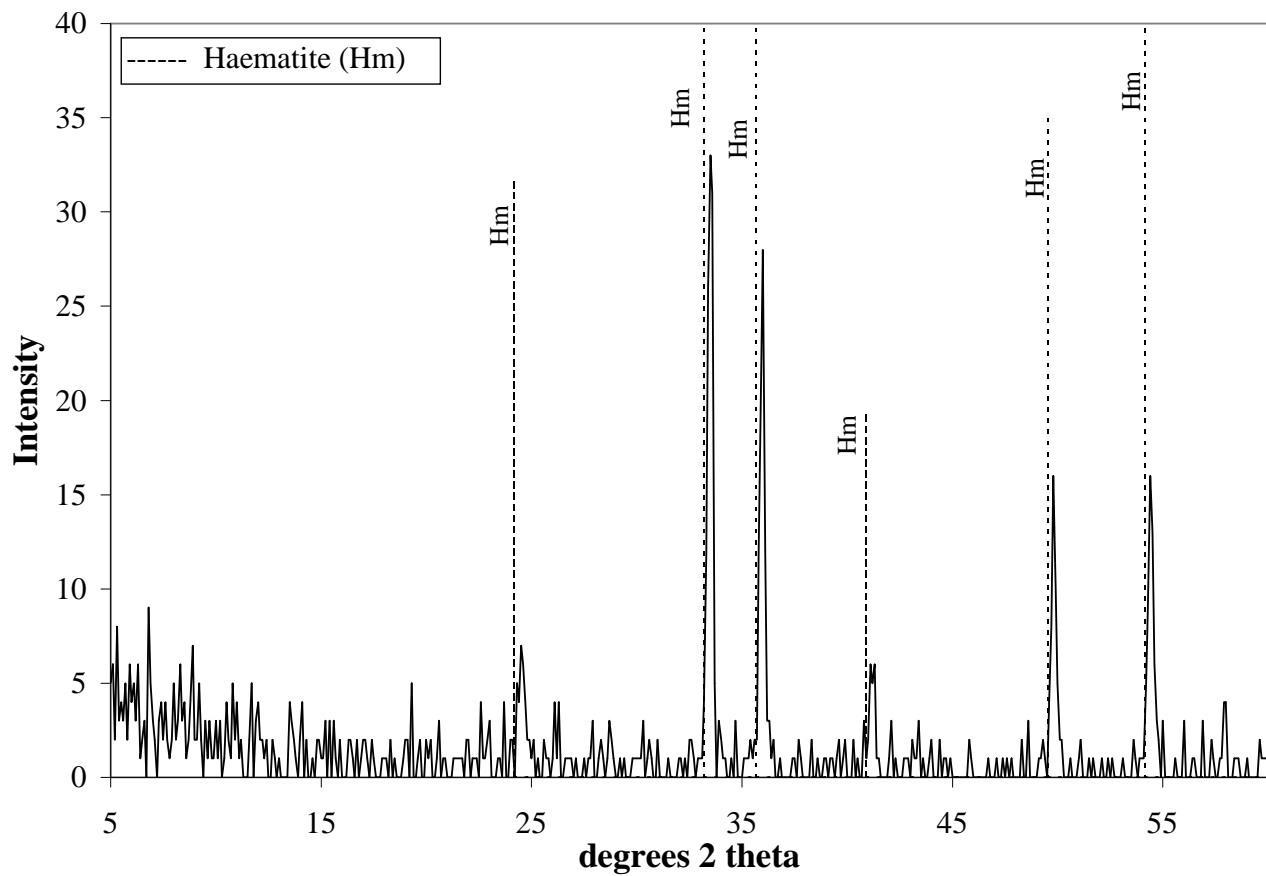
inverse geochemical calculations. U.S. Geological Survey Water-Resources Investigations Report 99-4259, 310 p.

64. Robb, G. and Robinson, J. **1995**: Acid mine drainage prediction and remediation. *Mining Environmental Management*, September, 19 – 21.
65. Schopf, J.M. **1956**: A definition of coal. *Economic Geology*, 51, 521 – 561.
66. Schwertmann, U. and Cornell, R.M. **2000**: Iron Oxides in the laboratory: Preparation and characterisation. 2nd Edition, Wiley-VCH, Germany.
67. Schwertmann, U. and Fitzpatrick, R.W. **1992**: Iron minerals in surface environments. In: Biomineralization Processes: Iron and Manganese. Skinner, H.C.W. and Fitzpatrick, R.W. (Eds), *Catena Supplement* 21, 7 – 30.
68. Schwertmann, U. and Jackson, M.L. **1964**: Influence of hydroxy aluminium ions on pH titration curves of hydronium-aluminium clays. *Soil Science Society of America Proceedings*, Colorado, 179 – 183.
69. Singer, P.C. and Stumm, W. **1970**: Acid Mine Drainage: The Rate Determining Step. *Science*, 167, 1121 – 1123.
70. Skousen, J., Hilton, T. and Faulkner, B. **1996**: Overview of acid mine drainage treatment with chemicals. Chapter 23, In: Acid Mine Drainage: Control and Treatment, Skousen, J.G. and Ziemkiewicz, P.F. (Eds.), 2nd Edition, West Virginia University, Morgantown, West Virginia.
71. Smith, B. **1999**: Infrared spectral interpretation: A systematic approach. CRC Press, Florida.
72. Smith, R.D. **1980**: The trace element composition of coal during combustion and the emissions from coal fired plants. *Progress in Energy and Combustion Science*, 6, 53 – 119.

73. Sposito, G. **1984**: The surface chemistry of soils. Oxford University Press, New York.
74. Stumm, W. **1992**: Chemistry of the solid-water interface: Processes at the mineral-water and particle-water interface in natural systems. John-Wiley and Sons, Inc. New York.
75. Summers, K.V., Rupp, G.L. and Gherini, S.A. **1983**: Physical-chemical characteristics of utility solid wastes. EPRI EA-3236, *Electrical Power Research Institute*, Palo Alto, CA, USA.
76. Taylor, E.M. Jr. and Schuman, G.E. **1988**: Fly ash and lime amendment of an acidic coal spoil to aid revegetation. *Journal of Environmental Quality*, 17, 120 – 124.
77. Thevenot, F., Szymanski, R. and Chaumette, P. **1989**: Preparation and characterisation Al-rich Zn-Al hydrotalcite-like compounds. *Clays and Clay Minerals*, 37, 5, 396 – 402.
78. Thompson, J.G. **1979**: Neutralization of acid mine waters, Soil and Irrigation Research Institute. *Report No. 902/8/79*. Department of Agricultural Technical Services, South Africa.
79. Thompson, J.G. **1980**: Acid mine water in South Africa and their amelioration. *Water SA*, 6, 130 – 134.
80. Tomlinson, I.R. **1994**: The amendment of acid soil with an ettringitic waste and its effects on plant growth. Masters Thesis, University of Cape Town, South Africa.
81. Van Niekerk, A. **2001**: Presentation at Coaltech 2020 Colloquium, Witbank Civic Theatre, March.
82. Waksman, S.A. and Jäffe, J.S. **1921**: Acid production by a new sulphur-oxidising bacterium. *Science*, 53, 216.
83. Warren, C.J. and Dudas, M.J. **1984**: Weathering processes in relation to leachate properties of alkaline fly ash. *Journal of Environmental Quality*, 13, 4, 530 – 538.

84. Webster, G.R **1996**: Experimental improvement of fly ash as a growth medium for plants through addition of selected solid wastes. Masters Thesis, University of Cape Town, South Africa.
85. Younger, P.L. **1995**: Hydrogeochemistry of mine waters flowing from abandoned coal workings in County Durham. *Quarterly Journal of Engineering Geology*, 28, S101 – S113.
86. Ziemkiewicz, P.F., Skousen, J.G., Brant. D.L., Sterner, P.L. and Lovett, R.J. **1997**: Acid Mine Drainage treatment with armoured limestone in open limestone channels. *Journal of Environmental Quality*, 26, 1017 – 1024.

**Appendix 1: XRD pattern of haematite formed by heating
 $\text{Fe}_2(\text{SO}_4)_3 \bullet \text{XH}_2\text{O}$**



Appendix 2: Reproducibility of potentiometric titrations

Figures A2.1 and A2.3 show titrations done in triplicate of $\text{Fe}_2(\text{SO}_4)_3$ and $\text{Al}_2(\text{SO}_4)_3$, respectively, titrated with NaOH in air. In both cases two of the titration curves are closely matched while the third may be considered an outlier and discounted.

Experiment 1: Components of SAMD titrated with different bases in oxic and anoxic environments

Figure A2.1: $\text{Fe}_2(\text{SO}_4)_3$ titrated with NaOH in air, repeated in triplicate

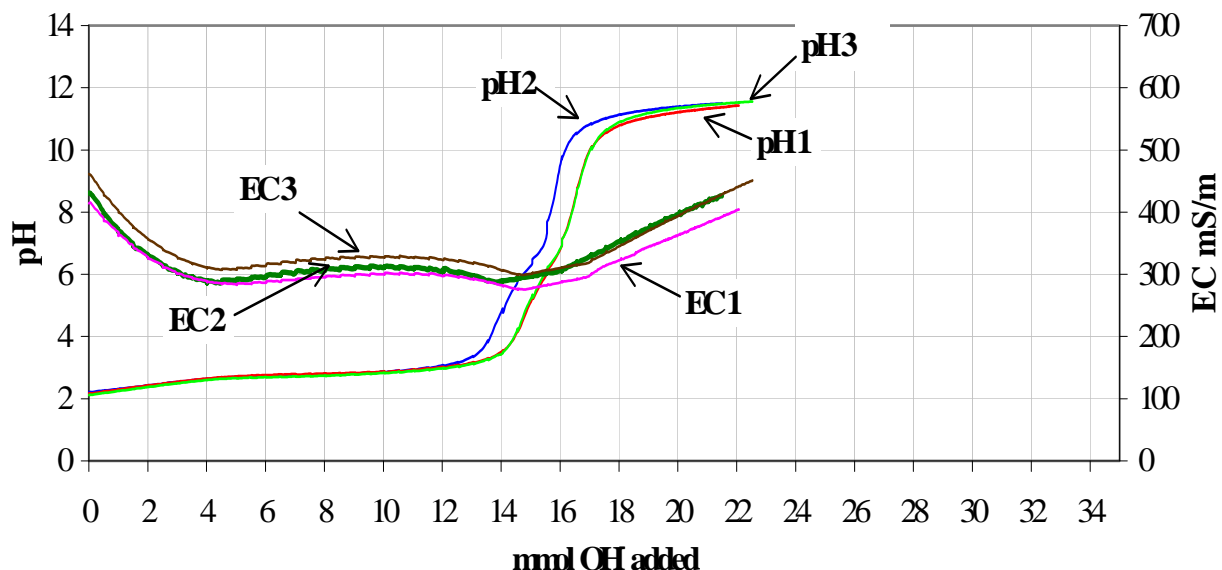


Figure A2.2: FeSO_4 titrated against NaOH in N_2 , repeated in triplicate

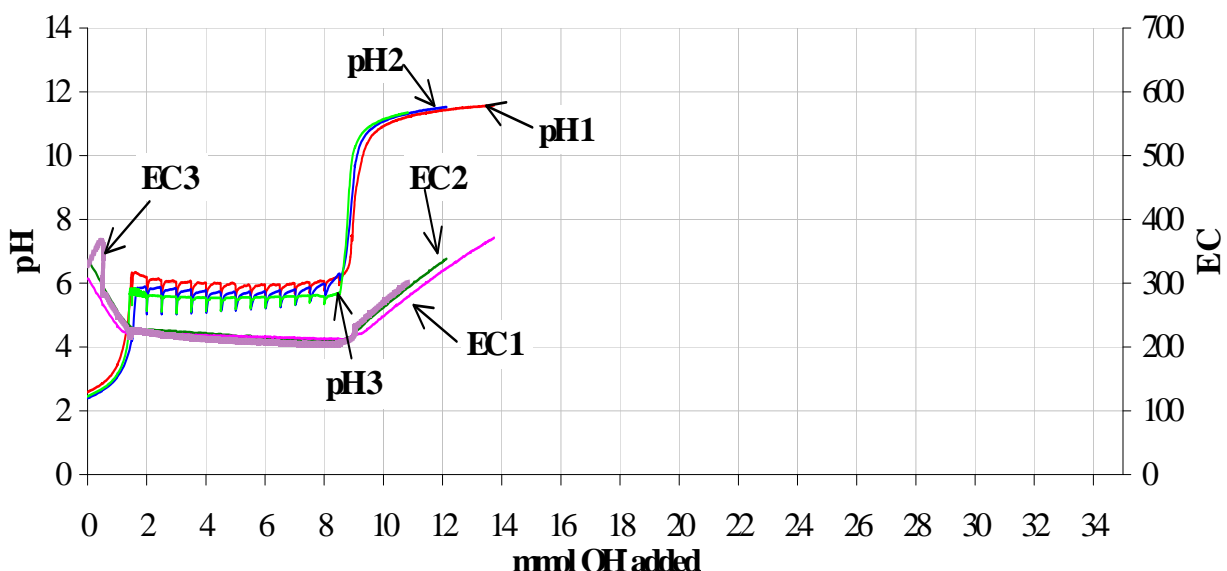


Figure A2.3: $\text{Al}_2(\text{SO}_4)_3$ titrated with NaOH in air repeated in triplicate

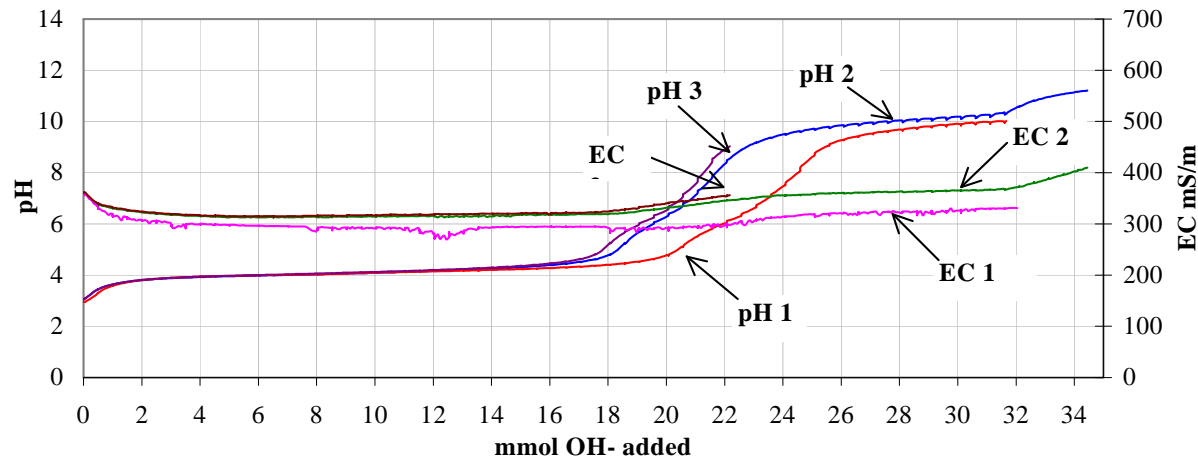


Figure A2.4: $\text{Fe}_2(\text{SO}_4)_3$ titrated with NaOH & CaCl_2 in N_2 repeated in triplicate

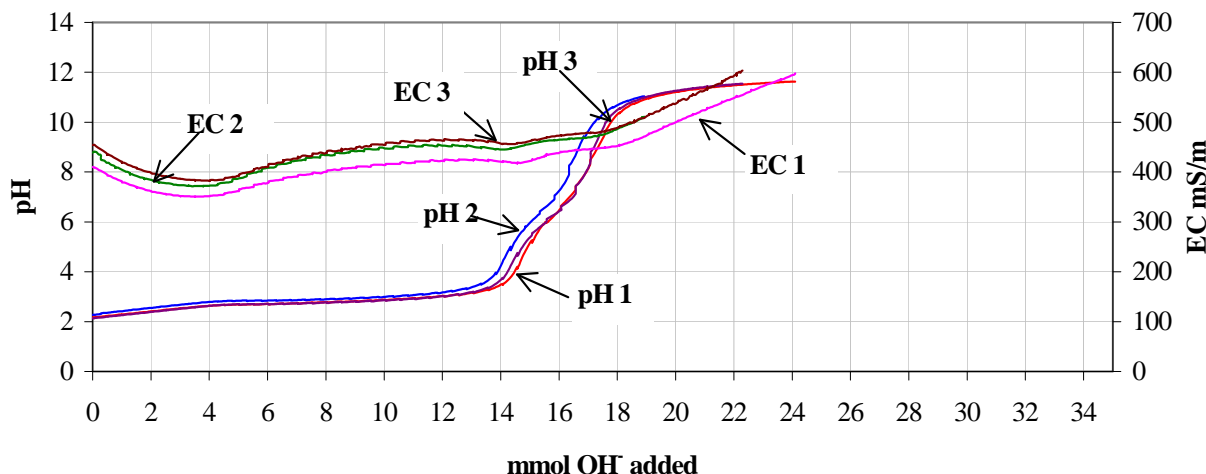


Figure A2.5: $\text{Fe}_2(\text{SO}_4)_3$ titrated with NaOH in N_2 repeated in duplicate

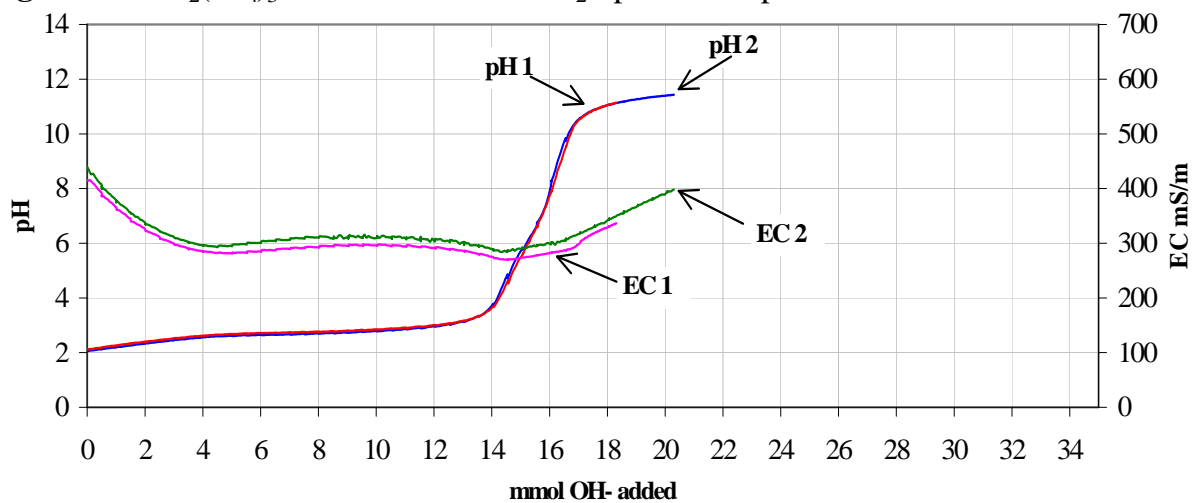
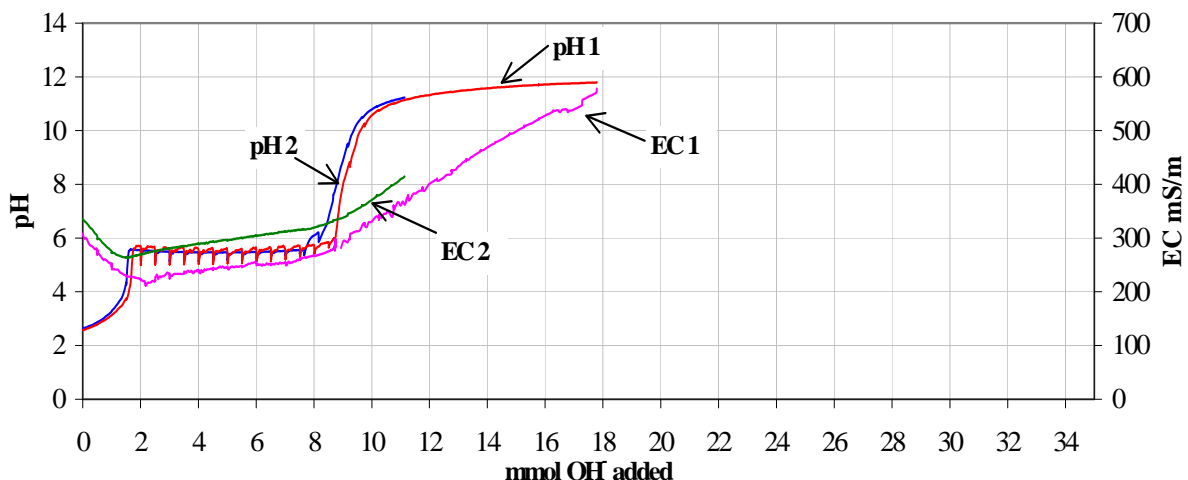


Figure A2.6: FeSO_4 titrated with NaOH and CaCl_2 in air repeated in duplicate.



Experiment 2: Acidic solutions with differing Fe:Al mole ratios

Figure A2.7: 6:1 $\text{FeSO}_4 : \text{Al}_2(\text{SO}_4)_3$ titrated with $\text{NaOH} & \text{CaCl}_2$ in N_2 in duplicate

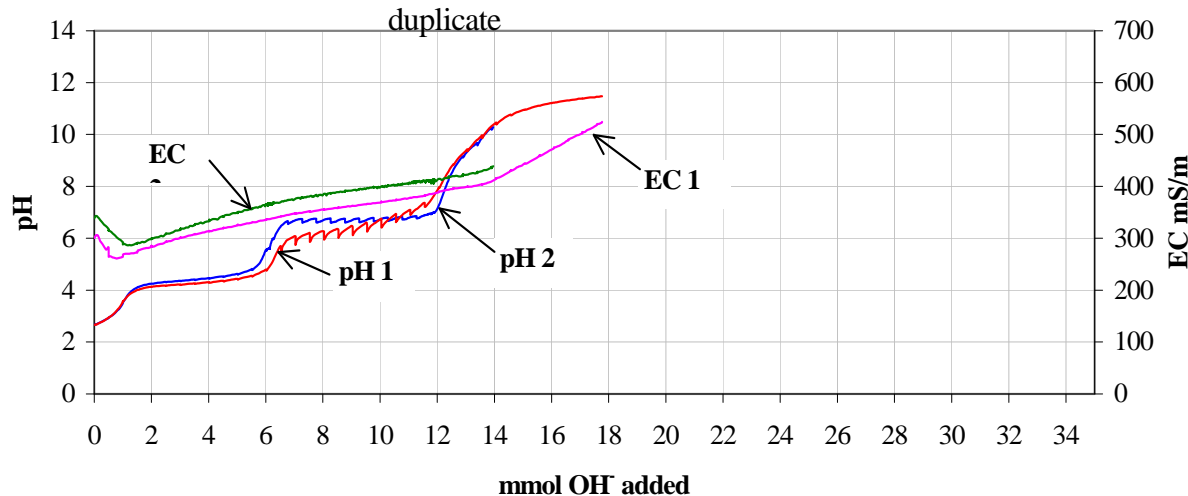
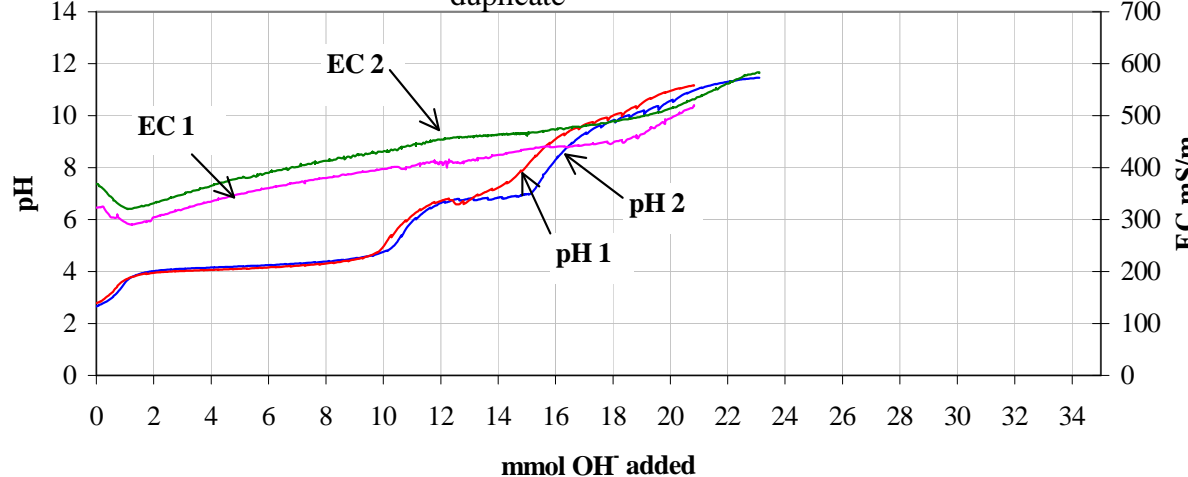
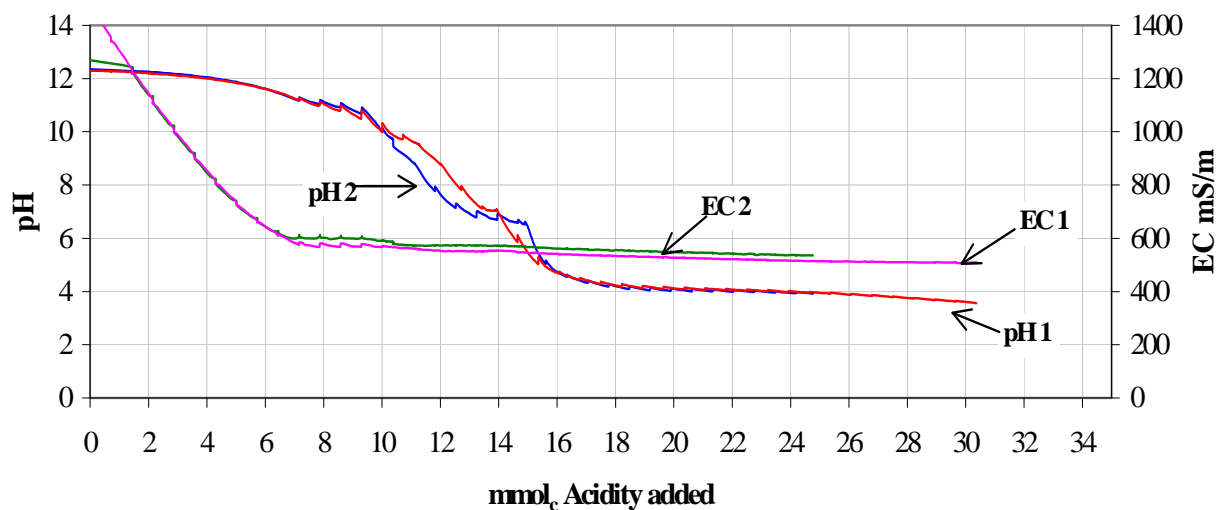


Figure A2.8: 1:2 $\text{FeSO}_4 : \text{Al}_2(\text{SO}_4)_3$ titrated with $\text{NaOH} & \text{CaCl}_2$ in N_2 in duplicate



Experiment 3: The SAMD/FAL system compared with simple acids and bases

Figure A2.9: NaOH and CaCl₂ titrated with SAMD in air repeated in duplicate



Appendix 3: A replot of Figure 3.2 in order to compare the difference between NaOH and the CaCl₂/NaOH solution

